Characteristics of fin whale vocalizations recorded on instruments in the northeast Pacific Ocean

Maria Michelle Josephine Weirathmueller

A dissertation
submitted in partial fulfillment of the
requirements for the degree of

Doctor of Philosophy

University of Washington

2016

Reading Committee:

William S.D. Wilcock, Chair

Kathleen M. Stafford

Julie E. Keister

Program Authorized to Offer Degree:
School of Oceanography

University of Washington

Abstract

Characteristics of fin whale vocalizations
recorded on instruments in the
northeast Pacific Ocean

Maria Michelle Josephine Weirathmueller

Chair of the Supervisory Committee:
Prof. William S.D. Wilcock
Oceanography

This thesis focuses on fin whale vocalizations recorded on ocean bottom seismometers (OBSs) in the Northeast Pacific Ocean, using data collected between 2003 and 2013. OBSs are a valuable, and largely untapped resource for the passive acoustic monitoring of large baleen whales. This dissertation is divided into three parts, each of which uses the recordings of fin whale vocalizations to better understand their calling behaviors and distributions.

The first study describes the development of a technique to extract source levels of fin whale vocalizations from OBS recordings. Source levels were estimated using data collected on a network of eight OBSs in the Northeast Pacific Ocean. The acoustic pressure levels measured at the instruments were adjusted for the propagation path between the calling whales and the instruments using the call location and estimating losses along the acoustic travel path. A total of 1241 calls were used to estimate an average source level of 189 $\pm$5.8 dB re 1μPa @ 1m. This variability is largely attributed to uncertainties in the horizontal and vertical position of the fin whale at the time of each call, and the effect of these uncertainties on subsequent calculations.

The second study describes a semi-automated method for obtaining horizontal ranges to vocalizing fin whales using the timing and relative amplitude of multipath arrivals. A matched filter is used to detect fin whale calls and pick the relative times and amplitudes

of multipath arrivals. Ray-based propagation models are used to predict multipath times and amplitudes as a function of range. Because the direct and first multiple arrivals are not always observed, three hypotheses for the paths of the observed arrivals are considered; the solution is the hypothesis and range that optimizes the fit to the data. Ray-theoretical amplitudes are not accurate and solutions are improved by determining amplitudes from the observations using a bootstrap method. Data from ocean bottom seismometers at two locations are used to assess the method: one on the Juan de Fuca Ridge, a bathymetrically complex mid-ocean ridge environment, and the other at a flat sedimented location in the Cascadia Basin. At both sites, the method is reliable up to $\sim$4 km range which is sufficient to enable estimates of call density.

The third study explores spatial and temporal trends in fin whale calling patterns. The frequency and inter-pulse interval of fin whale 20 Hz vocalizations were observed over 10 years from 2003-2013 on bottom mounted hydrophones and OBSs in the northeast Pacific Ocean. The instrument locations extended from 40°N to 48°N and 130°W to 125°W with water depths ranging from 1500-4000 m. The inter-pulse interval (IPI) of fin whale song sequences was observed to increase at a rate of 0.59 seconds/year over the decade of observation. During the same time period, peak frequency decreased at a rate of 0.16 Hz/year. Two primary call patterns were observed. During the earlier years, the more commonly observed pattern had a single frequency and single IPI. In later years, a doublet pattern emerged, with two dominant frequencies and two IPIs. Many call sequences in the intervening years appeared to represent a transitional state between the two patterns. The overall trend was consistent across the entire geographical span, although some regional differences exist.

TABLE OF CONTENTS

LIST OF FIGURES

LIST OF TABLES

ACKNOWLEDGMENTS

I am grateful to many people at the University of Washington and in the School of Oceanography. In particular I would like to thank my advisor, William Wilcock, who has provided incredible support and guidance throughout my time here. I am grateful for his patience and his willingness to take whatever time was needed to ensure that I got the most out of my research.

I would also like to thank my committee, Kate Stafford, Julie Keister, and Trevor Branch, who provided assistance and insights as I moved through my research. Kate has generously given hours of her time to help me understand and interpret the many surprising things I found in the data. She helped me to fathom how signals on my computer screen could tell a story about the complex and mysterious animals who produced them. Julie has a knack for asking big-picture questions that have made me think about my research in ways that I wouldn't have otherwise, and has been supportive whenever I've reached out for help. Trevor has provided valuable insights relating to my project, and has also been curious and enthusiastic any time we've met.

Thanks to thank Lora Weekly, Michelle Soule, Kim Leung, Jill Hurson, and Leah Stoller. I never would have survived graduate school without the support of my friends, family, and fellow graduate students. In particular I'd like to recognize my labmates and dear friends, Dax Soule and Robert Weekly. They have seen me through difficulties and triumphs, and have helped me navigate the often bumpy road through graduate school.

Finally, none of this would have been possible without the constant support of my husband, John Wray.

Chapter 1

INTRODUCTION

Many large baleen whales were hunted aggressively before whaling was finally banned in all oceans in the mid-1970s. Although several populations have at least partially recovered, they continue to be threatened in various ways by the increasing human presence in the worlds oceans. They are at risk from ship strikes, fishing gear entanglements, and also the increasing noise in the ocean, which is primarily linked to trans-oceanic vessel traffic, as well as active seismic experiments and pile driving.

To protect marine mammals from these effects, certain regions can be designated as protected areas, with regulations pertaining to things like vessel presence and speed, and fishing activity. But in order to establish these zones of relative safety, it is critical to have an adequate understanding of their ecology and habitat usage. Unlike terrestrial animals, marine mammals, particularly large baleen whale species, can be very difficult to observe. Often, their life history, migrations, feeding, and breeding grounds remain only partially understood, at best. In addition to benefits relating to the continued survival of the species, any additional information we learn will add to our somewhat sparse existing knowledge about this elusive animal.

Methods of observation include visual surveys, tagging experiments, and passive acoustic monitoring. Visual surveys can be used to estimate abundance (e.g. [31, 4, 30]) and have the benefit that individual animals can often be identified, and specific behaviors can be observed, such as feeding or social interactions. However, visual surveys are limited by light availability, and are therefore only possible during the day. They are also limited by weather, both due to the safety and comfort of human observers and vessel crew, but also to the fact that surfacing animals are more difficult to observe in rough waters. Tagging surveys are useful because

they give scientists a glimpse into the animals' behavior as they disappear below the surface. Short-term tags can record high-resolution diving and swimming patterns (e.g. [76, 41]), although it's possible that tagged animals may undergo a behavioral response shortly after deployment, which needs to be considered when analyzing the resulting data. Long-term tags can track individual animals over months or years, following them over large distances (e.g. [117, 67]). One downside to tagging experiments is that tags are challenging to deploy, and typically only a few individuals are tagged during a given experiment. Both visual and tagging studies can be particularly challenging for fin whales since they are fast swimmers and can leave an area quickly. Increasingly, passive acoustic methods are being used to observe these animals remotely [63]. One of the drawbacks of using acoustic monitoring to study marine mammals is that only vocalizing animals are recorded. This means that researchers need to know how often animals are calling, and what percentage of the animals are producing sounds in order to draw quantitative inferences from the data. Still, although the ability to understand the full context of the behaviors is sacrificed, researchers are able to deploy instruments for months or even years at a time at locations far from shore.

This study focuses in particular on fin whales (*B. physalus*) in the northeast Pacific Ocean. Fin whales are the second largest animals in the world after blue whales, and are known for their fast swimming speeds. Fin whales are filter feeders: they swim forward to engulf large volumes of water and filter their prey using fringed baleen plates. They are not as selective in what they eat as blue whales, and are known to consume various types of zooplankton as well as small schooling fish [64]. In the North Pacific Ocean, at least two sub-populations have been identified [32] but the details regarding the distributions and movements of fin whales in this region remain poorly understood.

This dissertation explores the use of passive acoustic monitoring to better understand movements, distributions, and calling behavior of fin whales in the northeast Pacific Ocean. Typical passive acoustic studies of marine mammals use instruments called hydrophones to measure sounds in the water column directly. In contrast, all three studies described herein use ocean bottom seismometer (OBS) data, which are datasets of opportunity. These studies

take advantage of the existence of extensive arrays of OBSs deployed to measure earthquake activity. OBSs measure ground motion and typically have sample rates of 50-100 Hz, which limits the upper frequency of observation. They record ground velocity in three perpendicular directions, with one vertical and two horizontal channels. These instruments fortuitously pick up the low frequency calls of two cetacean species: blue whales and fin whales. The most common fin whale calls are are downswept chirps with a duration of approximately 1 second, and are centered around a frequency of 20 Hz. The context or purpose of these vocalizations is not fully understood, although only male fin whales have been observed to produce the 20 Hz calls, and they are therefore believed to be linked to mating behavior [19]. The 20 Hz calls have also been attributed to groups of transiting animals [93, 57].

With multiple, closely-spaced OBSs, it is possible to locate individual calls using the arrival time of the calls on the different instruments [93, 57, 35]. However, for many OBS experiments, instruments are spaced too far apart to allow for this. Single OBS instruments are still useful, however, since the number of calls recorded on an instrument gives information about the presence of calling animals over time. To compare different instruments, call counts need to be normalized for differences in detectability. One way to do this is by using distance sampling methods to estimate animal density [10]. The three parts of this thesis describe studies that address different aspects of fin whale calling that can affect the estimation of call density.

Chapter 2 [119] describes the development of a technique to extract the source levels of fin whale vocalizations from seafloor seismometer recordings. If call amplitude is measured at the seafloor, and the position of the whale at the time of the vocalization is known, then the source level can be estimated by modeling the amplitude that is lost in propagation from the source to receiver. Seismometers do not directly measure the acoustic pressure level, so additional modeling is required to convert from the velocity measured at the seismometer. With knowledge of acoustic source levels, along with an adequate understanding of the local acoustic environment, fin whale calls can be used to estimate the communication range of vocalizing animals. Source levels are also required in the calculation of animal density using

the energy in the frequency band of fin whale vocalizations [62].

In Chapter 3 (submitted to the Journal of the Acoustical Society of America in September 2016), the timing and amplitude of fin whale call multipath arrivals are used to estimate range to vocalizing animals. Arrival times and amplitudes are initially modeled using ray-based propagation models, but the ray-theoretical amplitude estimates are improved upon by extracting information directly from the data using a bootstrap method. Since the direct path and first multiple are not always observed, three hypotheses for paths of the observed arrival are tested. The first hypothesis assumes the largest amplitude arrival is the direct path, the second assumes the largest amplitude arrival is the first multipath, and the third assumes the largest amplitude arrival is the second multipath. From these, the one that optimizes the fit between the data and the measured multipath timing and amplitude is selected. Ranges measured at two locations are used to demonstrate how they can be used to obtain estimates of call density.

Chapter 4 (submitted to PLOS ONE in November 2016) explores temporal and geographic shifts in calling patterns observed over a decade on eight instruments in the northeast Pacific Ocean. Both inter-pulse interval and call frequency are measured automatically and a total of more than 1.8 million calls are included in the analysis. Observing how patterns evolve over time and space can inform how these calls might be used to delineate acoustic populations of fin whales throughout the region. Another significant implication is that the conversion of call density to animal density requires knowledge of the characteristics of individual calling animals, and in particular, the calling rate. Therefore, observing a shift in calling patterns over a duration of several years has implications for the estimation of animal density.

Chapter 5 summarizes the results in Chapters 2-4, and discusses the implications and how they might be built upon in future work.

Chapter 2

SOURCE LEVELS OF FIN WHALE VOCALIZATIONS MEASURED IN THE NORTHEAST PACIFIC OCEAN

2.1 Introduction

Aggressive commercial whaling practices in the early-mid twentieth century led to the near-extinction of fin whale (*Balaenoptera physalus*) populations throughout the world's oceans [64]. They were listed in the Endangered Species Act of 1973, and by 1976 the International Whaling Commission (IWC) gave them full protection from commercial whaling in the North Pacific. By the late 1980s, this protection had extended to include all oceans. Since that time, there has been interest in monitoring their recovery and assessing ongoing effects of anthropogenic influences [19, 97].

The distributions and movements of fin whales are poorly understood [64]. Several observational techniques have been employed to assess fin whale populations, including visual and aerial surveys [31, 127], radio and satellite tagging [115, 117], genetic studies [32, 6], and the compilation of historic whaling records [42]. Passive acoustic monitoring provides an additional set of techniques, allowing for long-term, non-invasive observation of fin whale vocalizations. Fin whales produce high-amplitude, repetitive call sequences that can be reliably detected using automated methods [60]. A single acoustic recorder can be used to identify and count fin whale calls over time, and a fixed network of instruments can be used to locate a given call using relative arrival times at several instruments [118, 57, 35]. The source level of a fin whale call can be used to help distinguish between multipath arrivals and constrain the range to a calling whale measured on a single instrument [55]. Ranges to calling animals can then be used in estimating population density. Estimates of maximum communication range can also help assess the impact of anthropogenic noise.

Few studies estimating fin whale call source levels have been undertaken [79, 73, 115, 114, 17, 112], due in large part to the difficulty in acquiring a set of calls where the position of both the whale and the acoustic recorder are accurately known, and the received level at the instrument can be measured in terms of absolute pressure level. Previous estimates of source levels vary between 159-199 dB re 1μPa @ 1m. Charif et al. [17] reported source levels of 159-184 dB re 1μPa @ 1m in the northeast Pacific Ocean.

Globally distributed networks of ocean bottom seismometers (OBSs) are deployed to measure seismic activity, but are also sensitive to the low frequency sounds produced by both fin and blue whales. These instruments have been used to analyze calling patterns and to resolve tracks of fin and blue whales [57, 35, 27]. In this study, source levels of fin whale vocalizations are estimated using ocean bottom seismometer data recorded in the northeast Pacific Ocean between August 2003 and April 2004.

2.2 Methods

2.2.1 Fin whale dataset

The experiment was located at the Endeavour segment of the Juan de Fuca Ridge (48.5°N, 129.0°W), where a network of eight OBSs were deployed continuously between 2003 and 2006. The instruments were located along the axis of the mid ocean ridge, extending approximately 10 km in the along-axis direction, and 6 km across, with an average water depth of 2200 m (Figure 2.1). Each OBS was positioned using an ROV equipped with an ultra-short baseline (USBL) beacon, with an estimated absolute horizontal position error of less than 5 meters. Seven of the seismometers were short-period instruments sampled at 128 Hz with a flat frequency response between 1-90 Hz [103]. One of the instruments was a broadband seismometer, with a flat frequency response from less than 1 Hz to approximately 50 Hz, sampled at either 50 Hz or 100 Hz [86].

In addition to seismic activity, the instruments also recorded more than 300,000 fin whale vocalizations during the three year deployment, with most calls appearing during the winter

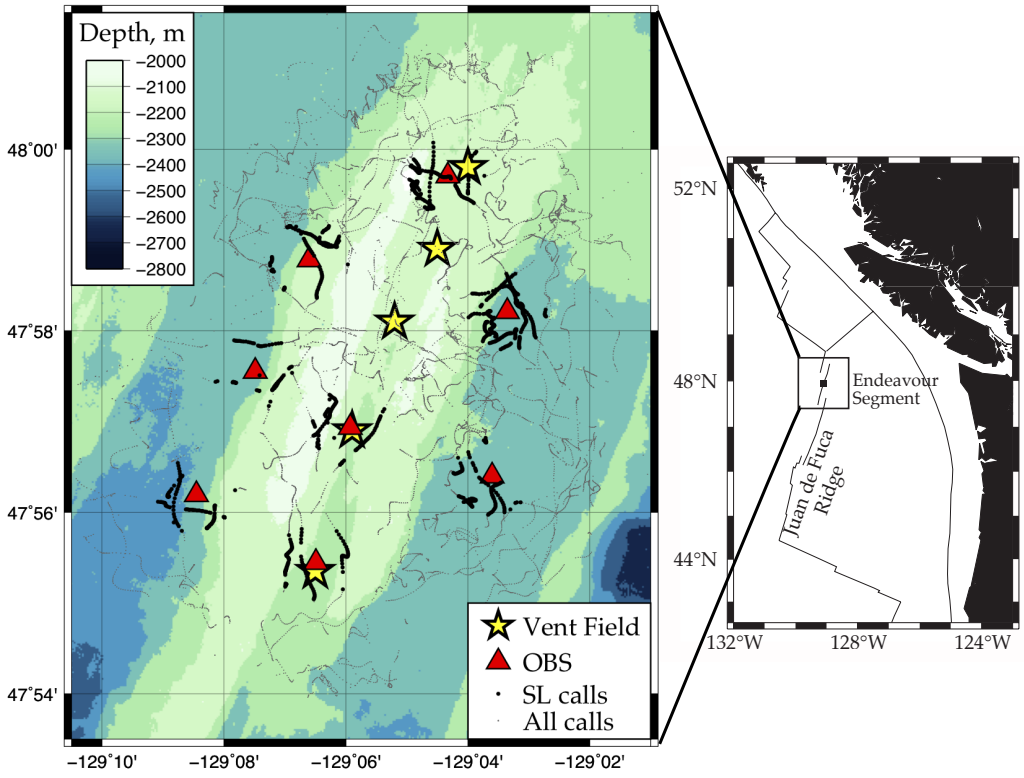

Figure 2.1: Experiment site on the Endeavour segment of the Juan de Fuca Ridge, in approximately 2200 m water depth. The seismic network extends approximately 10 km north-south, and 6 km east-west. Active hydrothermal vent fields in the axial valley are indicated by star symbols, and seismometers are shown by triangles. The darker circles show calls used in source level estimation. The smaller grey circles show calls that were analyzed but not included in final source level estimates.

months. Of the sounds produced by the fin whale, the low frequency "20-Hz pulses" [115] are most readily identifiable in the seismic dataset. The calls are approximately one second long and downswept in frequency, typically between 25-15 Hz. A location algorithm was developed which utilized the relative arrival times and multipath structure of whale calls observed on the OBSs [125]. During the first year of deployment (2003-2004), over 100 individual tracks were resolved from a dataset that included >100,000 calls [94]. Within the network, horizontal errors in final call locations were between 300 - 500 m. Call sequences were analyzed for patterns in inter-pulse interval (IPI) and frequency, where inter-pulse interval is defined as the space between the onset of one call and the one immediately before it. Four dominant IPI patterns are observed: 25-second simple IPI, 25/30-second dual IPI, 13/25-second dual IPI, and complex IPI. The 25-second simple IPI and the 25/30-second dual IPI are believed to represent single whales, while the 13/25-second dual IPI and the complex IPI are believed to represent two or more whales calling near the network. The most commonly measured call frequency was 19 Hz. Calls at distinctly higher frequencies were also observed, with an average frequency of 24 Hz. Lower frequency, lower amplitude backbeat calls were often associated with the 19 Hz calls. Backbeat calls were observed to occur primarily after rests (defined as a pause greater than 60 seconds and less than 2 hours), and also after 30-second IPIs.

The calculation of source level requires knowledge of the location of the OBS and the whale call, and the acoustic propagation path between the two. The tracking algorithm was optimized to find most, but not every call in a track. For this study, the missed calls in the tracks were detected using an automatic detection algorithm based on a spectrogram detection method [60]. The horizontal locations of the missing calls were interpolated based on time of call using a 300-second Gaussian smoothing operator. The analysis was restricted to a subset of the data where horizontal ranges between instruments and fin whale calls were less than 3000 m.

2.2.2 Source level estimation

The source level was estimated using the passive sonar equation [e.g. 48]:

$$SL = RL + TL, \tag{2.1}$$

where SL is the source level, RL is the acoustic pressure level at the receiver, TL is the transmission loss along the acoustic propagation path and all quantities are in decibels. Estimating the received acoustic pressure level is more complicted for an OBS than for a hydrophone. A voltage measured on a hydrophone with a known frequency response can be directly converted to acoustic amplitude. An OBS measurement differs in that it measures ground velocity, which has a more complex relationship with the amplitude of incident acoustic waves. The vertical component of the OBS is used for these measurements since coupling with the seafloor is more reliable in the vertical direction. The vertical particle velocity u_v is obtained by band-pass filtering the signal between 13 - 40 Hz, and using the instrument response to convert to ground velocity in meters per second. The root-mean-square (RMS) amplitude of the signal is calculated in a one-second window centered on the detection time (Equation 2.2). The measured amplitude u_v is corrected for the effects of noise using a one-second window immediately preceding the call:

$$u_v = \sqrt{\frac{1}{N}\left(\sum_{k=1}^{N}|h_k|^2 - \sum_{n=1}^{N}|h_n|^2\right)} \tag{2.2}$$

where h_k represents samples of the filtered signal in the time domain, h_n is the one second filtered noise measurement, and N is the number of samples in the one-second signal.

The Zoeppritz equations [45] are used to relate the particle velocity in the direction of the incoming acoustic wave to the seafloor particle velocity measured in the vertical direction (see geometry in Figure 2.2). The acoustic pressure wave incident on the seafloor is converted to both pressure P and shear S wave energy. The amplitudes of the transmitted P and S

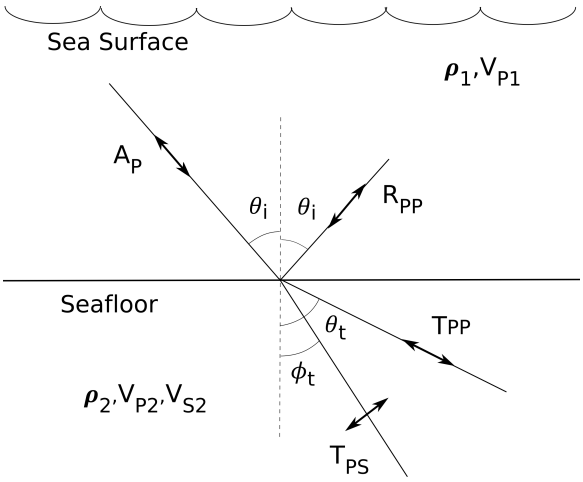

Figure 2.2: Geometry of the model used to calculate the amplitudes of the P and S waves transmitted into the seafloor. A_p is the incident P wave, T_{PP} is the transmitted P wave, T_{PS} is the transmitted S wave, and R_{PP} is the reflected P wave.

waves at a fluid solid interface, relative to an incident pressure wave of unit amplitude, are given by:

$$T_{PP} = \left(\frac{V_{P1}}{V_{P2}}\right) \times \frac{2B\rho_1 V_{P2}\cos(\theta_i)}{A_1\rho_2 V_{P2}\cos(\theta_i) + A_2\cos(\theta_i)\cos(\theta_t) + \rho_1 V_{P1}\cos(\theta_t)} \tag{2.3}$$

$$T_{PS} = \left(\frac{V_{P1}}{V_{S2}}\right) \times \frac{2C\cos(\theta_i)\ cos(\theta_t)}{A_1\rho_2 V_{P2}\cos(\theta_i) + A_2\cos(\theta_i)\cos(\theta_t) + \rho_1 V_{P1}\cos(\theta_t)} \tag{2.4}$$

where:

$$A_1 = \cos^2(2\phi_t) = B^2 \tag{2.5}$$

$$A_2 = 4\rho_2 V_{S2}\sin^2(\phi_t)\cos(\phi_t) \tag{2.6}$$

$$B = \cos(2\phi_t) \tag{2.7}$$

$$C = 2\rho_1 V_{S2}\sin(\phi_t) \tag{2.8}$$

and V_{P1} is the incoming P wave velocity, V_{P2} is the transmitted P wave velocity, V_{S2} is the transmitted S wave velocity, θ_i is the incidence angle of the incoming acoustic wave, θ_t is the transmitted P wave angle, ϕ_t is the transmitted S wave angle, and ρ_1 and ρ_2 are the densities in the fluid and solid layers respectively. The angles of the transmitted P and S waves are obtained from Snell's law:

$$\frac{\sin(\theta_i)}{V_{P1}} = \frac{\sin(\theta_t)}{V_{P2}} = \frac{\sin(\phi_t)}{V_{S2}} \tag{2.9}$$

The incidence angle is estimated using the location of the whale relative to the OBS. The measured vertical ground velocity, u_v, is scaled by the Zoeppritz equation to obtain velocity in the direction of the incoming wave u:

$$u = \frac{u_v}{T_{PP}cos\theta_t + T_{PS}sin\phi_t} \tag{2.10}$$

The acoustic pressure level p_m of the incoming wave is then calculated according to:

$$p_m = u\rho_1 V_{P1} \tag{2.11}$$

and the receive level RL, in dB, used in Equation 2.1 is obtained by:

$$RL = 20log_{10}\left(\frac{p_m}{p_{ref}}\right) \tag{2.12}$$

where p_{ref} is the reference level for underwater sound, 1μPa. Transmission loss was estimated assuming a spherical spreading acoustic environment:

$$TL = 20log_{10}(R) \tag{2.13}$$

where R is the slant range between the whale call and the OBS.

The sound speed and density of the water at the depth of the instrument are obtained using an average winter conductivity-temperature-depth profile from this location from the 2009 World Ocean Atlas using the formulation of [23]. Most of the instruments in the network are directly coupled to the exposed volcanic basalt layer, except for stations KESE and KESW which are installed in areas having a thin sediment layer. Seafloor properties used in this analysis are based on average density and sound speed to a depth of one wavelength ($\sim$75 m). Since the sediment layer, where it exists, is only a few meters thick, the average properties of the underlying basalt are used. P wave velocities of mid-ocean ridge basalts near the seafloor estimated at this location using surface refraction [20] and reflection data [113] and from the East Pacific Rise using seafloor refraction data range from 2.0-3.0 km/s with an average value of 2.5 km/s. Direct measurements for S wave velocities at the seafloor are not available for the Endeavour site, but the values of 0.4-0.6 km/s obtained from the East Pacific Rise [18] are consistent with indirect estimates from the Endeavour based on the arrival times of phase conversions form the base of the volcanic layer [124]. Measurement of the density of the shallow seafloor at this location range from 2190 - 2360 kg/m^3 [40].

The Zoeppritz correction in the vertical direction reaches a maximum at the critical angle. The parameter with the largest effect on the critical angle is the seafloor P wave velocity. Figure 2.3 shows the Zoeppritz correction for three P wave velocities: the lower and upper limits for typical mid-ocean ridge basalts, and an average value, which is used in source level calculations. This indicates that errors from incorrect estimates of seafloor P wave velocity are less than 2 dB at incidence angles less than 20°, but increase rapidly at larger incidence angles.

Both the transmission loss, TL, and the incidence angle, θ_i, were initially calculated for curved rays using BELLHOP acoustic propagation software from the Ocean Acoustics Toolbox [82]. The bias introduced by assuming a straight line propagation path is only 0.2 dB with the whale directly above an instrument, and increases to 0.4 dB at an incidence angle of 20°. Because this bias is small compared to other sources of error, a straight line travel path assumption was used for calculating incidence angle, and transmission loss was

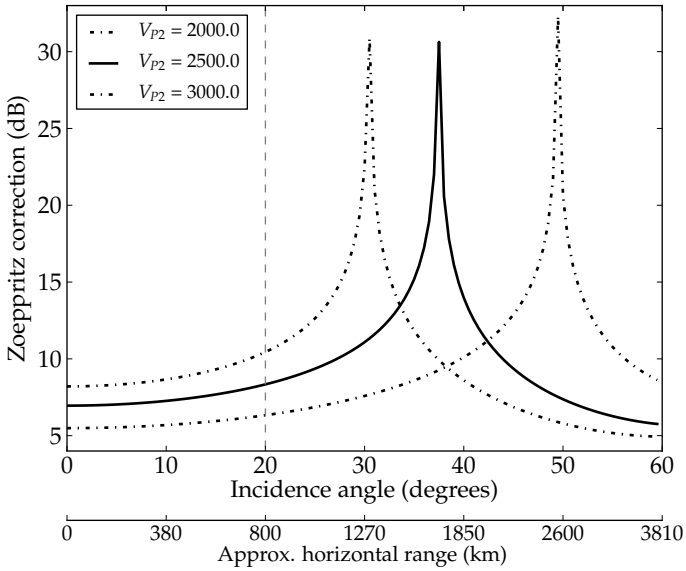

Figure 2.3: Zoeppritz correction to convert vertical ground velocity to the velocity of the incoming acoustic wave, displayed in decibel units. This function shows the sum of the P and S waves projected onto the vertical direction, as a function of incoming P wave incidence angle. The results for upper and lower limits of likely seafloor P wave velocity are shown by dashed lines, and are used to estimate the potential error resulting from an incorrect P wave velocity. The model is run using $V_{P1} = 1.5$ km/s, $V_{P2} = 2.5$ km/s, $V_{S2} = 200$ km/s, $\rho_1 = 1000\ kg/m^3$, and $\rho_2 = 1700\ kg/m^3$.

calculated assuming spherical spreading.

2.2.3 Variability in source level estimates

The amplitude of the Zoeppritz correction is a function of the incidence angle of the incoming P wave, which is dependent on the position of the whale relative to the instrument. An error in the whale's horizontal and vertical location would result in an incorrect incidence angle, which would give a biased estimate of the Zoeppritz correction. The uncertainty in the horizontal position of the whale in the vicinity of the OBS network is about 400 m. The location algorithm assumes that the whale is calling at the sea surface, so the vertical uncertainty is not resolved. Watkins et al. [114] report a calling depth of 50 m, but provide few details of the method or estimated uncertainties. The uncertainty in the Zoeppritz correction for a given uncertainty in the whale's position becomes larger as the incidence angle approaches the critical angle ($\theta_c = sin^{-1}(V_{P1}/V_{P2})$). For an upper-layer P wave velocity of 1.5 km/s, and a lower-layer P wave velocity of 2.5 km/s, the peak in the Zoeppritz correction corresponds to a critical angle of $\sim 37°$.

Another effect that is highly dependent on the three dimensional position of the whale relative to the OBS is the interference between the direct path and surface bounce acoustic arrivals. The effect of interference is described in [111], and discussed with respect to fin whale call source levels in [17]. The time delay between the direct and surface bounce arrivals produces an interference pattern that is highly sensitive to changes in horizontal range, call depth, and total water depth. The geometry is illustrated in Figure 2.4. For a tonal signal, the largest increase due to constructive interference will result in a doubling of signal amplitude, which is equivalent to a 6 dB increase in receive level. Perfect destructive interference would result in complete cancellation. The fin whale call is not a tonal signal, but a downswept chirp, so full constructive or destructive interference will not occur.

Interference between surface bounce and direct path arrival for the approximate geometry of this experiment was modeled for a series of different source depths and horizontal ranges. The input fin whale call was a linear chirp with a one-second duration, downswept from 25

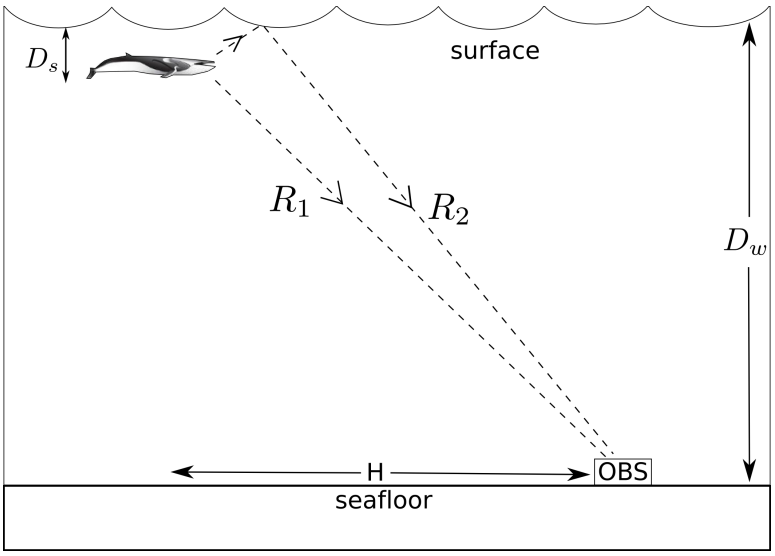

Figure 2.4: Schematic diagram of direct and surface bounce arrivals resulting in interference at the receiver. Depth of the calling fin whale D_s is believed to be near 50 m [114], and the water depth D_w in the region is approximately 2200 m.

to 15 Hz. The chirp amplitude was modulated over its duration using a one-second Hann window. The model assumes a single layer of water with uniform sound speed and a depth of 2200 m (Figure 2.4). The ranges, R_1 and R_2 can be estimated according to:

$$R_1 = \sqrt{(D_w - D_s)^2 + H^2} \tag{2.14}$$

$$R_2 = \sqrt{(D_w + D_s)^2 + H^2} \tag{2.15}$$

where D_w is the water depth, D_s is the source depth, and H is the horizontal range between source and receiver. The air-water interface is modeled as a pressure release boundary, resulting in 180° phase reversals of ray paths interacting with the surface [48]. The difference between these ranges, combined with the sound speed, gives the time difference between the arrivals, which can be used to calculate the interference. The ranges are also used to estimate

transmission loss, assuming simple spherical spreading for both the direct and the surface bounce paths. The validity of the spherical spreading assumption was verified by comparing with transmission loss modeled using BELLHOP [82]. The comparison showed a bias of <0.3 dB at $\theta_i < 20$ °.

The model output for source depths between 5-60 m, for ranges between 0-3000 m, is summarized in Figure 2.5. The root-mean-square amplitude of the input source level was scaled to unit amplitude. For a source depth of 5 m, the two travel paths arrive very close in time, but the surface-bounce path is phase shifted by 180°, resulting in mostly destructive interference and a low amplitude for all ranges. A high source level is predicted for a call depth of ∼20 m because the surface bounce lags by approximately half a wavelenth (where a full wavelength would be 75 m at 20 Hz and 1500 m/s), but with the 180° phase shift is nearly perfectly in phase with the direct path arrival. This results in almost complete constructive interference, and an increase of almost 6 dB.

The Zoeppritz correction and the effect of interference with the surface bounce arrival are both dependent on incidence angle, which is a function of range. Therefore, the average position uncertainty of 400 m is expected to cause scatter in the resulting source level estimates. A model was developed to quantify the effect of depth and horizontal position uncertainty on the final source level, given the effects of both interference patterns and the Zoeppritz correction. A series of horizontal locations were randomly generated within 3000 m horizontal range of an instrument. Depths for each location were randomly generated assuming a Gaussian distribution with a user-defined mean and standard deviation. These were treated as the *true* call locations. The same amplitude modulated chirp used in the interference pattern model was used as input to this model. The linear amplitude of the simulated signal was scaled so that the RMS level would be equal to a pre-defined starting source level. The *true* recieved level was calculated by combining the effect of both spherical spreading transmission loss and the interference between the direct path and surface bounce arrival for the *true* range and depth. From this, the vertical particle motion was calculated using the Zoeppritz equations for the particular range and depth. For the model, these were

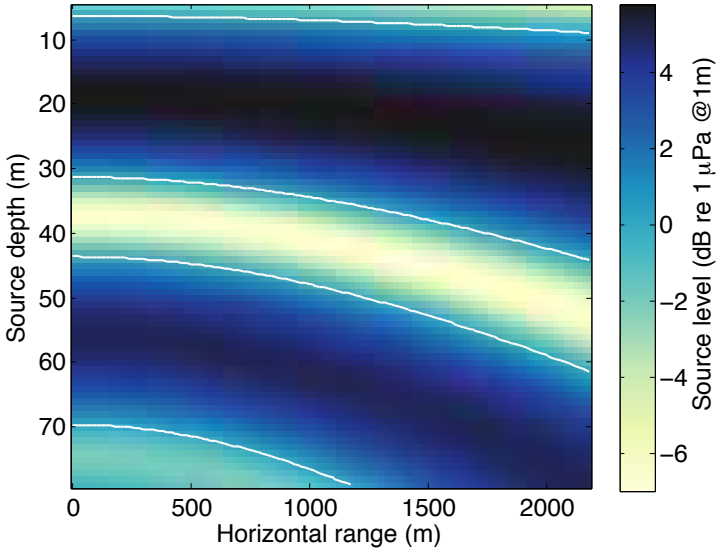

Figure 2.5: Result of interfernce between the direct path and surface bounce arrival for source depths between 5-80m. The interference model uses a starting RMS source amplitude of 1, and estimates propagation loss using spherical spreading over the distance of the propagation paths. White lines overlaid on the image indicate 0 dB contours where measured amplitude is equal to the input amplitude.

assumed to be equal to the measured vertical velocity. A second set of horizontal locations was generated by adding Gaussian errors with a standard deviation of 400 m to the *true* horizontal positions to produce *measured* positions. These were used to calculate the Zoeppritz correction to convert back to the direction of the incoming signal. Finally, this value was corrected to represent a *measured* source level using spherical spreading transmission loss over the range between the instrument and the *measured* position of the calling whale. Since the source depth was unknown, no attempt was made to correct apparent measured source levels for interference from the surface bounce arrival. The output of the model is shown in Figure 2.6a for a source depth of 50 m with a standard deviation of 10 m. The combination of uncertainties results in scatter about the *true* source level. The upper limit of the modeled source level output at very small incidence angles is limited to an increase of slightly less than 6 dB due to interference. The increase in this upper limit with increasing incidence angle, reaching a peak at the critical angle, is due to the Zoeppritz correction. There is increased scatter toward the smaller decibel values beginning near an incidence angle of 25°. This is a result of large errors in the Zoeppritz correction in the vicinity of the critical angle.

2.3 Results

2.3.1 Source levels

Measured source levels from all instruments are shown in Figure 2.6b. There are fewer measurements at close ranges. Due to the increased uncertainty in the Zoeppritz correction and the increased errors that would arise from incorrect seafloor properties at large incidence angles (Figure 2.3), calls used in source level estimates were restricted to those arriving at incidence angles $< 20°$. This reduces the dataset to a subset of 1241 calls from 32 individual whale tracks. Average source level within this subset is 189.9 dB $\pm$5.8 dB re 1μPa @ 1m.

The error bars in Figure 2.7 show the mean and standard deviation of the measured source level within 5° bins. The small standard deviation shown by the first error bar is likely the result of fewer data points, and even fewer tracks, within this range bin. The

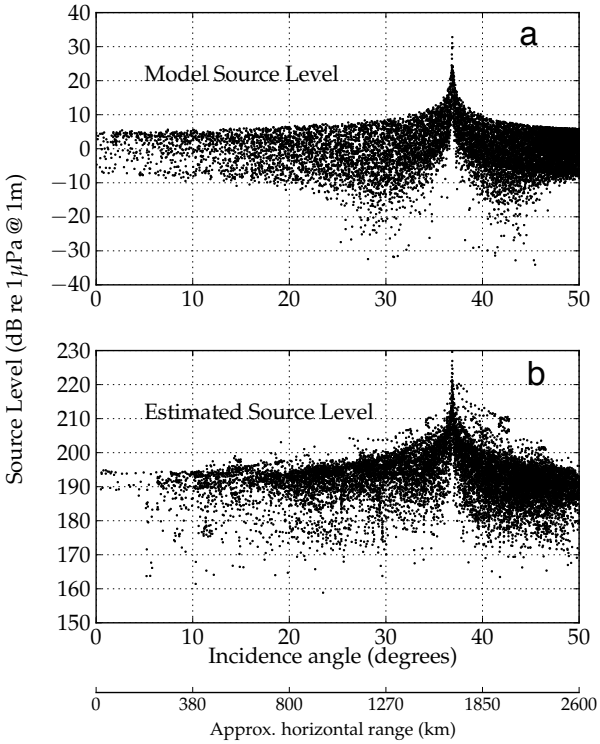

Figure 2.6: (a) Model source level output for an input source level of 0 dB, and the same seafloor properties used in calculating the measured source levels. (b) Measured source levels. Both are plotted versus incidence angle, but a second X-axis shows approximate range for a call generated at the surface and a water depth of 2200 m.

dashed lines shows the mean and standard deviation of the model for the same 5° bins, with a starting source level of 190 dB.

The standard deviation of source levels of all measured calls at less than 20° incidence angle is 5.8 dB. Interference effects were modeled for a variety of depths and standard deviations. Only very shallow source depths (<10 m) resulted in variability greater than that in the observed data. At source depths with standard deviations >10 m and 10-20 m respectively, standard deviation in the modeled source levels is approximately 4-5 dB. This is 1-2 dB less than the measured standard deviation, suggesting that there may be some variability in the true source level. To test this, the model was repeated several times with Gaussian errors added to the input source level. A standard deviation of 4 dB added to the starting source level in the model resulted in a standard deviation of 5.7 dB within the first 20° of the model output (shown by dot-dashed lines in Figure 2.7), which is close to the standard deviation of the data. The variability matches the model up until the cutoff frequency of 20°, where it begins to diverge, although there is a range dependent bias observed below 20°. Figure 2.5 shows that for a whale calling very consistently at a depth of 25-35 m, the apparent amplitude of its call would increase gradually with increasing range. The same phenomenon would be observed at a consistent depth of between 65-70 m. If a fin whale were swimming consistently in one of these specific depth ranges, it could explain the divergence between the measured data and the model (Fig. 2.6a and b). Alternatively the range dependent bias might arise because the model does not fully describe the physics of the interactions of acoustic waves with the seafloor and in particular, the generation of interference waves at larger incidence angles[28, 72].

Source levels were measured on all eight stations, and the mean and standard deviations of these are summarized in Table 2.1. The lowest mean source level is measured by KEBB, the one broadband instrument, at 183.3 dB. The highest mean source level, 194.2 dB, is measured at station KEMO.

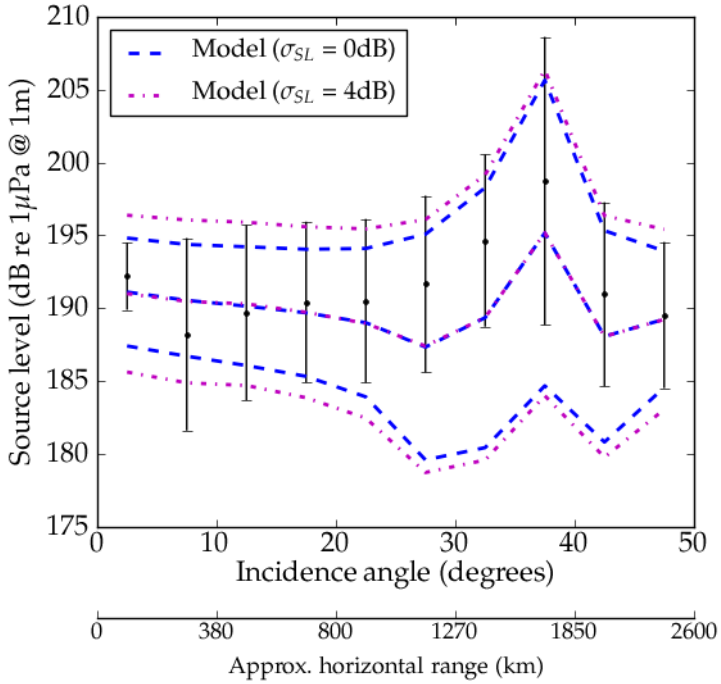

Figure 2.7: Comparison of the variability between modeled and measured source levels. Variability in source levels is estimated by calculating the mean and standard deviation within 5-degree bins of incidence angle. The error bars show the variability in the source level measurements (Figure 2.6b), the dashed lines show the mean and standard deviation in the source levels calculated using the model (Figure 2.6a), and the dot-dashed lines show the mean and standard deviation in the model where a 4 dB standard deviation has been added to the input source level.

Table 2.1: Summary of source level results for all stations. Decibel measurements are relative to 1 μPa at 1 m.

Station	μ_{SL} (dB)	σ_{SL} (dB)	n_{meas}
All	189.9	5.9	1241
KESQ	191.8	4.1	212
KEMF	186.4	7.8	110
KEMO	194.2	3.4	113
KESE	188.0	7.1	130
KENE	191.2	4.1	317
KENW	190.2	3.4	151
KESW	188.5	7.4	123
KEBB	183.3	4.5	85

2.3.2 Amplitude variation

A small number of track segments contained sufficient consecutive calls to investigate relationships between the inter-pulse interval, call frequency, and source level. Both the 25 second simple IPI and the 25/30 second dual IPI are believed to originate from a single vocalizing whale. A total of two simple IPI and six dual IPI tracks were used in the analysis of amplitude variation. A typical single-whale track is shown in Figure 2.8. Calls immediately following a gap longer than 27 seconds are consistently lower in amplitude and frequency, and are believed to be backbeat calls [114, 44]. The backbeat calls for all tracks of this type are, on average, 2.7 dB lower in amplitude and 1.1 Hz lower in frequency.

Complex IPI tracks are believed to represent two or more whales calling together. A total of four complex IPI tracks were resolved. Figure 2.9 shows an example of a complex IPI track with two dominant frequencies. The mean of the lower frequency group is 19.7 Hz, and the mean of the higher frequency group is 24.0 Hz. Mean source level is 192.7 dB for the lower frequency group and 191.8 for the higher frequency group. Figure 2.9a

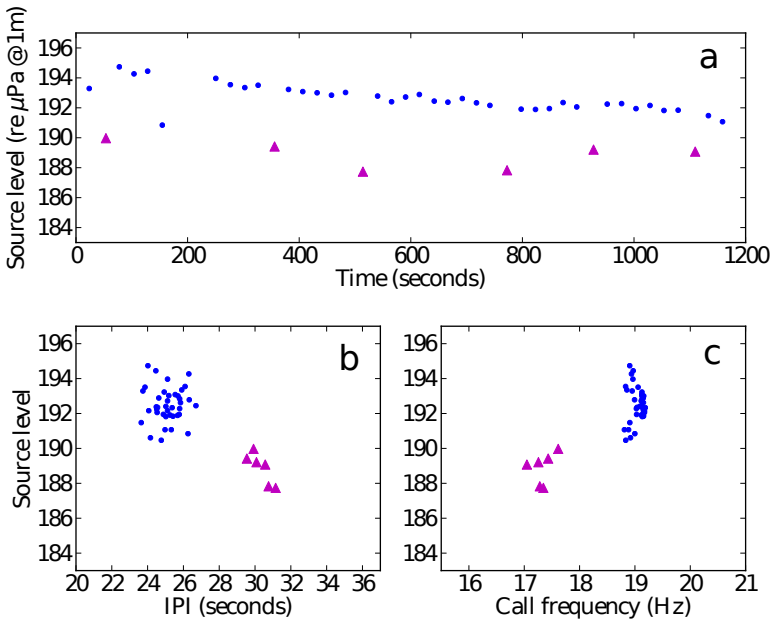

Figure 2.8: Example of a track with dominant IPIs near 25 and 30 seconds, interpreted as a single whale. (a) source level measured over time, (b) source level versus IPI, and (c) source level versus call frequency. In all three panels, calls following an IPI less than 27 seconds are indicated by circles, and calls following IPIs longer than 27 seconds are indicated by triangles.

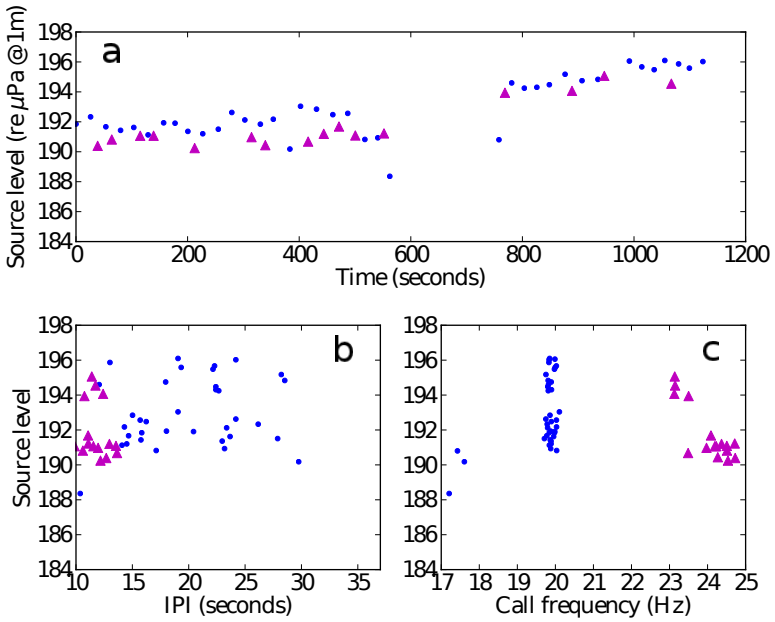

Figure 2.9: Example of a track with two whales calling, plotted with the same conventions as Figure 2.8, except symbols are assigned based on call frequency: calls with center frequency $<$21 Hz and $\geq$21 Hz are indicated by circles and triangles, respectively.

shows the source levels over time with different symbols for the different frequency groups. The calls alternate between the two frequencies over the duration of the track, possibly indicating communication. Figure 2.9a also shows a gradual increase in source level over time of approximately 5 dB.

Figure 2.10 shows an example of a complex IPI track with at least three different frequencies. The mean source levels for the frequency groupings shown in Figure 2.10 are 184.1 dB for 15-20 Hz, 186.2 dB for 20-25 Hz, and 175.7 dB for $>$25 Hz. This track shows a large spread in source levels for all three frequency groups.

Figure 2.11 shows the amplitude of several calls, plotted versus time since the last rest, where a rest is defined as a pause in calling that is greater than 60 seconds, and less than 20 minutes [114]. Figure 2.11a shows dives from a 25/30 second dual IPI track, and Figure 2.11b shows dives from a 25 second single IPI track. The lack of systematic trends suggests

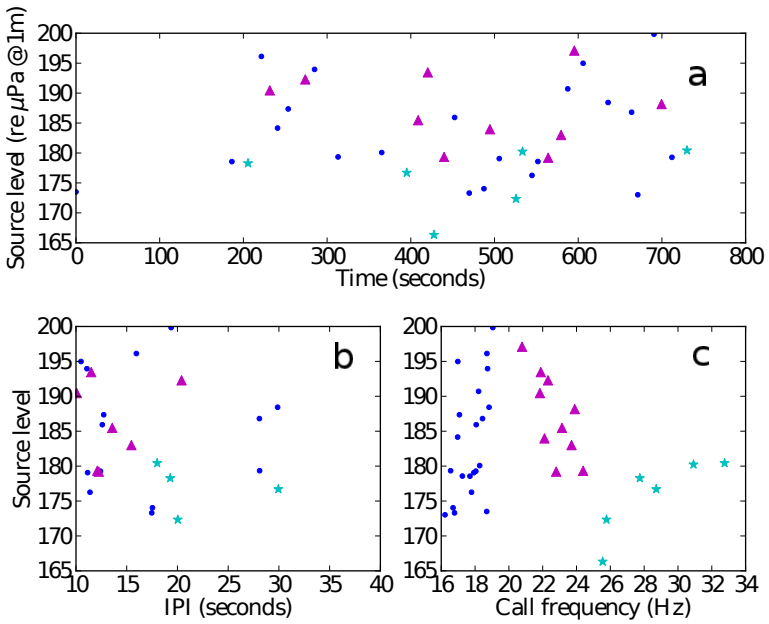

Figure 2.10: Example of a track with three or more whales calling together, plotted with the same conventions as Figure 2.8, except symbols are assigned based on call frequency: calls with center frequency < 20 Hz, between 20-25 Hz, and ≥ 25 Hz are indicated by circles, triangles, and stars, respectively.

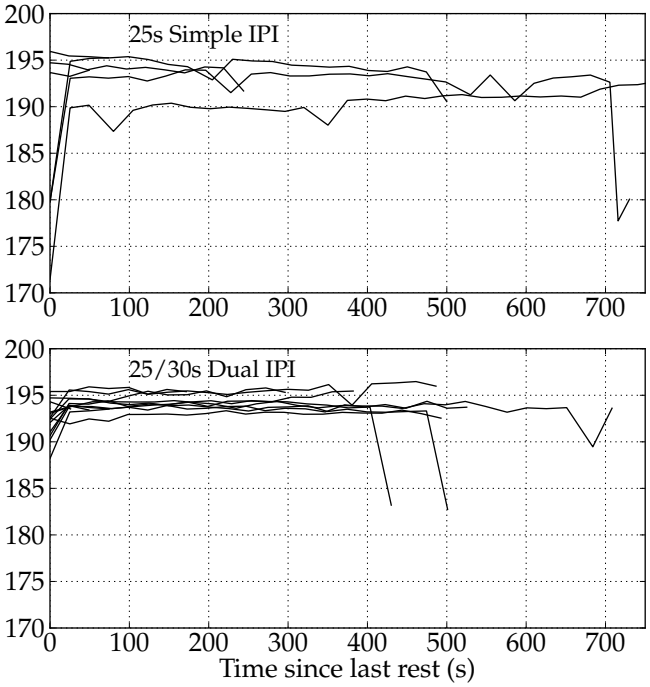

Figure 2.11: Source levels plotted versus time since the end of the last rest for (a) a 25s Simple IPI track, and (b) a 25/30s Dual IPI track.

that source levels do not gradually increase or decrease with time since the last rest.

2.4 Discussion

The average source level of 20 Hz fin whale calls measured in this study is 189 ±5.8 dB re 1μPa @ 1m. This is generally consistent with other studies (Table 2.2), although it is at the higher end of the reported range. Charif et al. [17] report the only other measurements of source levels of fin whale calls in the northeast Pacific, and they are significantly lower than those reported here. This may be due in part to differences in processing method. Charif et al. [17] measure RMS amplitudes of individual calls over a three-second window centered on the call. Since a fin whale call is approximately one second in length, the calculated amplitude will be reduced by a factor of 2/3, or ∼9.5 dB, compared to the one-second measurement

Table 2.2: Previous fin whale call source level measurements. Source levels are in units of dB re 1μPa @ 1m.

	Source Level	n_{meas}	Location
Patterson and Hamilton [79]	180	-	Bermuda
Northrop et al. [73]	164-199	20	Central Pacific
Watkins et al. [115]	180-185	-	North Atlantic
Watkins et al. [114]	160-186	-	Atlantic, Pacific
Charif et al. [17]	171 (159-184)	37	NE Pacific
Sirovic et al. [112]	189 (185-193)	83	Southern Ocean
This experiment	190 (184-196)	1241	NE Pacific

used in this study. Additionally, the amplitude for a given call described by Charif et al. [17] is obtained from the loudest of four hydrophones. The loudest call is assumed to result from nearly complete constructive interference, and is conservatively corrected using a reduction of 6 dB. For the geometry of the experiment, it is possible that the results could be biased by several decibels depending on the depth of the calling whale relative to the hydrophone array. Once these differences in methodology are taken into account, the results are closer to those described here, although average source level is still lower by about 5-10 dB. Source levels of fin whale calls are reported more recently by [112] for the Southern Ocean. Source levels in this study were estimated using bottom-mounted hydrophones, where ranges to fin whale calls were estimated using the spacing between successive multipath arrivals recorded on single instruments. Their average source level of 189±4 dB is similar to the results obtained in this study, despite being measured in a different region.

Uncertainty in the horizontal and vertical position of the fin whale was shown to introduce a large degree of scatter in the results, as shown by the model (Fig.2.6a). However, the model does not describe all of the variability in the data. One explanation is that there is inherent variability in the sound levels produced by the whales. Some whales might vocalize more

loudly than others, or individuals might produce calls at different amplitudes. Figure 2.11 showed very little variation within a single sequence, with the exception of backbeats, and calls immediately following a 30-second gap. However, Figure 2.10 showed $> \pm 4$ dB of variability from one frequency group to the next, and also within calls from a single group. This may be indicative of differences in source level between individuals or it could be a result of different depths of vocalization.

Source level estimates depend on knowledge of the water and seafloor properties. The P wave velocity was shown to have the largest effect on the Zoeppritz correction in the vertical direction (Fig.2.3). Error in the estimate of P wave velocity could reach up to 2 dB at an incidence angle of 20°. In addition to differences in overall scatter, the model results shown in Figure 2.6a have a different distribution of source levels than the measured source levels shown in Figure 2.6b. The measured calls show larger overall spread in the range of source levels, with a larger number of low amplitude calls relative to the mean, which may be a result of low amplitude backbeat calls.

Another source of uncertainty in this type of measurement may arise from sub-bottom arrivals that reach the instrument very close in time to the acoustic arrivals from the water column [83]. If the seafloor in the Axial valley is modeled as a sheeted dike layer (4.5 km/s) overlaid by a 500 m thick extrusive volcanic layer (2.5 km/s), the closest horizontal range at which this effect is likley to be observed is approximately 1.4 km ($\theta_i \sim 33°$). Since the source levels reported in this paper are limited to a maximum incidence angle of 20°, the effect should not be significant.

Fin whales are believed to produce vocalizations for communication, likely during mating and feeding [81, 19]. If the acoustic environment is well understood, and source levels of vocalizing whales are known, then it is possible to estimate the maximum communication range between animals. The maximum communication range is important for understanding the acoustic ecology of a species. The most significant noise sources in the frequency band of the 20 Hz vocalizations are seismic background, turbulent pressure fluctionations, and shipping noise [120]. All of these background noises can potentially mask fin whales' calls,

effectively reducing the maximum communication range. The extent of this masking can only be estimated if the source level of the call is known. Recent studies [37, 56] have described a decrease in blue whale call frequency in different ocean basins over several years which may indicate a response to a changing acoustic environment. It should be noted that acoustic communication between fin whales has developed over an evolutionary history of millions of years and the introduction of anthropogenic noise to their environment has been relatively recent. Studies of maximum communication range need to consider that the development of the acoustic communication method took place mostly in a much quieter environment [81].

Another important use of source levels is for range estimation between a calling whale and a calibrated hydrophone or OBS, provided a reliable transmission loss model is available [63]. This assumes that maximum source levels are consistent within a series of calls, or at least that the statistical distribution of the received levels can be accurately characterized [56]. Range can also be estimated using the spacing of multipath arrivals [56, 112] or by analyzing the received signal in terms of normal mode propagation models for calls produced in shallow water waveguides [122]. Both of these methods may be constrained by source levels and by the variability of source levels of calls produced by fin whales. Once range is known, it can be used in estimating the abundance or density of fin whales within a specified area. This has important management implications for the study and conservation of pelagic, endangered whales by providing a new tool for population assessments.

Chapter 3

ESTIMATING RANGE TO A VOCALIZING FIN WHALE USING THE TIMING AND AMPLITUDE OF MULTIPATH ARRIVALS

3.1 Introduction

Fin whales are currently listed as an endangered species throughout their range. Despite the moratorium on commercial whaling imposed in the 1980s, they are still at risk from human activities in the ocean [51, 76, 126]. To quantify the recovery of populations and understand their use of habitat, it is critical to understand their distributions, however, this metric remains poorly constrained throughout most of their range, including in the northeast Pacific Ocean [64, 65, 97]. Traditional visual surveys can be challenging due to fin whales' speed and pelagic habitat. Additionally, visual surveys are restricted by light and weather conditions, making surveys difficult at night and during the winter months. Tagging surveys allow for tracking of individual animals over large geographic ranges [67, 115, 117], but tag deployment is difficult and often expensive, which restricts the number of animals that can be tagged in a given experiment.

Since fin whales produce repetitive, low frequency vocalizations, passive acoustic monitoring can provide a valuable complement to tagging and visual surveys. Fixed acoustic monitoring instruments, usually hydrophones, can be deployed for long periods of time, and are not affected by adverse weather conditions or light availability. The most commonly observed fin whale calls are 1-second chirps, sweeping from ∼25-15 Hz (Figure 3.1(a-b)) and these calls typically have an inter-pulse interval between 6 and 46 seconds [15, 49, 75, 35, 93, 114]. An individual whale can call for many hours at a time, with short pauses occurring fairly regularly while they are breathing at the surface and longer irregularly spaced gaps.

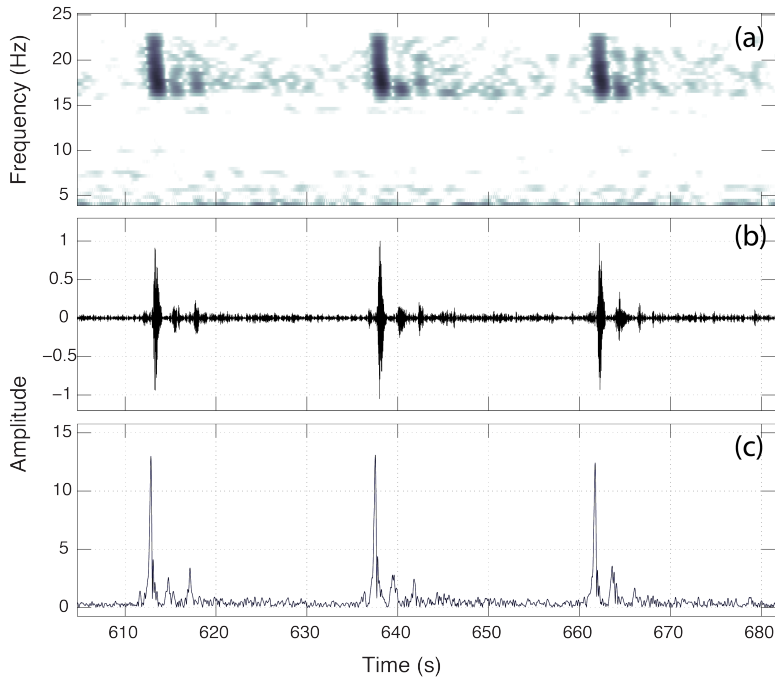

Figure 3.1: Example of three fin whale calls recorded at the Endeavour site shown as (a) a spectrogram, (b) a time series after applying a 15-25 Hz bandpass filter and (c) the output of the matched filter cross-correlation used for call detection.

Ocean bottom seismometers (OBSs) provide an additional opportunistic source of passive acoustic recordings. These instruments are designed to detect ground motions resulting from earthquakes or active source seismic experiments, but are also sensitive to ground motions induced by the low frequency fin whale calls. Closely-spaced networks of OBSs have been used to localize fin whale calls to obtain a better understanding of distributions and swimming patterns [57, 35, 93].

However, for some experiments, the OBSs are too widely spaced to track whales. For example, the Cascadia Initiative experiment [109] deployed 70 OBSs from 2011-2015 on the Juan de Fuca and Gorda tectonic plates off the West coast of the United States and Canada. These instruments cover a significant portion of the potential migratory range of fin whales [64], and thus provide an opportunity to correlate the spatial and temporal distribution of whales with regional scale oceanographic and environmental variables. To do this requires a quantitative comparison of the number of whales observed at different locations across the region. However, the OBSs in this experiment are spaced up to 70 km apart, which precludes conventional tracking because a given fin whale call will typically only be detected on one instrument. Because there are large differences in the acoustic environment between instrument locations, it is very unlikely that call detectability is uniform between instruments. This invalidates direct comparisons of call counts and motivates methods to estimate call density as the metric for comparison.

Call density can be obtained using various methods. Küsel et al. [50] describe a single hydrophone method that uses the total received energy from beaked whales in specific frequency bands to estimate population density for a given time period. This method is also being developed for use with energy bands from fin whale calls in OBS data [62]. Another method, point transect distance sampling, uses the distance between the sensor and the vocalizing animal to model the probability of detection as a function of range [10, 53]. Point transect distance sampling techniques were originally developed for terrestrial applications, but have since been adopted for use in the marine environment [10]. The primary requirement for point transect distance sampling is that the range to the detection may be

obtained. One way to obtain range to a vocalizing fin whale is to use the relative particle motions measured on three orthogonal components of an ocean bottom seismometer to estimate the orientation (azimuth and incidence angle) of incoming acoustic energy from a fin whale call [43, 54]. The incoming call orientation can be combined with depth to estimate horizontal range.

Another method of obtaining range from a single instrument uses the timing and relative amplitudes of multipath arrivals to estimate range to a sound source using single-instrument recordings. Multipath arrivals measured on hydrophones have been used to estimate range to vocalizing cetaceans [3, 55, 108]. In particular, McDonald and Fox (1999) demonstrate the use of multipath timing and amplitude to manually estimate range to fin whales using data recorded on a single hydrophone located north of Oahu, Hawaii and use the resulting ranges to estimate call density. This paper builds upon previous work by exploring the use of a semi-automated multipath ranging technique that can be implemented on large datasets. The work is motivated by the availability of the Cascadia Initiative OBS dataset, and our initial testing is conducted at two contrasting locations in the northeast Pacific which demonstrate the technique and illustrate the challenges encountered in different acoustic settings.

3.2 Multipath Ranging

3.2.1 Datasets

The dataset comprises records from two OBSs. Only data from the vertical channel is used because horizontal channels are often not well-coupled to the seafloor (e.g., Trehu [110]). The first OBS is from the Endeavour Segment of the Juan de Fuca mid-ocean ridge (48.5°N, 129.0°W), where eight ocean bottom seismometers (OBSs) were deployed from 2003-2006 (Fig. 3.2). Bathymetry at the Endeavour Segment is complex and rough with depths varying from 2100-2800 m. The ridge is characterized by exposed basalt. On nearby flanks a thin layer of a few meters of pelagic sediment cover fills bathymetric lows. A thick (<100 m) turbidite layer extends from the continental margin to within ∼20 km of the ridge axis

(Davis et al., 1997), but is largely outside the area considered in this study. The OBSs were located at an average water depth of 2200 m and the network extended 10 km along the direction of the mid-ocean ridge axis, and ∼6 km across. For the first year of deployment (2003-2004), 154 fin whale tracks were obtained [93], which allows the single-sensor method to be tested against independently estimated ranges. The instrument used for testing is KEBB, a broadband seismometer located on the west side of the array at a depth of 2377 m (Figure 3.2(b)). The instrument sampled at 50 Hz and had a flat frequency response up to ∼22.5 Hz [103]. A total of 37 days of recording were used in this analysis, between 24 November 2003 and 6 April 2004. This subset was manually selected to include the longest sequences of calls to assess the performance of the ranging algorithm, but the entire 139 days of the dataset are later used to make preliminary estimates of density.

The second seismometer is part of Ocean Networks Canada's Neptune Observatory. It is located 124 km southeast of the Keck instrument, at the Cascadia Basin site (47.76°N, 127.76°W, Fig. 3.2(a)) at a water depth of 2660 m. This site is approximately midway between the Endeavour Segment to the west and the continental slope to the east. It sits on a thick layer of sediment (300-600 m), which overlies a basalt basement [33]. Bathymetry at this location is much flatter than at the Endeavour segment, exhibiting bathymetric characteristics typical of abyssal plain environments. The only notable bathymetric features nearby are two isolated outcropping seamounts located 6-10 km to the northeast. The OBS sampled at 100 Hz and had a flat frequency response up to ∼40 Hz. A total of 28 days of recordings were used in this analysis, between 15 October 2011 and 27 February 2012. These were also manually selected for assessment of the ranging algorithm. The entire 150 days of the dataset are later used to estimate call density.

3.2.2 Multipath ranging technique

The technique described here uses the timing and amplitude of multipath arrivals to estimate range. The underlying geometry used in developing the amplitude and timing models is shown in Figure 3.3. We assume that the direct path arrival travels through the water

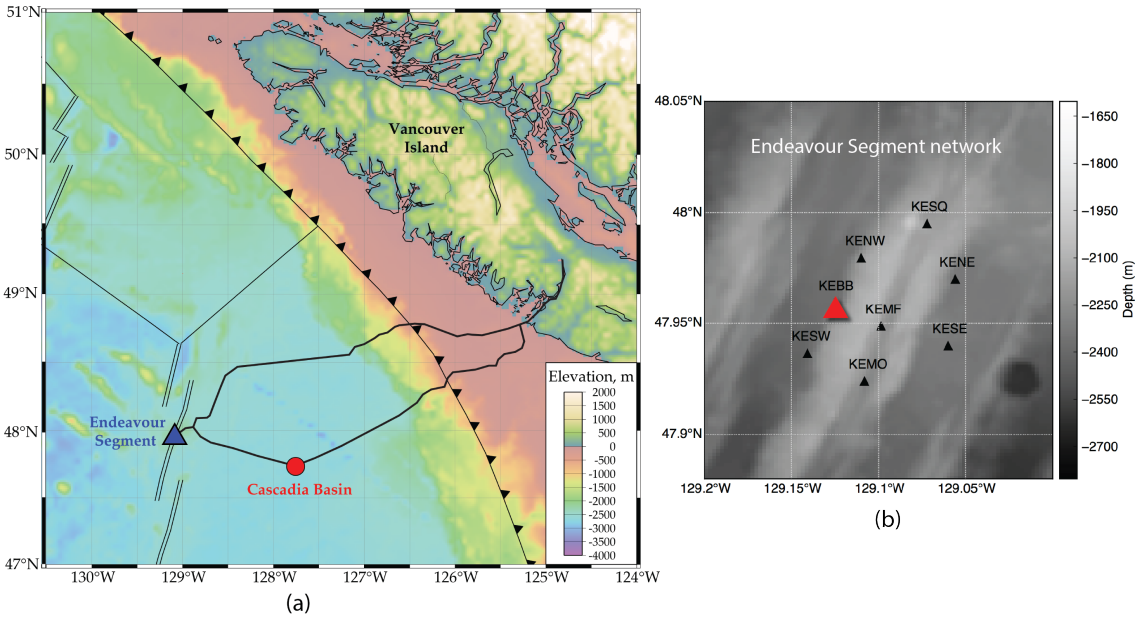

Figure 3.2: Map showing locations of the Endeavour Segment (blue triangle) and Cascadia Basin (red triangle) ocean bottom seismometers (OBSs) used in testing the multipath ranging technique in the northeast Pacific Ocean. The bold black line connecting Vancouver Island to the OBSs indicates the Ocean Networks Canada cable route and thin black lines indicate tectonic plate boundaries, with the double line representing a mid-ocean spreading ridge. The inset figure shows the configuration of the eight OBS network used previously to track whales at the Endeavour [93], with the instrument used in this study (KEBB) labeled.

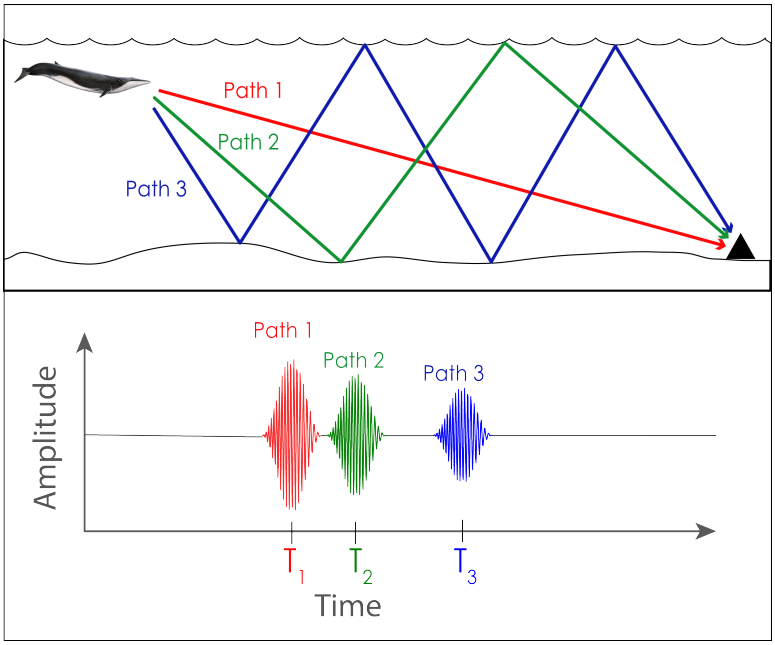

Figure 3.3: Cartoon illustrating the geometry ray paths and timing of arrivals for the direct path and first two multipaths. Both the timing and amplitude of the multipath arrivals are potentially diagnostic of range to the vocalizing whale.

without interacting with any boundaries. Multipaths interact with the seafloor and sea surface a number of times before reaching the receiver. The method consists of four parts: (i) modeling the received multipath structure at specified range increments, (ii) automatic detection of fin whale calls, (iii) automatic detection of multipath arrivals, and (iv) combining the modeling and detections to estimate horizontal range to a vocalizing fin whale. The optimal value of various parameters used in the method [Table 3.1] are set based on the analysis of eight days of data at each location, comprising 8141 and 16,675 calls at the Endeavour and Cascadia Basin sites, respectively.

Modeling amplitude and arrival times

Multipath times and amplitudes are modeled at 200-meter range increments between 0 km and 25 km (Fig. 3.4). For simplicity, seafloor depth is modeled as range and azimuth

Table 3.1: Summary of parameters used in the multipath detection and ranging method that were optimized based on the analysis of test data sets at the two sites.

Detection/Ranging parameter	Value
(a) SNR detection threshold	7 dB
(b) minimum time between calls	10 s
(c) stacking correlation coefficient threshold	0.8
(d) multipath amplitude threshold	5% of largest peak; 3x median standard deviation in segment
(e) multipath picking time allowance	0.2 s
(f) SNR threshold for using 2 peaks	20 dB
(g) complex arrival threshold	30% of largest peak
(h) width of Gaussian peaks in model	0.4 s
(i) hypothesis minimum correlation value	0.25
(j) hypothesis close correlation time	0.1
(k) combined residual weighting factor	1
(l) nearby call maximum range	1 km
(m) nearby call maximum time difference	6 minutes

independent, and assigned the depth of the instrument being tested. Fin whales vocalize at approximately 20-50 m depth [104, 114] with surface bounce interference resulting in amplitude fluctuations [119], although for simplicity, we assume that the whale vocalizes at the surface. The depth-varying sound speed profile is obtained using an average conductivity-temperature-depth profile from this location from the 2009 World Ocean Atlas [2, 52] using the formulation of del Grosso [23]. Based on prior work [93, 123], we expect to observe a maximum of five distinct multipath arrivals, so the model is constructed using the first five modeled arrivals.

Relative arrival times of multipaths are estimated using BELLHOP ray tracing software

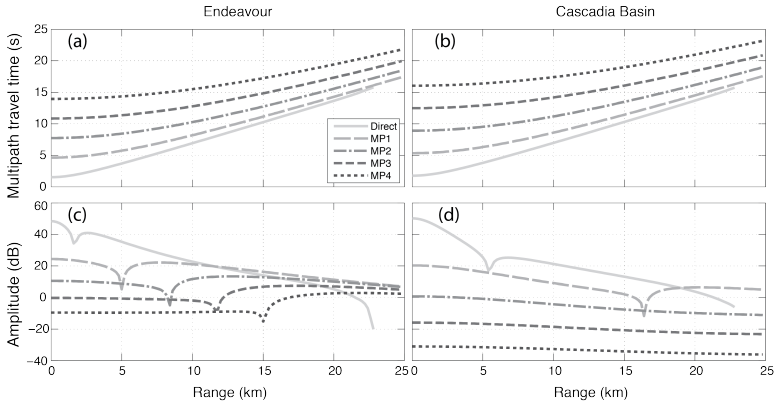

Figure 3.4: Modeled multipath timing and amplitude for the vertical channel of the OBSs. (a-b) Travel times as a function of range from 0-25 km for the direct path and first four multipaths at (a) the Endeavour and (b) Cascadia Basin OBS sites. (c-d) Relative amplitudes predicted from ray divergence and the application of the Zoeppritz equations at (c) the Endeavour and (d) Cascadia Basin OBS sites.

[82], and are plotted as a function of range in Fig. 3.4(a-b) for both instrument locations. When the whale is vocalizing directly over the instrument, the delay between successive multipath arrivals is equal to the two-way travel time, the time it takes for the sound to travel vertically from the sea surface to the seafloor and back again. As the range increases, successive multipath arrivals are closer together.

Relative amplitudes are obtained using BELLHOP-derived ray paths to estimate energy losses using ray divergence. Reflection coefficients at the seafloor interface were modeled using the boundary conditions at a fluid-solid interface, as described by the Zoeppritz equations [45], which are dependent on the characteristics of both the fluid and solid media as well as the incidence angle of the incoming acoustic signal. We do not include absorption in our calculations of amplitude loss since this is expected to be a small effect at 20 Hz [48].

At the Endeavour OBS location, the sediment layer is much thinner than the wavelength of a fin whale call, so properties of the underlying basalt layer were used in the amplitude model. P wave velocities of mid-ocean ridge basalts are estimated to be 2500 m/s, based on surface refraction and reflection data from this ridge segment [20, 113]. S wave velocities

are estimated to be 500 m/s based on measurements on young crust at the East Pacific Rise [18], similar to that at the Juan de Fuca ridge. A density of 2200 kg/m^3 is used [40]. At the Cascadia Basin location, the instrument sits on a 300-600 m thick layer of sediment, which overlies a basalt basement. The P wave velocity of the sediment layer is estimated to be 1625 km/s, the S wave velocity 200 m/s, and the density 1500 kg/m^3 [87].

When acoustic energy from the water column interacts with the seafloor, most of the energy is either reflected back into the water column or transmitted into the seafloor. The energy that is transmitted into the seafloor propagates in two modes, pressure waves and shear waves, the sum of which are measured by the seismometer. The particle motions sensed by the OBS are dependent on the incidence angle of the incoming acoustic wave. The predicted multipath amplitudes for the vertical channel of the ocean bottom seismometer are shown Fig. 3.4(c-d), where abrupt drops in amplitude coincide with ranges where the incidence angle is equal to the critical angle for total reflection.

Automatic detection of calls

Two methods of automatic detection are assessed: matched filtering and spectrogram correlation [60]. The template call used for both methods is a downswept chirp, varying linearly over a duration of one second from 25 Hz to 15 Hz. The amplitude is modulated using a Hann window to approximate the amplitude variation observed in fin whale calls. Prior to cross correlating, both the template call and received time series are quadrature demodulated using a 3rd order Butterworth filter with a bandwidth of 10 Hz (15-25 Hz). Figure 3.1(c) shows an example of the cross correlator output for the matched filter with peaks corresponding to the onset times of three calls.

A quantitative comparison with a supervised detection algorithm shows that the matched filtering technique is slightly more reliable in counting fin whale calls in this dataset, and is used for all subsequent detections. Table 3.2 summarizes the results of the comparison between the two methods with a baseline dataset in both high and low signal to noise ratio (SNR) environments, where signal level is defined as the value of the cross-correlator

output at the detection and noise level is computed as the 90th percentile value of the cross correlator output within 20-minute increments. This high SNR case contains calls where SNR was mostly greater than 10 dB, while the low SNR case contains calls where SNR is mostly in the range 5-10 dB. In the case of high SNR, the two methods are comparable: 97% of calls are correctly detected with the matched filter, and 94% with the spectrogram correlation method. In the case of low SNR, the matched filter correctly detects 72% of calls, while the spectrogram correlation method only correctly detects 59%. The number of false alarms is similar between the two methods in both SNR cases.

Table 3.2: Results of comparison between matched filter and spectrogram correlation automatic detectors for both high and low signal to noise ratio cases.

		High SNR			Low SNR	
	Baseline[a]	M. Filt[b]	Spec.Corr.[c]	Baseline	M. Filt	Spec.Corr
Total picks	2585	2608	2582	253	223	189
Match		2499(97%)	2436(94%)		181(72%)	149(59%)
Missed		86(3%)	149(6%)		72(28%)	104(41%)
False Alarms		109(4%)	146(6%)		42(17%)	40(16%)

[a] manually detected calls

[b] number of calls detected using matched filter detector

[c] number of calls detected using spectrogram correlation detector

For multipath ranging, the SNR detection threshold is set to 7 dB (Table 3.1(a)). Most sequences of fin whale calls observed in our datasets have inter-pulse intervals (IPIs) between 13 s and 30 s, and multipath sequences are typically up to 10 s long. To avoid triggering the detector several times on multipath arrivals from the same call, we force adjacent detections to be at least 10 s apart (Table 3.1(b)).

Local earthquakes are common sources of false positives, particularly in the Endeavour

dataset. Earthquakes are attenuated impulsive signals, with local earthquakes generally dominated by energy below 5-15 Hz, but they contain some energy at higher frequencies. To ensure that that earthquakes are not accidentally flagged as fin whale calls, the energy in the range 15-25 Hz (typical fin whale call frequencies) must be equal to or greater than the energy in the range 5-15 Hz.

Low amplitude multipaths are boosted by summing the correlator output of nearby calls. This is done by cross-correlating the matched filter output of each call segment with other segments within 3 minutes. Alignment is determined using the delay corresponding to the maximum value of the cross correlation. If the correlation coefficient exceeds a threshold of 0.8, the aligned call is included in the sum (Table 3.1(c)). This also has the approximate effect of imposing a 6-minute smoothing filter on range sequences.

Identification of multipath arrivals

The automatic detection of multipath arrivals uses the cross correlator output in the vicinity of each call, since multipath arrivals appear as peaks (Fig. 3.1(c)). Potential multipaths are initially narrowed down using a two-step threshold test: (1) peaks must exceed 5% of the amplitude of the largest amplitude peak, and (2) peaks must be greater than three times the median absolute deviation above the median correlator output in a 20-minute window surrounding the call (Table 3.1(d)). These threshold values are selected based on visual examination of the test datasets and are chosen to maximize the number of true multipaths selected while avoiding peaks that result from noise.

Peaks that pass the threshold tests are further filtered to ensure that only the largest peaks separated by at least one second are kept. This is done to avoid picking more than one peak on a single noisy arrival. Assuming a sound speed of 1500 m/s, and a water depth of 2300 m, the spacing between the direct path and first multipath arrival reduces to one second by a range of $\sim$10 km, but by then the direct path is not observed [123]. The first and second multipaths arrive within one second of each other at approximately 21 km, which lies beyond the maximum distance at which our method works. So this filter should not reject

any true arrivals within our range of interest.

The final set of peaks are selected using constraints based on patterns in predicted multipath times. In particular, moving from one multipath arrival to the next, successive delay times must increase monotonically (Fig. 3.4). The first step is to select the largest arrival. Looking later in time, the second arrival must occur with a maximum time delay equivalent to the vertical two-way travel time, subject to a variability of 0.2 seconds (Table 3.1(e)). If there are no peaks within that interval, the call is not used for multipath ranging. If a second arrival is found, then the search continues for a third arrival, this time constraining the delay to be less than that between the first (largest) and the second to ensure that the time delays are monotonically decreasing, again, subject to a variability of 0.2 seconds. This continues until a maximum of four peaks beyond the largest is found. Then, moving earlier in time from the largest arrival, similar logic is employed with up to two earlier arrivals being stored. When only two peaks are detected, it is often at shorter ranges, where more energy is lost at each bottom bounce due to the low incidence angle. It also occurs at larger ranges where the earlier arrivals are no longer detectable. For the short-range case, amplitude is much larger, so we use it as a discriminator. If the SNR of the largest arrival is greater than 20 dB, we assume those two peaks are the direct path and first multipath, and determine the range using the time difference between them. If only two peaks are detected and the SNR is less than 20 dB, that detection is rejected (Table 3.1(f)).

In some cases, call sequences are more complicated, with multiple whales vocalizing simultaneously [55, 93]. When this happens, overlapping calls can corrupt the multipath ranging process. In order to flag occurrences of potentially overlapping call sequences, the amplitude of the largest arrival is compared with any peaks that fall outside the set of detected arrivals but within a window of 10 seconds of the largest arrival. If any of the extraneous peaks is larger than 30% of the amplitude of the largest arrival, that call is not used for multipath ranging (Table 3.1(g)). This also discards calls that have unidentified noise spikes in the vicinity of the multipath arrivals, since those might corrupt the multipath ranging solution.

Range estimation

Wilcock [123] reported that at the Endeavour Segment location, direct path arrivals were not detectable beyond ∼8-10 km. The implication is that for a given set of detected multipaths, we do not have a priori knowledge of which arrival corresponds to which path. This leads to the fundamental challenge in implementing the multipath ranging method: resolving the ambiguities that arise from not having the ability to identify specific multipaths in advance. We address this by testing three possible hypotheses for labeling arrivals (Fig. 3.5). The basis for these hypotheses is that the largest amplitude arrival could be the direct path arrival (hypothesis 1), the first multipath (hypothesis 2), or the second multipath (hypothesis 3). Each set of detected multipaths is labeled three times, once for each of the hypotheses. For each hypothesis, we find the horizontal range, x, that optimizes the fit to the travel times by minimizing the normalized timing residual, t_{res}(x) given by

$$t_{res}(x) = \left(\sum_{i=1}^{n} \frac{(O_i - C_i)^2}{\sigma_i n} \right)^{1/2}, \tag{3.1}$$

where i is the index of the arrival, n is the number of arrivals, O_i are the observed travel times, σ_i are estimates of the timing uncertainty, and C_i represents the modeled travel times assuming a call origin time, T_o, given by

$$T_o = \frac{\sum_{i=1}^{n} \frac{T_i - C_i}{\sigma_i^2}}{\sum_{i=1}^{n} \frac{1}{\sigma_i^2}}, \tag{3.2}$$

where T_i are the measured arrival times. In Equations 3.1-3.2, the estimate of the timing uncertainty is selected to weight the earliest arrivals more heavily than later arrivals. At the Endeavour location, where the basaltic seafloor is highly reflective, at least three strong arrivals are typically detected and sometimes up to five are observed. Based on inspection of the data the first three arrivals are assigned an uncertainty of 0.025 s with those of subsequent arrivals set four times larger. At Cascadia basin, where the sedimented seafloor

is less reflective, there are often only 2-3 observed arrivals. Here, the first two arrivals are also assigned an uncertainty of 0.025 s, with those of subsequent arrivals four times larger.

For each of the three hypotheses, a model multipath time series corresponding to the range that minimizes the timing residual is constructed and compared with the correlator output for that call. The model time series is created by first generating impulse responses corresponding to modeled times and amplitudes. The series of impulse responses is then convolved with a Gaussian function to generate a simulated multipath structure. The final multipath model is calculated as a function of time t by summing Gaussian functions centered at the modeled multipath arrival times according to

$$\hat{\Gamma}(t) = \sum_{k=1}^{5} \alpha_k e^{-\frac{1}{2}\left[\frac{(t_k - t)}{\phi}\right]^2}, \tag{3.3}$$

where the multipath arrival index k runs from 1 to 5, for the direct path and four multipaths, and α_k is the modeled multipath amplitude. The parameter ϕ controls the width of the Gaussian and is set equal to 0.4 s based on the observed width of fin whale calls in the correlator output (Table 3.1(h)).

The correlation coefficient $\bar{\phi}_{xy}$ between the model $\hat{\Gamma}(t)$ and the cross-correlator output for that call is computed as

$$\bar{\phi}_{xy} = \frac{max(\phi_{xy}(t)}{\sqrt{\phi_{xx}(0))\phi_{yy}(0)}}, \tag{3.4}$$

where $\bar{\phi}_{xy}$ varies between -1 and 1. The quantities $\phi_{xx}(0)$ and $\phi_{yy}(0)$ are the zero-lag autocorrelations of the two input time series and $\phi_{xy}(t)$ is the correlation value between the model $\hat{\Gamma}(t)$ and the cross-correlator output.

The observed direct path amplitude is consistently lower than predicted using the ray divergence amplitude model, and subsequent arrivals also tend to decrease in amplitude with increasing range more rapidly than predicted. This is addressed in a rudimentary way by checking whether all of the predicted arrivals prior to the largest are represented by a

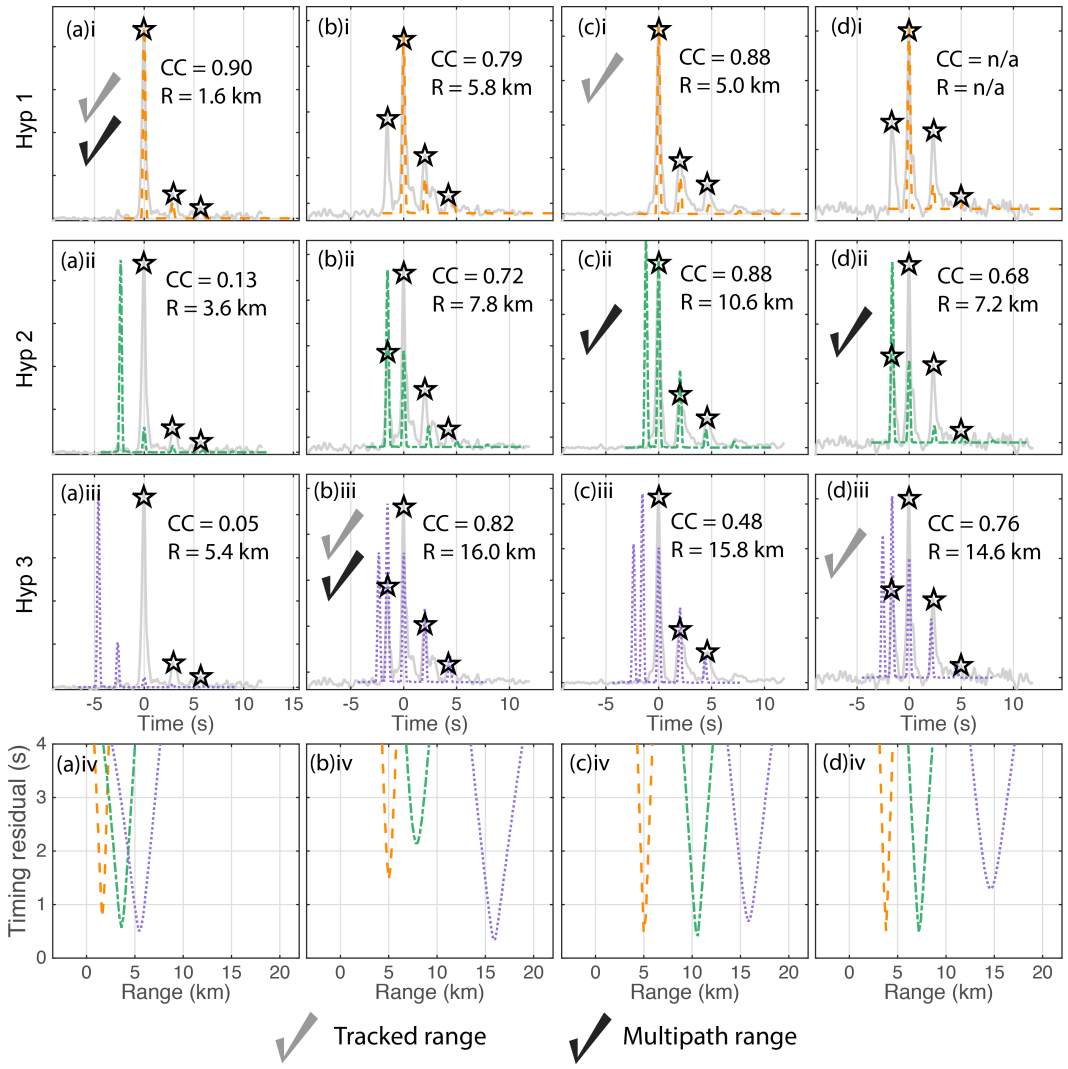

Figure 3.5: Four examples showing multipath ranging solutions. In each example, the upper three panels (i-iii) show the cross correlator output (gray solid line) overlaid by the model that minimizes the travel time residual (interrupted lines) for the three hypotheses, with amplitude normalized to 1 in all cases. The lower panel (iv) shows the travel time residual as a function of range for the three hypotheses (hypothesis 1 - orange dashed line; hypothesis 2 - green dot-dashed line; hypothesis 3 - dotted line). (a) An example where hypothesis 1 is correctly selected. (b) An example where hypothesis 2 is correctly selected. (c) An example where hypothesis 2 is selected but hypothesis 1 is correct. (d) An example where hypotheses 2 is selected by hypothesis 3 is correct.

detection in the data. If not, the corresponding model peak is not used in the correlation calculation. Additionally, if there is an arrival detected prior to the largest peak, hypothesis 1 is immediately rejected because hypothesis 1 assumes that the largest peak is the direct path.

If the correlation coefficient between the model and correlator output time series for a particular hypothesis is less than 0.25 (Table 3.1(i)), that hypothesis is immediately rejected. If the highest correlation coefficient is at least 0.1 greater than all other remaining hypotheses, it is selected as the preferred hypothesis. If the difference between the two largest remaining correlation coefficients is < 0.1 (Table 3.1(j)), further steps are taken to determine which of the range hypotheses will be selected. Both the travel time residual and amplitude can potentially help discriminate between hypotheses. Since the divergence amplitude models do not fit the observations well, the travel time residual [from Equation 3.1] is used as the tiebreaker when using these models. When an empirical amplitude model can be extracted from the data, we also use a combination of the travel time residual and the amplitude residual for the largest arrival. The combined residual tiebreaker method uses multipath amplitudes and standard deviations extracted directly from the data, and the normalized amplitude residual, γ_{res}, is calculated for each hypothesis as

$$\gamma_{res,j} = \frac{|a_m - a_{pred}(r_j)|}{\sigma}, \tag{3.5}$$

where j is the index of the hypothesis, a_m is the measured amplitude of the largest arrival, $a_{pred}(r_j)$ is the predicted amplitude corresponding to the largest measured arrival at the predicted range r_j, $\sigma_{pred}(r_j)$ is the standard deviation of the empirically derived amplitude with a_m, a_{pred}, and σ_{pred} in linear units. The combined residual for the j-th hypothesis, $C_{res,j}$, is then given by

$$C_{res,j} = \gamma_{res,j}^2 + wt_{res,j}^2, \tag{3.6}$$

where w is a weighting factor that assigns relative importance to the two residual values. It was set to 1 since there we find no evidence that either the amplitude or timing residuals are more reliable in predicting the correct range (Table 3.1(k)).

In the final step of processing, a simple sequence filter is applied to take advantage of the repetitive nature of fin whale vocalizations is used to either accept or reject ranges. We only keep calls if there are at least six other multipath-ranged calls are present within 1 km (Table 3.1(l)) and 6 minutes (Table 3.1(m)). The sequence filter is a rudimentary method of filtering out ranges when they are not consistent with a significant number of other solutions.

3.3 Results

3.3.1 Endeavour

A total of 64,385 calls were detected in the Endeavour dataset. Of those detections, 9705 (15%) were flagged as being part of overlapping call sequences and 5156 (8%) were flagged because they only had two detected arrivals but with SNR less than 20 dB. The number of calls flagged by the sequence filter because their ranges were inconsistent with others varied from 9433 to 10,670 (15-17%) for the different amplitude models. The remaining 38,459-40,091 calls were used to assess the method and, of those, 19,812-20,858 had corresponding calls in the tracked dataset that could be used to evaluate multipath range solutions.

Figure 5 shows four examples of multipath ranging solutions for the Endeavour location. The first example (Fig. 5(a)) shows a call where the multipath ranging algorithm selects the correct hypothesis. In this case, hypothesis 1 is selected because it has the largest correlation coefficient, and that correlation coefficient is at least 0.1 units greater than the next largest. The final range estimate for this call is 1.6 km. Figure 5(b) shows an example where hypothesis 3 is correctly selected. In this case, all three hypotheses have correlation coefficients within 0.1 units of each other. The minimum travel time residual is used as a tiebreaker, with hypothesis 3 having the lowest travel time residual of all three. In Fig. 5(c), correlation coefficients for hypothesis 1 and hypothesis 2 are very close. Hypothesis 2 is

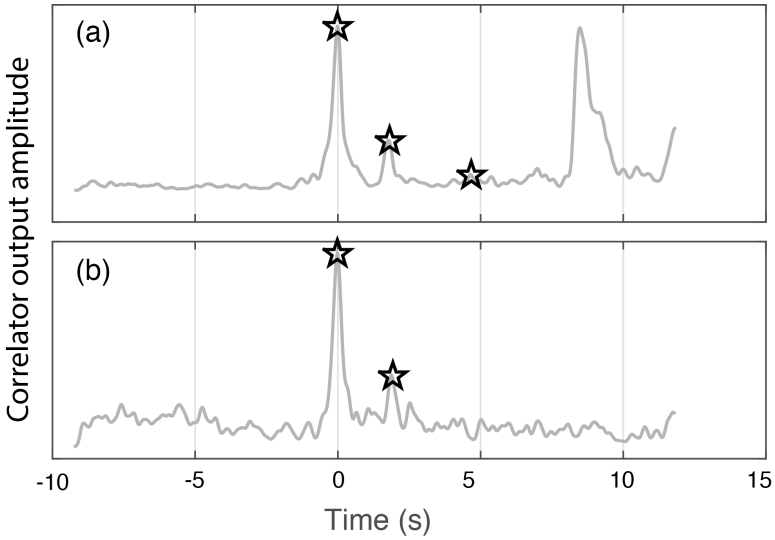

Figure 3.6: Two examples of the cross-correlator output for calls that are rejected prior to multipath ranging. Amplitudes are normalized to 1 in both cases. (a) A call that is part of an overlapping sequence with a high-amplitude arrival that part of another call within 10 s. (b) The lower panel (b) shows a call that is rejected because there are only two detected peaks and the highest peak has a signal to noise ratio below 20 dB.

selected since it has a slightly smaller travel time residual, but hypothesis 1 corresponds to the correct range. Figure 5(d) shows an example where hypothesis 1 is immediately rejected because there is a detection prior to the largest. Since the remaining two hypotheses are within 0.1 of each other, the travel time is used as a tiebreaker. Hypothesis 2 is selected because it has a lower travel time residual, although hypothesis 3 corresponds to the correct range.

Figure 3.6 shows examples of calls that were immediately rejected and therefore not used in ranging solutions. In Fig. 6(a), the call is rejected because there is another nearby peak, indicating that this is likely part of an overlapping or noisy sequence. In Fig. 6(b), the call is rejected because only two peaks are found by the automatic detector, but the signal to noise ratio is less than 20 dB.

Two examples of ranged call sequences for the Endeavour OBS are shown in Figure 3.7, along with ranges derived independently from tracking [93]. These two sequences include

all the example solutions shown in Fig. 3.5. The sequence in the upper panel (Fig. 3.7(a)) has long stretches of time where there is a clear path and ranges of < 10 km, and where the range varies gradually and is a reasonable pattern for a whale swimming near an instrument. However, there are still examples of clearly incorrect ranges. For example, at approximately 05:00 and again at 08:00, several ranges are placed $\sim$5 km beyond the track. Between $\sim$13:00-15:00, the sequence becomes less clear, with ranges jumping back and forth, though it is worth noting that there are no tracked ranges. The bottom panel (Fig. 3.7(b)) shows an example of a track at a larger range where the incorrect hypothesis is selected for many of the calls. Nearly all of the errors in range were a result of ambiguities arising from selecting the incorrect hypothesis (hypothesis 2 instead of 3).

The direct path amplitude was consistently lower than predicted by the divergence model of amplitude and was rarely observed at all beyond approximately 8-10 km (e.g., Fig. 3.5(b,d)). Because of this discrepancy, the divergence model was not used when implementing the combined residual tiebreaker method, since the absolute amplitudes were unreliable. Since there were independently located calls at the Endeavour location, it was possible to extract the amplitudes of multipath arrivals directly to build an empirical amplitude model for comparison. Amplitudes were extracted on a call-by-call basis and binned in 2 km increments up to 24 km. Figure 3.8(a) shows the mean and standard deviations of the resulting amplitude model, and Fig. 3.8(b) shows the mean and standard deviations of the first three amplitude ratios in each range bin. On average, the direct path is the largest amplitude arrival up to $\sim$5 km, the first multipath is the largest amplitude arrival from $\sim$5-11 km, and the second multipath is the largest amplitude arrival from $\sim$11-17 km. However, the amplitudes show a large amount of variation for a given arrival and range and they overlap substantially between arrivals at all but the shortest range. One might infer that the amplitudes do not provide a strong additional constraint on range although the empirical model has the advantage that the direct path amplitude is more accurate; the divergence model consistently predicted a higher direct path amplitude than was observed in the data which impacts the values of the normalized correlation coefficient computed with

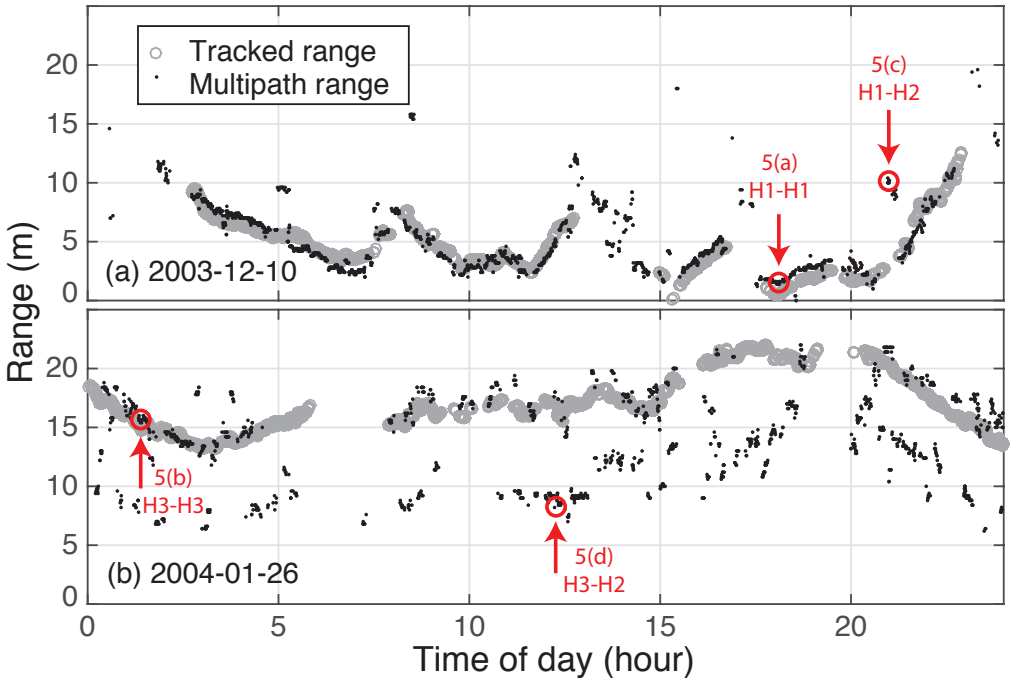

Figure 3.7: Range sequences plotted as a function of time of day at the Endeavour site for two example days, (a) December 10, 2003 and (b) January 26, 2004. The ranges estimated using the multipath ranging method with the ray divergence amplitude model are indicated by black dots, and the tracked ranges are indicated by grey circles. Panel (a) shows long tracked segments at <10 km range with only a few instances where incorrect hypotheses are selected while panel (b) shows long tracked segments at >10 km range where many calls are assigned incorrect ranges. Red circles and labels correspond to the 4 examples shown in Figure 5 with label listing the correct hypothesis followed by the selected hypothesis.

Equation 3.4.

Range distributions from the Endeavour instrument are shown in Fig. 3.9. The distribution of all tracked ranges (Fig. 3.9(a)) is complex and reflects the non-uniform spatial distribution of tracked [93]. Figure 3.9(b) shows the distribution of ranges to independently located calls that have a corresponding multipath range. The most notable difference is that the more distant calls were less likely to be selected for multipath ranging. This is because distant calls often have a signal to noise ratio below the 7dB threshold. The darker histogram bars in Fig. 3.9(c) show the distribution of multipath ranges for calls that were tracked, obtained using the ray divergence model of amplitude. It is similar to the tracked ranges up to 4-5 km, then shows a drop in call counts at $\sim$5.5 km and a second peak at 7-8 km. These features are also present in the tracked ranges though are less prominent. The two versions of the empirical model ranging solution (travel time residual and combined residual tiebreaker methods) are shown in Fig. 3.9(d-e). They are both similar to the divergence model solution up to $\sim$10 km, particularly below 5 km. The drop in calls around 5.5 km is less prominent in the combined residual model histogram.

Figure 3.10 shows the distribution of ranges obtained for the different amplitude models and hypothesis selection techniques for calls with tracked ranges. This figure gives an overview of the nature of the multipath ranging errors. In all cases, up to 4 km, the ranges are generally assigned the correct hypothesis and range errors are small. For ranges of tracked 4-8 km, a significant number of the multipath ranges are too large (10-16 km), but there is a clear decrease in the number of erroneous solutions when empirical amplitudes are used, particularly with the combined residual tiebreaker. From 8-16 km, all three range solutions are generally unreliable, and show a large scatter and comparable results.

Most range errors occur as a result of choosing the incorrect multipath hypothesis. Figure 3.11 illustrates how the estimated ranges change for the first two hypotheses if three arrival times are available. When the whale is directly over the instrument, the time between successive multipaths is equal, and the estimated range is equal in either case although at such short ranges the direct arrival would always be observed. As the animal moves

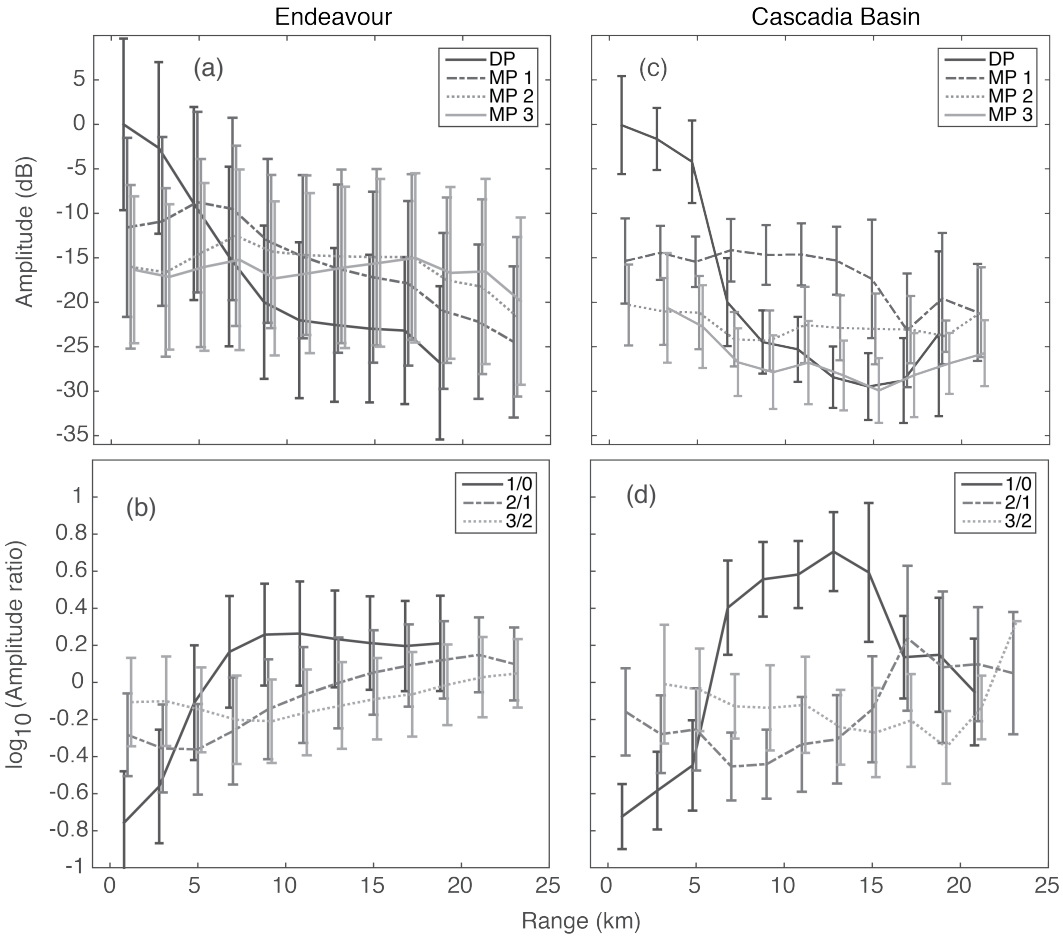

Figure 3.8: (a) Mean and standard deviation of observed amplitudes in 2 km range bins normalized to the amplitude of the direct arrival at 0-2 km range for the Endeavour site. Ranges were obtained from a previous tracking study [93]. (b) Mean and standard deviation of amplitude ratios in 2 km range bins at the Endeavour site. (c-d) is the same as (a-b) but for the Cascadia Basin site and with ranges determined by an iterative supervised bootstrap method (see text).

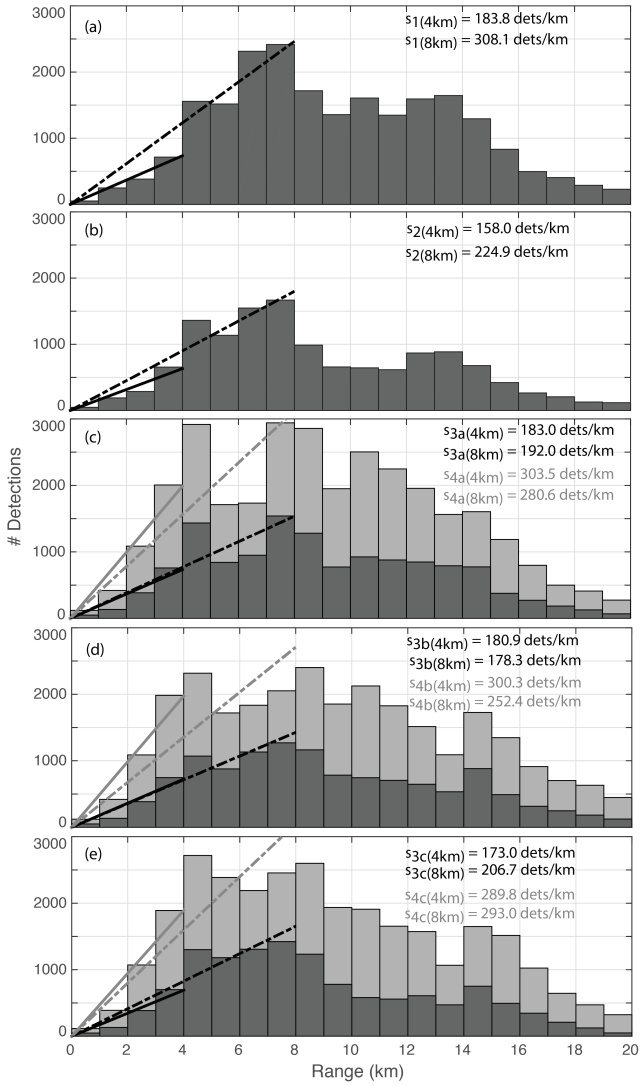

Figure 3.9: Distribution of calls by range at the Endeavour site for (a) all the tracked calls [93]; (b) the subset of tracked calls for which there are multipath ranges using the ray-divergence amplitude model; (c) multipath ranging with the ray-divergence model of amplitude; (d) multipath ranging with the empirically-derived model of amplitude and the travel time residual tiebreaker; and (e) multipath ranging with the empirically derived amplitude model and the combined residual tiebreaker. In panels (c-e), the darker histogram bars show the subset of multipath ranged calls used for the comparison. These are underlaid by lighter gray bars that represent the entire multipath ranged dataset. The dashed lines show the best linear fit that is constrained to go through the plot origin and up to either 4 km (solid lines) or 8 km (dashed lines). Lines fitted to the full set of detections are plotted as lighter gray.

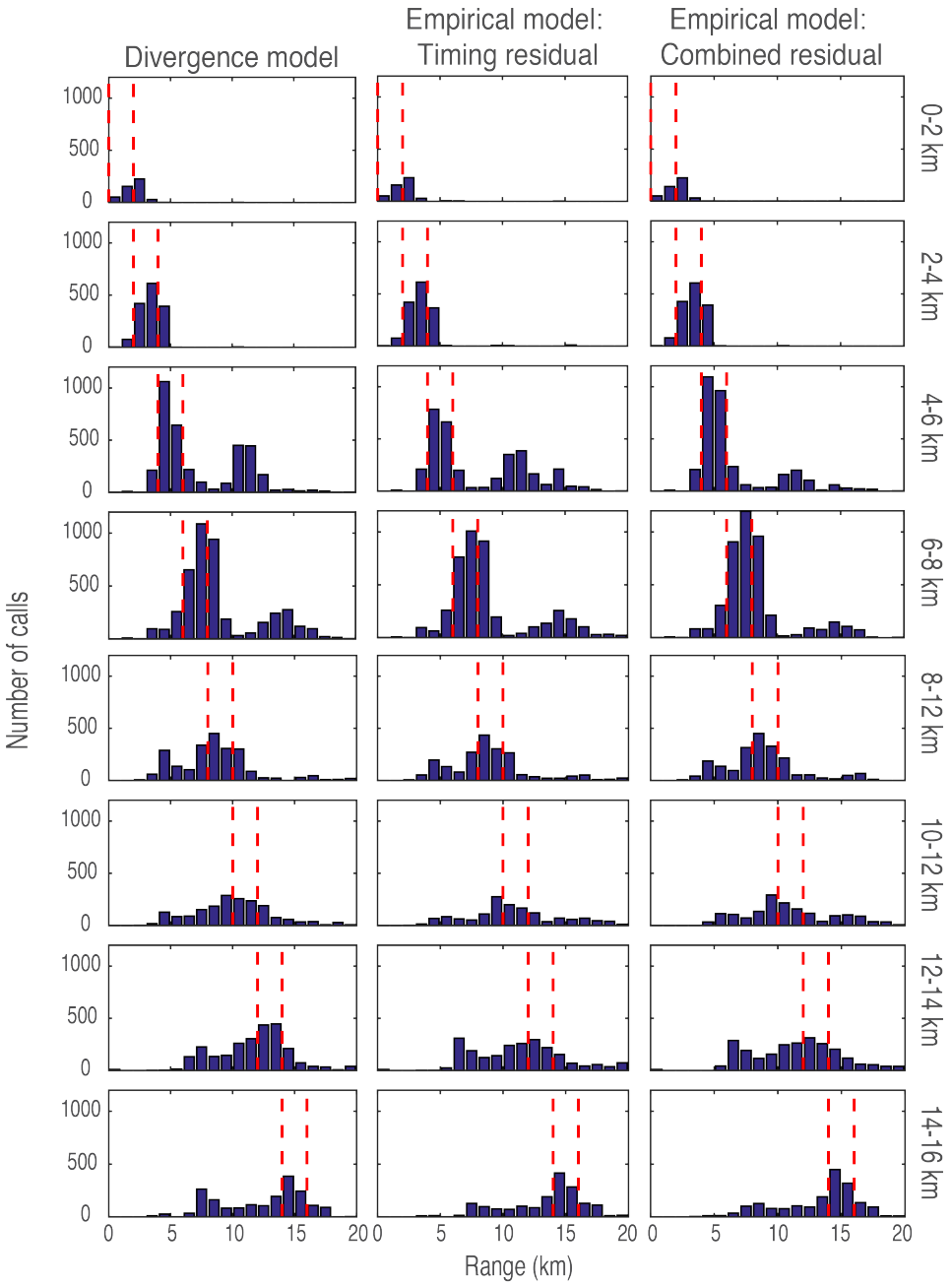

Figure 3.10: Distribution of multipath ranges as a function of tracked ranges at the Endeavour site. Each row represents a 2-km bin of tracked ranges, and the histogram bins show the distribution of multipath range solutions for that subset of calls. The left column shows results for the divergence model of amplitude, the middle column shows results for the empirical amplitude model using the travel time residual tiebreaker, and the right column shows the empirical amplitude model using the combined residual tiebreaker.

further from the instrument, the two estimates of range diverge. For example, a gap of 2.0 seconds between the first and second arrivals might correspond to either a range of 5.2 km for hypothesis 1 where the first observed arrival is assumed to be the direct path or 10.8 km for the hypothesis 2 where the first observed arrival is assumed to be the first multiple. Differentiating between them using a third arrival requires a time resolution on the order of 0.3 seconds. This is a challenge at the Endeavour location, where depth over relatively short ranges varies in the vicinity of the network by hundreds of meters. Using the assumption of flat bathymetry in a location as bathymetrically complex as Endeavour leads to multipath timing errors, which can result in the selection of the wrong hypothesis. For example, a change in depth of 425 m for bounce point of the first multiple at 10 km range will lead to a timing error of 0.3 s. Additionally, the complex bathymetry increases the errors in picking arrival times; it tends to smear out waveforms because each multipath arrival can travel along several paths with different bounce points and there is significant scattering from the rough seafloor. Absolute or relative amplitudes could be used to discriminate between hypotheses, but the large degree of scatter in amplitudes at the Endeavour [Fig. 3.8(a-b)] makes these only a weak discriminator.

Table 3.3 presents a comparison of the hypothesis number selected by the multipath ranging method with the hypothesis that corresponds most closely to the solutions derived independently from tracking. Compared to the divergence model solution, the solution that uses the empirical amplitude model with the travel time residual solution lowers the number of solutions in three of the six incorrect hypothesis categories, but increases it significantly in the remaining three and yields a smaller percentage of correct solution (69% versus 73%). The solution that uses the empirical model with the combined residual tiebreaker method reduces the number of solutions in five of the six incorrect hypothesis categories and yields the highest percentage (76%) of correct solutions. Thus, there appears to be a slight advantage to using empirical amplitudes and the combined residual tiebreaker method, but the improvement is limited by the large variability in absolute amplitudes at this location.

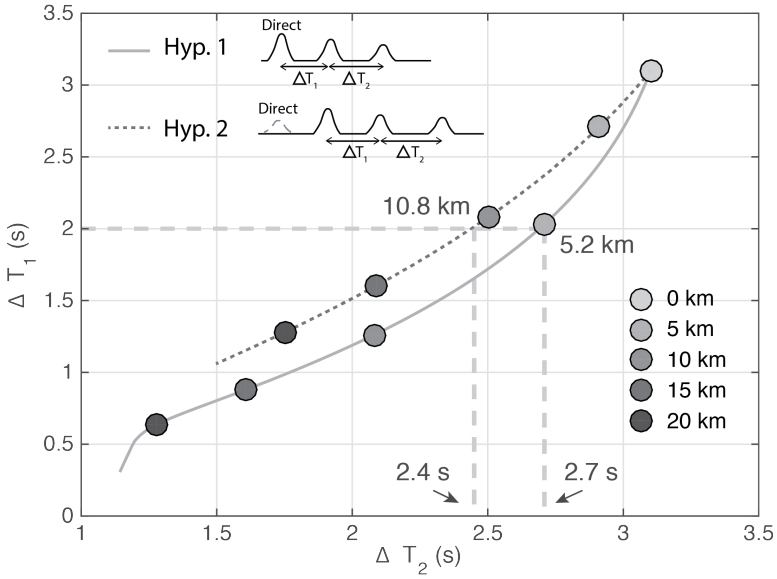

Figure 3.11: Sketch illustrating the challenge of using multipath timing to determine range when the path of the arrivals is not known. For hypothesis 1 (light gray solid line), the direct path arrival is detected. For hypothesis 2 (dark gray dashed line) the direct path arrival is not detected. Lines with grey shaded circles show the predicted time between the first and second arrivals (ΔT_1) and second and third arrivals (ΔT_2) as a function of range for the two hypothesis. For the two hypotheses the observed time difference between the first and second arrival predicts two ranges, and discriminating between the hypotheses requires picking the time difference between the second and third arrival to an accuracy of a few tenths of a second. A specific example shows how a time difference $\Delta T_1 = 2$ seconds would correspond to either 5.2 km (hypothesis 1) or 10.8 km (hypothesis 2) depending on whether the time difference ΔT_2 is 2.7 or 2.4 km.

Table 3.3: Summary of how hypotheses are selected at Endeavour. The hypothesis that most closely matches the independently derived range from tracking is indicted on the left of the arrow in the first column, and the hypothesis that is selected by the multipath ranging algorithm is on the right side of the arrow. Total calls for the three solutions are shown, where the Divergence model and Empirical model 1 use the travel time residual as a tiebreaker to select the preferred hypothesis, while the Empirical model 2 uses the combined residual as a tiebreaker .

True → MP solution	Divergence model	Empirical model 1	Empirical model 2
H1 → H1	6255	5150	6148
H2 → H2	4870	4767	5243
H3 → H3	4026	3768	3746
Total correct	15151(73%)	13685(69%)	15137(76%)
H1 → H2	1007	1185	729
H1 → H3	310	768	277
H2 → H1	1721	1145	1196
H2 → H3	1505	1754	1151
H3 → H1	198	151	130
H3 → H2	966	1124	1219
Total incorrect	5707(27%)	6127(31%)	4702(24%)
Total calls	20858	19812	19839

3.3.2 Cascadia Basin

At Cascadia Basin, a total of 95,889 calls were detected. Of those, 11,155 (12%) were flagged as being part of overlapping call sequences, and 16,548 (17%) were flagged because they only had two detected arrivals and a SNR less than 20 dB. Using the combined residual tiebreaker solution, an additional 19,972 (21%) were not used in the final analysis because they did not meet the sequence filter requirements. The remaining 48,214 (50%) were used to assess the method. The Cascadia Basin instrument is in a much flatter location than

the Endeavour instrument. This improves timing resolution, but the sedimented bottom also has a lower reflection coefficient, meaning that multipath arrivals have lower amplitudes and are thus, more difficult to detect at a given range than at the Endeavour. We used an iterative supervised bootstrap method to extract root-mean-square (RMS) amplitudes for individual arrivals after they had been labeled as part of the ranging process. Extracting empirical amplitudes from the Cascadia Basin 8-day data subset began with the ranging results from the ray divergence amplitude model. Multipath range solutions for the three hypotheses were plotted versus time, a day at a time with the preferred range. A user would then manually define what appeared to be the most likely ranges based on the continuity of ranges, and if necessary, the inspection of individual solutions; if the user was uncertain of the correct solution they would select none. The range hypotheses were then re-selected based on the user input and the resulting amplitudes were used to create a new amplitude model for multipath ranging. This process was repeated three times to obtain the final empirical multipath amplitudes and amplitude ratios (Fig. 3.8(c-d)).

The empirical model shows that the direct path amplitude (Fig. 3.8(c)) drops rapidly above 6 km. This coincides closely with a drop in the amplitudes predicted at ∼5-7 km for the ray divergence model (Fig. 3.4(d)) that is a result of an amplitude minimum predicted by the Zoeppritz equations at the critical angle [45]. The empirical amplitudes for the direct path (Fig. 3.8(c)) do not increase at ranges beyond the critical angle as predicted by the ray divergence model (Fig. 3.4(d)) which may indicate that these equations, which assume plane waves, infinite frequencies and no gradients in seismic properties on either side of the interface, do not predict post-critical amplitudes well (e.g. [54]). At the Endeavour, which has a higher velocity basaltic seafloor, the critical angle is predicted at <2 km range (Fig. 3.4(b)) which is too short a range to observe with our analysis, especially given the limited number of short range observation in our data set. It might, however, explain why direct path amplitudes at the Endeavour are apparently over predicted by the ray divergence model at all ranges.

The empirically derived amplitude model at the Cascadia Basin instrument shows con-

siderably less variability than observed at the Endeavour. The direct path amplitude is significantly larger than the other arrivals at ranges up to 6 km, and from 6-16 km the first multipath arrival is largest and is nearly two standard deviations larger than other arrivals up to 14 km. This decreased variability is presumably due to flatter bathymetry and uniform seafloor characteristics and suggests that amplitude information may be more useful for discriminating between hypotheses at this location than at the Endeavour.

Two examples of ranged calls sequences are shown in Fig. 3.12, with the results from both the ray divergence model and from the empirical model with the combined residual tiebreaker (Equation 3.5). Figure 3.12(a) shows two long sequences from 0:00-4:00, and 5:30-13:00 that likely originate from the same whale. The ray divergence model incorrectly places many of the 10-12 km calls in this sequence at larger ranges. During the second sequence there are a few instances where both amplitude models lead to the wrong hypothesis but the empirical model has less outliers. Between ∼11:00-13:00, both amplitude models occasionally jump to lower ranges. Between ∼14:00-15:00, the two solutions diverge, although it is unclear which, if either, is correct. Beyond 17:00, there is no clear track, although there are scattered solutions, with the empirical solutions often yielding larger and more consistent ranges. Figure 3.12(b) shows another example with a clear segment from 5:00-11:00 that is well resolved with both models. Before and after this there are scattered solutions; no clear track is resolved with either model although the empirical amplitude model tends to give slightly more self-consistent solutions.

Figure 3.13(a) shows the multipath range distributions for solutions obtained using the ray divergence amplitude model. At the shortest ranges (∼2 km) there are more detections than would be expected from a uniform areal density of whales which suggests that some calls are being consistently placed at too short a range. Inspection of the call sequences shows that in some instances groups of calls in tracks that approach the OBS are placed at zero range (Fig. 3.14). The calls that are placed at zero range tended to exhibit a common pattern; the first multipath arrival has a double peak, with the second peak higher and occurring at a time that is delayed by just over the two-way vertical travel time from the

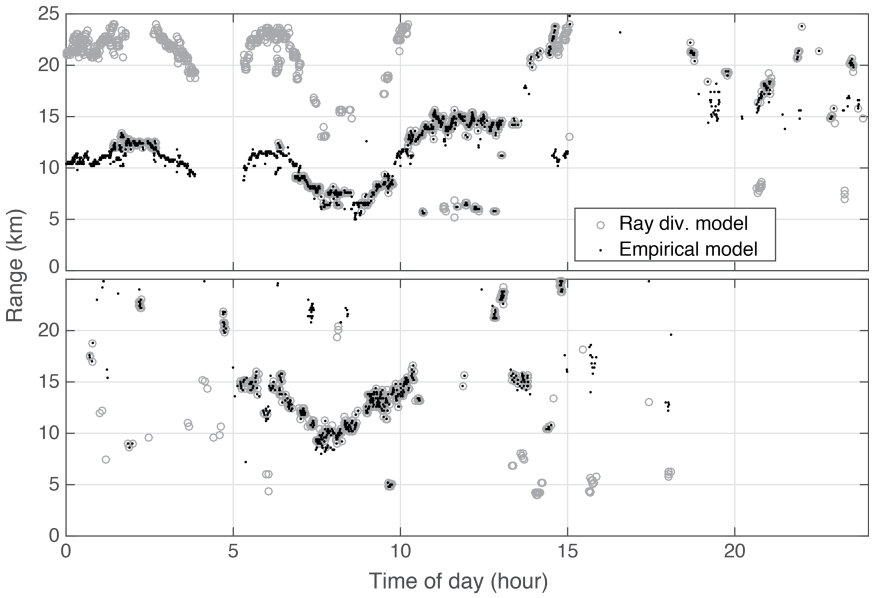

Figure 3.12: Range sequences plotted as a function of time of day at the Cascadia Basin site for two example days, (a) February 9, 2012 and (b) November 11, 2011 showing the ranges estimated using the multipath ranging method with the ray-divergence amplitude model (gray circles) and with the empirical amplitudes and the travel time residual tiebreaker (black dots).

direct arrival (Fig. 3.15). Because the multipath detector looks for the largest peak within a certain search window (with a 0.2 s timing variability), the second peak is selected and the range estimated to be 0 km. Similarly, for some calls with short ($< \sim$2 km) but non-zero ranges, a double peak is also apparent with second higher amplitude peak occurring at a time that is delayed from the direct arrival by just under the two-way travel time.

The double peak arises at Cascadia Basin because there is a 300- to 600-m-thick layer of sediment overlying a basalt basement and the first multipath arrival is the sum of both a fully water-borne multiple which reflects from the seafloor and a slightly delayed basement / water-column multiple that is sum of two arrivals both of which include a basement reflection as illustrated in (Fig. 3.16). If the basement / water-column multiple has a larger amplitude than the water-borne multiple, then it will be picked by the multipath ranging algorithm and the call will be placed at too short a range.

A simple model of the relative timing and amplitude of the first water-borne and basement / water-column multipaths shows that such ranging errors may arise at Cascadia Basin for calls at ranges up to $\sim$4.5 km. The model uses Snells law to track rays and calculate divergence, the Zoeppritz equations to get reflection and transmission coefficients and includes attenuation in the sediment layer. In the basement, we assume a P-wave velocity of 3500 m/s based on seismic reflection imaging across this site [68] and use observed relationships at other sites to estimate an S-wave velocity of 1000 m/s [106] and a density of 2300 kg/m^3 [13]. In the sediment layer, we consider P-wave velocities of 1530 m/s, 1600 m/s and 1700 m/s which span the range of feasible values and assume an S-wave velocity of 0.2 km/s, a density of 1500 kg/m^3, and a Q-value for P waves of 50 [87].

Figure 3.17 shows the predicted relative amplitudes and time differences between the water-borne multiple and the basement / water-column multiple as a function of range for a sediment thickness of 450 m. Depending on the P-wave velocity being used, the potential delay between the two arrivals between 0.45 s and 0.59 s and the amplitude of the basement reflection is slightly larger than the water-borne arrival out to $\sim$4.5 km in all three cases. Figure 3.18 shows the relative timing and amplitude of the two arrivals at zero range plotted

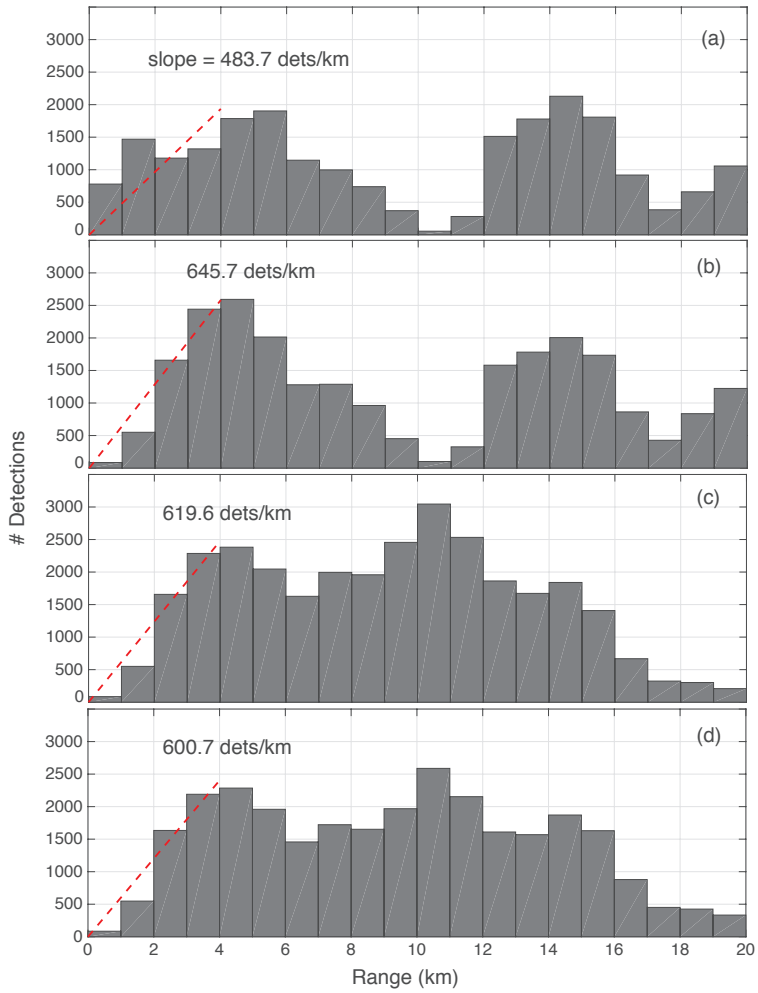

Figure 3.13: Distribution of calls by range at the Cascadia basin site for (a) multipath ranging with the ray-divergence model of amplitude and no correction for the influence of basement reflection at short ranges; (b) multipath ranging with the ray-divergence model of amplitude and a correction for the influence of basement reflection at short ranges (see text) (c) multipath ranging with the empirically-derived model of amplitude, a correction for basement reflections, and the travel time residual tiebreaker; and (e) multipath ranging with the empirically derived amplitude model, a correction for basement reflections, and the combined residual tiebreaker. The labeled dashed lines show the best linear fit that is constrained to go through the plot origin to the range distributions from 0-4 km.

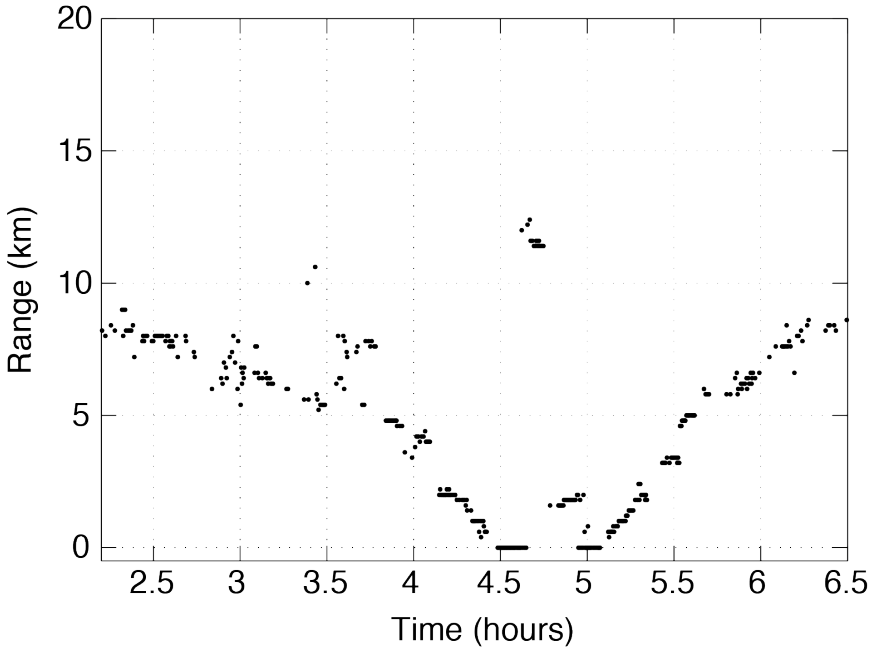

Figure 3.14: A sequence of call ranges at the Cascadia Basin site plotted as a function of time on 31 January 2012 showing an example where calls that are incorrectly placed at a range of 0 km due to the influence of basement reflections (see text).

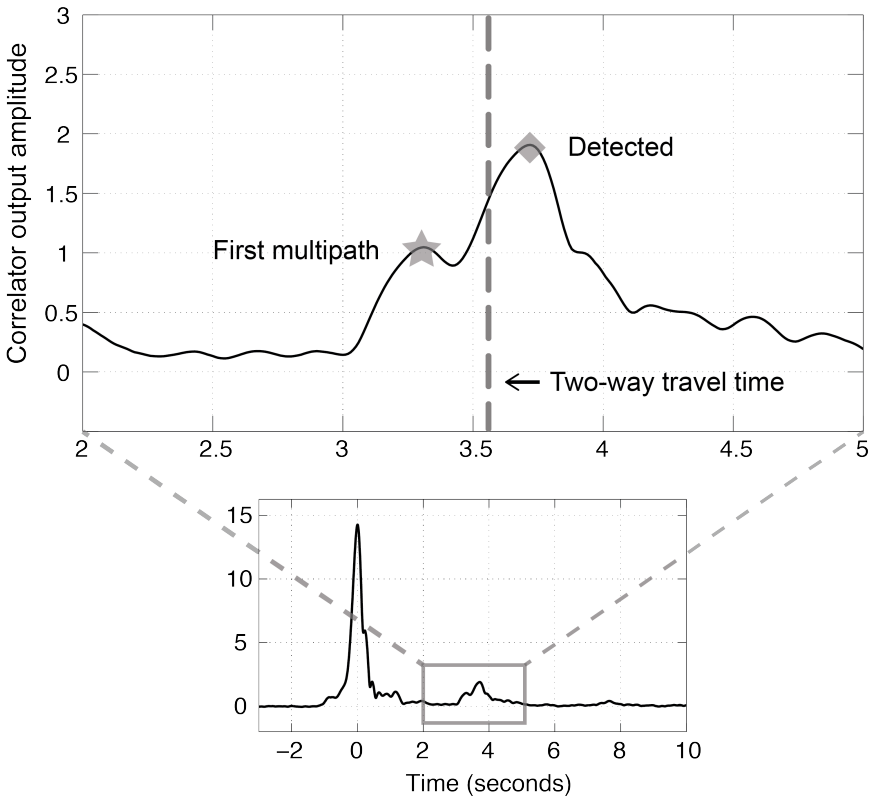

Figure 3.15: Example of the cross-correlator output for a call at a short range at the Cascadia Basin site showing a double-peak for the first multipath arrival due to the influence of basement reflections. When the basement reflection multiple has a higher amplitude than the water-borne multiple, it is picked by the detector and the range estimate is too small.

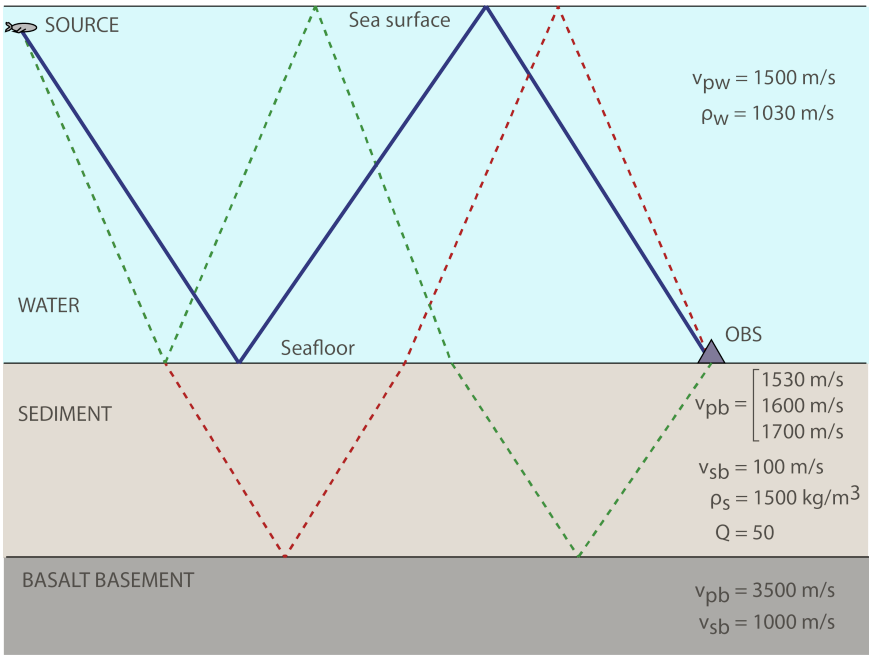

Figure 3.16: Sketch of first-multiple ray paths for an OBS at a sedimented site. The water-borne arrival (bold solid line) is the path assumed for the multipath ranging. The two basement reflection paths (dashed lines) sum to produce a basement reflection that arrives just after the water-borne multiple. The sketch is labeled with the layer properties used to create a model of the relative timing and amplitudes of the water-borne and water-column / basement multiples.

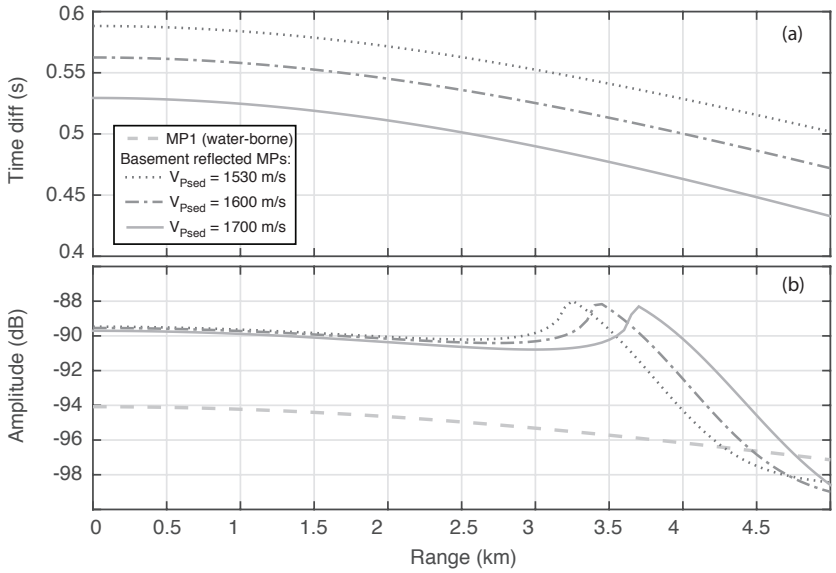

Figure 3.17: (a) Modeled time difference between the first water-borne multipath and the basement reflection / water column multipath as a function of range for an average sediment thickness of 450 m for 3 different choices of sediment P-wave velocity. (b) Modeled amplitudes for the basement reflection / water-column multiples as a function of range compared with that of the water-borne multiple.

as a function of sediment thickness. For a sediment thickness of ∼700 m, the predicted amplitude of the water-borne and basement / water-column multiples are similar. Once the sediment thickness reaches ∼1 km, the basement / water-column multiple is sufficiently attenuated as it travels through the sediment layer that it is unlikely to appear larger in amplitude than the water-borne multipath. If the sediment thickness is less than ∼100 m, the basement / water-column multiple is delayed by less than 0.1 s and is unlikely to be resolved as a separate peak in the cross correlator output. Thus, we infer that basement reflections may influence the multipath ranging out to ranges of ∼4.5 km when the sediment thickness is in the range 100 m to 1 km.

In order to correct for effect of basement reflections, we added an additional step to the multipath detection process. When searching for a second arrival after the largest detection, we look for the next largest peak that follows within the two-way travel time, subject to an

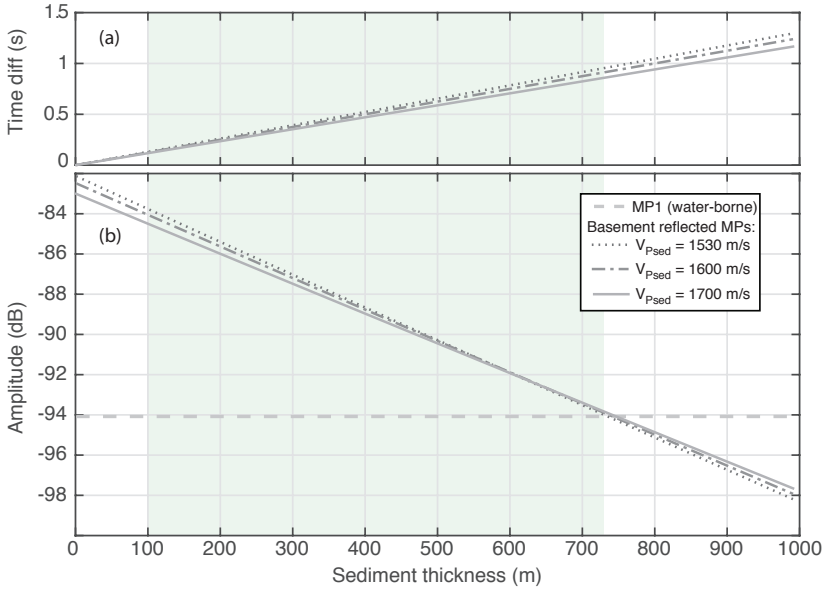

Figure 3.18: (a) Modeled time difference between the first water-borne multipath and the basement reflection / water column multipath at 0 km range as a function of sediment thickness for 3 different sediment P-wave velocities. (b) Modeled amplitudes for the basement reflection / water-column multiples at zero range as a function of sediment thickness compared with that of the water-borne multiple. The shaded area indicates the range of sediment thicknesses in which double peak errors in multipath ranging are most likely to arise.

additional 0.2 seconds to account for uncertainty in picking. Then, if there is an earlier peak no more than 1 s in front of the second arrival that is at least 50% of its amplitude, we select the earlier peak as the second arrival instead.

After implementing this step, the resulting range distribution for the ray divergence amplitude model (Fig. 3.13(b)) no longer has an unexpectedly large number of calls at very short ranges. The number of detections increases out to 3-4 km, then decreases to near zero at 10 km before increasing to a second peak at 14 km and a third at ∼20 km.

Figure 3.13(c) shows multipath ranging results using the empirically derived amplitude model with the travel time residual tiebreaker. The solution is similar to that for the ray divergence model out to about 6 km but at larger ranges, the distributions are quite different. For the empirical amplitude model, there are more detections between 6 km and 12 km with the maximum at 10 km where the ray divergence amplitude model yields almost none, and beyond 16 km there are markedly fewer detections. Both solutions show a drop in the number of detections from 5-6 km, a range that coincides with an abrupt drop in the direct arrival amplitude (Fig. 3.8(c)) at the critical angle for seafloor reflections. This drop in amplitudes is also very apparent when inspecting call sequences that traverse these ranges and we infer that the drop in the number of detections at this range reflects a decrease in fraction of calls that are successfully ranged.

Figure 3.13(d) shows the results of the empirical amplitude model using the combined residual tiebreaker. It is very similar to the distribution obtained for the travel time residual tiebreaker. This is likely because at Cascadia Basin, the bathymetry is flat and seafloor properties are relatively uniform, leading to reliable predictions of both multipath timing and amplitude. The addition of the empirically derived amplitudes to the tiebreaker does not significantly alter the final range solutions because the travel times are equally diagnostic.

3.4 Discussion

In this paper, we have described a semi-automated method to range to fin whales using the timing and amplitude of arrivals recorded by a seafloor hydrophone or seismometer. The

method relies on estimates of timing that are based on the simplifying assumption of a flat seafloor and estimates of amplitude which are best obtained from the data by a bootstrap method. The following sections discuss in turn the performance of the multipath ranging method at the two test sites, its use for density estimation, and its strengths and weaknesses relative to other methods.

3.4.1 Performance of method

The analysis at the Endeavour benefited from an independent dataset of tracked ranges [93]. The Endeavour is characterized by a rough basaltic basement and significant bathymetric relief. The composition of the seafloor at this site results in a strong impedance contrast which means that most received vocalizations have many multipath arrivals. However, the rough bathymetry leads to complex variations in timing that are not modeled under the flat bathymetry assumption which increases the probability that the observed arrivals are associated with the wrong multipath and adds uncertainty to locations even when the multipaths are correctly assigned. The rough bathymetry at the Endeavour also leads to a lot of variability in both absolute and relative amplitudes; there is significant overlap in amplitude as a function of range between the different multipath arrivals. This means that the amplitudes alone cannot be used to reliably identify multipaths. However, the combined residual method that utilizes both travel time residuals and amplitude residuals for the empirical amplitude model produces the best solution indicating that both timing and amplitude contribute usefully to the solution. With this method, ranges are very reliable out to 4 km and most ranges out to 8 km are correctly assigned (Fig. 3.10).

The Cascadia Basin instrument is in a flat, sedimented environment, which means that timing errors are smaller, but the lower impedance contrast with the seafloor results in a reduction in multipath amplitude. At least three multipath arrivals are required to obtain a solution using the multipath timing, but quite often only two are visible arrivals for a given call. However, at this site the amplitudes are also more distinct for different paths and it is possible to infer with a high degree of certainty that a first arrival is a direct path if it has

a cross-correlator signal to noise ratio 20 dB; this allows ranging to nearby arrivals. This two-arrival case was also sometimes observed at the Endeavour site, but far less frequently (only 8% of total detections) and nearly always for arrivals that we inferred to be distant. Although, we have no independent dataset of ranges at Cascadia Basin, we infer that both the times and empirical amplitudes are more reliable and thus more diagnostic of range. Unlike the Endeavour the combined residual method does not substantially improve the solutions over the timing residual method, presumably because the times alone are sufficient to distinguish between multipath hypotheses and are thus diagnostic of range. At Cascadia Basin, we infer that the ranges are very reliable out to 4 km because here the histogram is reasonably consistent with the linear increase in detection counts predicted assuming full detection and accurate ranging. At 5-7 km a sharp drop in amplitudes of the direct path near the critical angle coincides with a sharp drop in the number of ranges obtained presumably because the calls are either not detected or discarded because they only have two arrivals of insufficient amplitude. Without independent tracking, it is not possible to infer the accuracy of ranges that are obtained in this range interval or at larger ranges.

At short ranges, reflections from the base of the sediment layer create a double-peak for the first multipath which requires the method pick the first peak from the seafloor reflection even if the second peak from basement reflection has a higher amplitude. Simple modeling suggests that such a correction may be necessary for sediment layers with thicknesses between $\sim$100 m and $\sim$1 km. In future applications to data from the Cascadia Initiative OBS experiment or other sedimented sites, it will be important to verify that this approach works for a range of basement depths.

The bootstrap method used to estimate empirical amplitudes appears to work well, yielding a set of amplitudes that are quite diagnostic for the first three arrivals out to $\sim$15 km (Fig. 3.8(c-d)). In the Cascadia Basin where the seafloor is flat and likely quite uniform, much of the observed variation in amplitudes for a given arrival is likely due to the calls themselves. Fin whales vocalize near the sea surface, at 20-50 m depth [104, 114], which means that there will be interference between the direct path arrival and the arrival that

is reflected off of the sea surface [119]. This effect causes the amplitude of the call to vary as a function of both call depth and range to the instrument. This effect can result in a doubling of amplitude (6 dB increase), when fully constructive interference occurs, or it can theoretically result in a complete cancellation in the case of fully destructive interference [17] and thus may account for much of the variability in amplitudes (typically ±5 dB) seen in the Cascadia Basin data (Fig. 3.8c).

The fact that fin whales tend to call in long sequences is a powerful piece of information that could be exploited to improve the ranging algorithm. In this paper, we used a rudimentary filter to only exclude calls without at least six other calls nearby in both range (±1 km) and time (±6 minutes). A more advanced approach might incorporate a sophisticated tracking algorithm, such as a Kalman filter (e.g. [8]), to incorporate information from adjacent calls in a sequence to help select the correct multipath hypothesis and thus, improve the reliability and success rate of the range estimates.

3.4.2 Density estimation

A common formula used for point-transect distance sampling to estimate density of animals using vocalizations detected on an acoustic sensor is

$$\hat{D} = \frac{n(1-\hat{c}_{fd})}{\pi w^2 \hat{P}_{det} T \hat{r}_{cue}}, \tag{3.7}$$

where n is the number of detections, $\hat{c}_{fd}$ is the proportion of false detections, w is the truncation distance, $\hat{P}_{det}$ is the probability of detection at ranges less than the truncation distance, T is the duration of monitoring, and $\hat{r}_{cue}$ is the cue rate [10, 43, 53]. Information on cue rate for fin whales was not available so like other studies [43, 55] we only estimated call density. In our data, there is a band of noise near 20 Hz that results from the presence of distant calling fin whales. These calls are indistinct, but combine to produce background noise. We are able to identify and discard earthquakes based on their spectral characteristics. Since there are no other source of impulsive signals near 20 Hz, we assume that "false

detections" are distant fin whale calls, so we assumed that $\hat{c}_{fd} = 0$.

For traditional point transect distance sampling, the probability of detection is estimated from the range distributions by fitting a detection function with a simple form [10]. At short ranges where full detection is assumed, the function would increase because the area for each range increment increases linearly with range. The slope of the distribution would then smoothly decrease and the function taper to zero, because of the effect of decreasing acoustic detectability with range. Although they do initially increase linearly, our range distributions become more complex at larger ranges (Figs. 3.9 and 3.13). There are two reasons for this. First, tracking data at the Endeavour shows that the underlying distribution is not uniform [93]. Second, there are very likely unmodeled, range-dependent detectability issues that occur when using an OBS for multipath ranging. For example, at the Cascadia Basin site the rapid drop off in the amplitude of the direct path at 5-7 km (Fig. 3.8(c)) appears to be reflected in the histograms of detections obtained with the empirical amplitude model (Fig. 3.13(c-d)). Rather than trying to fit a detection function, we adopt an alternative approach. We assume full detection out to a specified range and use this to estimate a density of detected calls, subject to some corrections described below. We then use the total number of calls in the detection histogram to estimate an equivalent range of full detection R_{fd} which replaces $w^2\hat{P}_{det}$ in Equation 3.7.

At the Endeavour location, comparisons of multipath ranges with tracked ranges showed that there is very good agreement at ranges below 4 km and reasonable agreement out to ∼8 km (Fig. 3.10). Slopes are computed out to 4 and 8 km for each of the distributions shown in Fig. 3.9. Two corrections for biases are made to slopes estimated from the full sets of multipath ranges (s_{4a}, s_{4b} and s_{4c} in Fig 3.9(c-e), respectively). First, the method does not range to all nearby calls because overlapping calls are discarded before ranging and the sequence filter eliminates multipath ranges that are isolated or part of only short sequence. We correct for this bias by comparing the slope of the full tracked dataset (Fig. 3.9(a), s_1) with the slope of the subset of tracked calls for which there are multipath ranges (Fig. 3.9(b), s_2) yielding a correction s_2/s_1. We note that this correction itself may be biased because the

tracking also preferentially locates calls in sequences. Second, the slopes of the multipath range distributions may be biased by systematic errors in the ranges. We correct for this by comparing the slope of the tracked subset for which there are multipath ranges (Fig. 3.9(b), s_2) with the slope of the multipath ranges for the same subset (Fig. 3.9(c-e), s_{3a}, s_{3b} and s_{3c}), yielding a correction s_3/s_2. Combining these two corrections gives a corrected slope estimate S^*:

$$S^* = s_{4\#} * \frac{s_1}{s_{3\#}}, \tag{3.8}$$

where the # symbol indicates letters a-c, depending on which multipath solution is used. Using the corrected slope, along with the total number of detected calls in the test dataset N, the equivalent range of full detections, R_{fd},is computed as

$$R_{fd} = \sqrt{\frac{2N}{S^*}}. \tag{3.9}$$

The simplified formula for estimating density then becomes

$$\hat{D} = \frac{n_{total}}{\pi R_{fd}^2 T}, \tag{3.10}$$

where n_{total} is the total number of detections over the interval of interest (T=139 days for the full duration of the data set at Endeavour). Using the combined residual method to estimate corrected slope S^* and the equivalent range of full detections R_{fd}, the final estimates of call density at Endeavour over the entire 139 days is 0.56 calls/km^2/day for the 4 km slope, and 0.80 calls/km^2/day for the 8 km slope.

At the Cascadia Basin site, a different approach is required because there are no independent range estimates. There is no way to make the second correction for biases in the multipath range estimates because we do not know what the true ranges are. However, this correction is only $\sim$9% for combined residual method at the Endeavour and is likely

even smaller at the Cascadia Basin site because the flat sedimented bathymetry leads to more predictable times and amplitudes and thus, presumably to more consistent ranges. To correct for detections that are excluded from multipath ranges, we calculate the fraction of calls, f_c, that are discarded because they are in overlapping call sequences. Assuming these are equally probable at all ranges, the corrected slope S^* can be computed as

$$S^* = s_{\#}\frac{1}{1-f_c}, \tag{3.11}$$

where the # symbol again indicates the multipath solution used (slopes s_a, s_b and s_c in Fig. 3.13(b-d), respectively). Some calls at short ranges will also be discarded by the sequence filter. If we assume that these are all correctly ranged calls that are part of isolated or short sequences, rather than erroneous ranges, an alternative corrected slope can be written as

$$S^* = s_{\#}\frac{1}{(1-f_c)(1-f_s)}, \tag{3.12}$$

where f_s is the fraction of multipath ranges at short ranges discarded by the sequence filter. The slopes estimated with Equations 3.11 and 3.12, likely bracket the true value. Using the combined residual method multipaths (Fig. 3.13(d)) and slopes fitted out to 4 km range, we estimate call densities over the entire 150 days at Cascadia Basin of 2.93 calls/km^2/day and of 3.70 calls/km^2/day using Equations 3.11 and 3.12, respectively.

Burd et al. [12] and Burd and Thompson [11] describe experiments showing increased concentrations of zooplankton at all depths in the vicinity of the Endeavour hydrothermal vent field. Since fin whales eat zooplankton, the increased concentrations near the vent site might draw fin whales to that area. Soule and Wilcock [93] showed that at the Endeavour site, there were higher concentrations of fin whale calls near the network and to the north and east. It was hypothesized that this might be related to advection of zooplankton biomass above the vent fields by the prevailing near surface current. Given this observation, higher call densities might be expected at the Endeavour site relative to Cascadia Basin since there

is a potential food source for fin whales at Endeavour. However, we observe a call density that is about 5-6 times higher at Cascadia Basin than the Endeavour. The increased density at Cascadia Basin could be linked to the fact that it is closer to the coast, since proximity to the coast is correlated with increased biological productivity [1]. It may also be a result of the changes in the fin whale population as it recovers from the effects of whaling (the Cascadia Basin data was collected in 2011-12 and the Endeavour data in 2003-4) or just year to year variations in ocean climatology (e.g. [97]). A more extensive and contemporaneous dataset would be required to understand how environmental factors might be influencing call density.

3.4.3 Comparison with other methods

The two other methods developed for fin whale density estimation are the energy band technique [62] and the 3-component ranging method [43, 54]. The 3-component method was developed in the Gulf of Cadiz using from data from OBSs at depths ranging from 2 to 5 km. At this site the estimated critical angle of 56° yields ranges of critical reflection of 3 to 7 km. For two OBS at ∼4 km depth, airgun shots were successfully ranged out to offsets of ∼4 km. Matias and Harris [54] find that reducing the amplitude of horizontal channels by a factor of 0.5 improves the estimates of range, and propose that modeling amplitudes using the Zoeppritz equations is insufficient since it assumes infinite frequencies and plane wave incidence. Synthetic seismograms generated using the reflectivity method with a typical fin whale call as the source wavelet reproduce this empirically derived correction factor. Fin whale calls have a lower amplitude and narrower frequency content than an airgun and thus cannot be ranged to as large a distance. For a day of test data, full detection is limited to ∼1 km range and the probability of detection of is ∼0.3 for a truncation distance of 3 km [43]. Matias and Harris [54] also evaluated the method on the Mid-Atlantic Ridge using data from OBS at ∼2 km depth. At this site the range of critical reflection is just over 2 km and calls from a single fin whale track were successfully ranged up to ∼1.8 km.

The Cascadia basin site is a sedimented site with a water depth of 2.7 km and thus similar

to that of the shallower OBS in the Gulf of Cadiz experiment. At Cascadia Basin the critical angle is 65° which corresponds to a range of ∼6 km. The range of full detection for the multipath method of 4 km is thus quite similar to the maximum ranges that would be attainable using the 3-component method. One of the challenges of the multipath method at Cascadia Basin is that the reflections have low amplitudes at short ranges. At sedimented sites that are substantially deeper than Cascadia Basin it is not clear whether the 1st multipath would be always be detectable at short ranges; multipath arrivals are not clearly apparent in the example spectrogram shown for the Gulf of Cadiz (Figure 6 in Harris et al. [43]). Thus, the 3-component method might be more suited to deep sedimented sites. The Endeavour site is similar in depth and bottom properties to the Mid-Atlantic Ridge site investigated by Matias and Harris [54]. Here the shallow depths and larger seafloor impedence contrast limit the 3-component method to a maximum range of 2 km while the multipath method is successful out to 4-8 km range. Furthermore, because the amplitudes of multipaths are higher and more variable in such settings, it may be more challenging to distinguish direct from multipath arrivals as required by the 3-component technique.

Since the 3-component and the multipath ranging method are optimal in different environments, they may be complementary techniques that can used together. Both methods require correction at each new site to account for differences in acoustic environment. The 3-component method includes a correction factor for horizontal amplitudes that may need to be calculated when seafloor properties and water depth change [54]; the multipath ranging method is improved if an empirical amplitude model is extracted directly from the data using a bootstrap methodology. Using the methods together would increase the confidence in the results.

The 3-component method uses a parameter called the coherency factor, which describes the degree to which the horizontal and vertical seismometer channels are correlated with each other to identify whether a direct path arrival is at sub-critical ranges [54]. We explored the use of the coherency factor with our test data sets to resolve range ambiguities. Sub-critical calls clearly show a higher coherency on average, but there is a large degree of scatter which

make it an unreliable metric to apply to individual calls. However, it would provide a useful means to verify that call sequences are indeed placed correctly at sub- or post-critical ranges.

The energy band method [62] extracts density estimates from a single station that extends over a much wider area than either the 3-component or multipath ranging method since it does not use individual detections. The limited radii of distance sampling methods allow studies of finer scale phenomena, while the energy band method can provide continuity between widely spaced sensors. One of the challenges in using the energy band method is that it requires a full acoustic propagation model [62]. It can be difficult to obtain sufficiently detailed knowledge of environmental conditions to effectively constrain a propagation model and the most sophisticated models are computationally expensive, so this method would benefit from calibration using the multipath and 3-component ranging methods.

3.5 Conclusions

This study shows that a semi-automated process can be used range to vocalizing fin whales using the timing and amplitude of multipath arrivals received on an ocean bottom seismometer or hydrophone. Tests with OBSs at two environmentally distinct locations in the NE Pacific Ocean: one at a mid-ocean spreading ridge with rough basaltic seafloor, and the other at a sedimented, mid-plate location, suggest that ranges up to 20 km can be obtained and that ranges out to ∼4 km were complete and reliable enough to estimate call density.

The most common errors observed at either location are ambiguity errors. Since we do not know a priori which multipath arrivals are detected, we find the best fit among three different multipath labeling hypotheses. For future work, modeling times and amplitudes in azimuthal segments might improve the multipath ranging method in bathymetrically complex environments such as continental slopes or mid ocean ridges. Furthermore, if bathymetry surrounding the instrument is sufficiently heterogeneous, it might enable solutions for both range and azimuth, which would provide two-dimensional tracking information [55].

Both our test sites were at ∼2.5 km depth and it will be important for future studies to determine the range of water depths for which the method will work. The shallow limit will

likely be ∼750 m, since at shallower depths, the multipaths will be <1 s apart and so the ∼1-s-long 20 Hz calls traveling along the different paths will overlap Additionally, shallow water propagation effects will be much more pronounced, making ray tracing methods far less reliable. A deep water limit at sedimented locations may arise because of the low amplitude of multipaths. Harris et al. [43] show an example from the a deep site in the Gulf of Cadiz where only the direct path arrival is clearly identifiable.

Future studies should also evaluate the performance of the multipath ranging method for density information relative to the 3-component [43, 54] and the energy band [62] methods. Each method is based on assumptions or modeling that could be usefully validated by independent density methods.

Chapter 4

SPATIAL AND TEMPORAL TRENDS IN FIN WHALE VOCALIZATIONS RECORDED IN THE NE PACIFIC OCEAN BETWEEN 2003-2013

4.1 Introduction

Large whales, particularly those that spend most of their lives well offshore and range widely throughout ocean basins, can be extremely difficult to study. Many baleen whale species, including fin whales (Balaenoptera physalus) are currently listed as endangered under the United States Endangered Species Act [14] and the International Union for Conservation of Nature (IUCN) Red List [84] and understanding the population structure of these species is of particular importance for management and recovery efforts. Passive acoustic data have been used to successfully determine regions and seasons where different species of large whales occur, which has provided important information on the offshore distribution of endangered whales. Passive acoustic data also hold the promise of identifying different populations of large whales based on stable acoustic signatures. For instance, the clear geographic variation in blue whale (*B musculus*) songs has led some authors to propose that there are acoustic populations of blue whales and the signatures of each have been used to examine the population identity and geographic range of blue whales in all oceans [9, 58, 61, 70, 95, 100, 101, 102, 96].

Like blue whales, fin whales produce simple, repeated signals that have appeared to be relatively invariant over time. The "20 Hz pulse" is the most commonly observed vocalization produced by fin whales and has been recorded throughout the world's oceans [15, 57, 65, 112, 115, 117, 114]. The pulses (hereafter "notes") are arranged into stereotyped sequences that can last for several hours [114]. Each call is centered at approximately 20 Hz and is a

downswept chirp, covering a frequency range of ∼8-20 Hz [107, 114]. The interval between calls (interpulse interval, or IPI) is typically between 15-25 seconds with longer pauses of a few minutes that have been hypothesized to be surface intervals. The long series of 20 Hz calls are produced seasonally, usually from late fall until early spring [69, 73, 88, 89, 107, 114, 116]. The precise behavioral function of these calls is not known, although to date only male fin whales have been observed to produce these sounds, and their seasonality has been matched to the seasonality of fin whale reproduction, therefore it has been widely assumed that these long bouts have a reproductive function [19]. Because of this association with a reproductive display, and based on the repeated pattern of 20 Hz calls, the long series of these calls have been called "song" [58, 70, 88].

There is evidence that some baleen whale species have song patterns that are related to specific geographic regions. Male humpback whales (Megaptera novaeangliae) from the same population sing the same song in the same year, and while that song changes during the season all males adopt the changes [34]. Song also changes from year to year, with striking changes observed over several years duration [71, 80]. Blue, Brydes (B edeni), and minke (B acutorostrata) whales also show evidence for geographic differences in song type but unlike humpback whales, their songs appear to be much simpler and conserved over time in a given location [58, 102]. Over time, the fundamental frequencies of some song notes of blue whales have decreased in frequency [37, 56]. In some instances, this decrease appears to be quasi-continuous, whereas in others there is evidence of an annual "reset" in the fundamental frequency [56].

A number of studies have suggested that fin whale songs can be geographically distinct. The IPI of fin whales has been shown to vary in the Mediterranean Sea, and the North Pacific and North Atlantic Oceans [15, 26, 66, 107]. In some regions, fin whales produce a higher frequency pulse associated with the 20 Hz call, and the frequency of that pulse has also been used to suggest geographic variation in fin whales around the Antarctic [38, 90] . Additionally, 20 Hz call series may be composed of both a single pulse type or of two to three pulse types (e.g. [95, 57, 25]). Because fin whales have been documented to change both the call used

and the IPI intra-annually [74, 91], this study focuses on winter months (November through March) when fin whale 20 Hz songs are the predominant signals produced by this species [100, 107, 116, 37]. Here we present 10 years of data from a small region in the NE Pacific Ocean and contemporaneous data from nearby locations to examine the IPI and frequency characteristics of fin whale calls to determine how robust IPI and call characteristics are over a relatively long time scale and whether there is local geographic variation in these characteristics.

4.2 Methods

4.2.1 Datasets

Four datasets were used in the analysis for this project. A map of the locations of the sites is shown in Fig 4.1, along with the corresponding dataset timeline. The longest recording was from a NOAA-PMEL ocean bottom hydrophone (OBH) that was located at Axial Seamount (45.96°N, 130.01°W) in a water depth of 1550 m. We used data collected on the Axial instrument over a duration of 7 years, from 2006-2013. The data were collected at a sample rate of 100 Hz. This dataset was used to examine long time-scale variation in fin whale calling behavior at a single location.

The other instruments used in the study were all ocean bottom seismometers (OBS), which were designed to detect ground motions caused by earthquakes. These instruments have three channels: one vertical and two horizontal. Only the vertical channel was used in this analysis since because horizontal channels are often not well-coupled to the seafloor (e.g. Trehu [110]). These instruments were used to compare geographic variation among different sites in the same general region and the same year.

We used a subset of five OBSs from the Cascadia Initiative (CI) experiment, which is an onshore-offshore seismic and geodetic experiment that was deployed from 2011-2015 [109]. We selected instruments deployed from 2011-2012 along the western periphery of the array, spanning from 40°N-48°N. This allowed us to monitor a north-south geographic span of

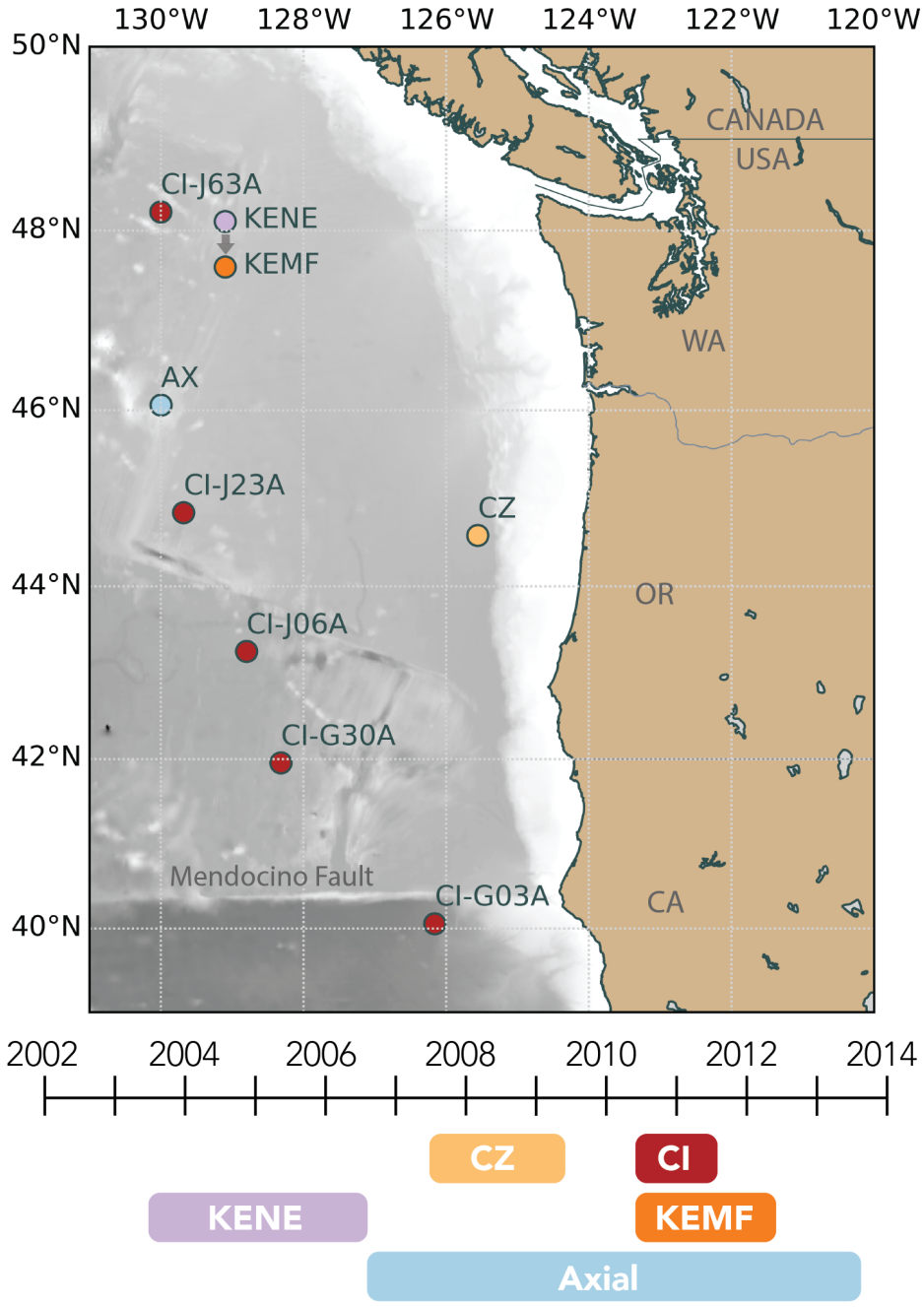

Figure 4.1: Regional map of the northeast Pacific Ocean showing locations of all instruments used in this study, along with a timeline indicating when they were deployed. At the scale of this map, KENE and KEMF are effectively co-located, but KENE is displayed slightly offset to the north for clarity (AX=Axial, CI= Cascadia Initiative, CZ = Colza).

nearly 1000 km over a time period that corresponds to one year of the Axial dataset. North of the Mendocino transform fault, instrument depth varied between 2650 m - 3200 m. The one instrument south of the Mendocino transform fault (CI-G03A, Fig 4.1) was at a depth of 4055 m. The CI instruments used in this study all sampled at 50 Hz.

One instrument from the Central Oregon Locked Zone Array (COLZA) was used. It was situated at 44.58°N and 125.56°W in a water depth of 2880 m and was located at the base of the continental shelf. This instrument was deployed from 2008-2010 and recorded at a sample rate of 100 Hz.

Two instruments located at the Endeavour segment of the Juan de Fuca Ridge (∼340 km offshore of Washington State) were used in this study (KENE and KEMF). This site is characterized by rough, mid-ocean ridge topography with active hydrothermal vents. The KENE instrument was deployed between 2003-2006 and was part of an 8-station seismic experiment [59]. It was located at 47.97°N and 129.06°W in a water depth of 2330 m. The KENE instrument sampled at 128 Hz. The KEMF instrument was part of the Ocean Networks Canada Neptune array and was located approximately 4 km to the south-west at 47.95°N and 129.10°N in a water depth of 2205 m. At KEMF, the sample rate was 100 Hz.

All of the instruments had a flat response over the frequency range of fin whale calls (between 15-30 Hz), with the exception of the Cascadia Initiative instruments. At the Cascadia site, the instruments were sampled at 50 Hz, but the instruments' anti-aliasing filters limited the effective upper frequency of observation to ∼23.5 Hz. Instruments sampled at higher rates were low-pass filtered at 35 Hz.

4.2.2 Automatic detection of calls

Fin whale calls were automatically detected using a time series matched filter (e.g. [98]). The template call was designed to span a wide enough bandwidth to pick up calls that varied slightly in frequency, so long as they remained consistent in the rate of change of frequency. The template call consisted of a linear chirp decreasing from 30 to 15 Hz over a duration of 2.25 s. This can cause a slight shift in the timing of the correlator output peak, so we

introduced additional logic to find the time of the peak amplitude of the signal envelope within 0.5 seconds of the correlator output detection. Since peak amplitude of recorded fin whale calls was typically observed to occur within the first third to half of the call, and calls are usually ∼1 second in duration, this is procedure is expected to introduce no more than 0.5 seconds in timing variation.

A spectrogram was computed for each 30-minute segment of the input time series (the FFT used a 1-s Hann window with 90% overlap). The peak frequency of each call was extracted using the weighted mean of a subset of the spectrogram within ±0.5 seconds of the call detection time, and within the frequency bandwidth of the template call. The detection threshold for the cross-correlator output was set to 5 dB relative to the median signal level within half an hour of the detection.

For calls measured at the Cascadia Initiative sites, the upper limit on frequency is low as a result of instrument sample rate. Higher frequency calls were detected but frequency estimates are inevitably skewed low since the full call bandwidth could not be used in the weighted frequency estimation. The inter-pulse interval was calculated as the time between the peak amplitude of the current call and the call immediately preceding it, and was independent of call frequency.

One of the most common sources of false detections in this dataset was from earthquakes. These broadband energy sources often overlapped with the typical energy band of fin whale calls and could trigger the matched filter. To minimize this type of error, we used the spectrogram to compare the energy in between 15-25 Hz, and 5-15 Hz. Any calls with higher energy content in the lower frequency band were assumed to be earthquakes and were discarded.

There is a consistent band of low-frequency noise near 20 Hz that has been attributed to distant fin whale 20 Hz pulses. This means that even when individual calls cannot be identified, the background noise is actually the signal of interest, just further away and indistinct (e.g. Curtis et al. [21]). This makes the traditional assessments of false positive and false negative detections challenging. We instead chose to only accept calls that were

clearly part of a sequence, since this study is an exploration of patterns observed in call sequences. Details on the extraction of sequences are given in the following section.

4.2.3 Computing note statistics

Since our goal in examining this dataset was to look for patterns in IPI, note frequency, and the relationship between these two features, we restricted our analysis to only the loudest and most consistent note sequences. We accomplished this by first subsetting the entire dataset to calls with signal-to-noise ratios (SNR) greater than 5 dB and IPI less than 40 s. From these, we defined sequences as any series of calls with no gaps greater than 20 minutes. Only sequences containing at least 20 calls were used in the analysis.

To visualize the relationship between frequency and IPI, we computed a two-dimensional (2D) histogram for each month of each instrument year. IPI was binned from 5-45 s in increments of 1 s. Frequency was binned from 15-26 Hz in increments of 0.4 Hz. The focus of our analysis was on call patterns rather than on absolute number of calls in a given month. To normalize for the large degree of variation in total calls among different months, we scaled call counts to reflect the proportion of calls, as a percentage, relative to the total detections within that month. Peaks in the 2D histogram indicate distinct call-type patterns in frequency-IPI space. To allow for further quantitative analysis, we extracted the coordinates and corresponding counts for each peak by finding local maxima using SciPy's image processing maximum filter tool [47]. If the maximum number of detections corresponding to a particular peak was fewer than 50, that element was not retained for further analysis.

4.3 Results

4.3.1 Song and note types

Over 1.8 million notes from more than 8,000 sequences recorded at 8 sites in the northeast Pacific Ocean were used to examine singing patterns in fin whales from 2003-2013. Two patterns were recorded most frequently at all sites and can be best described as consisting

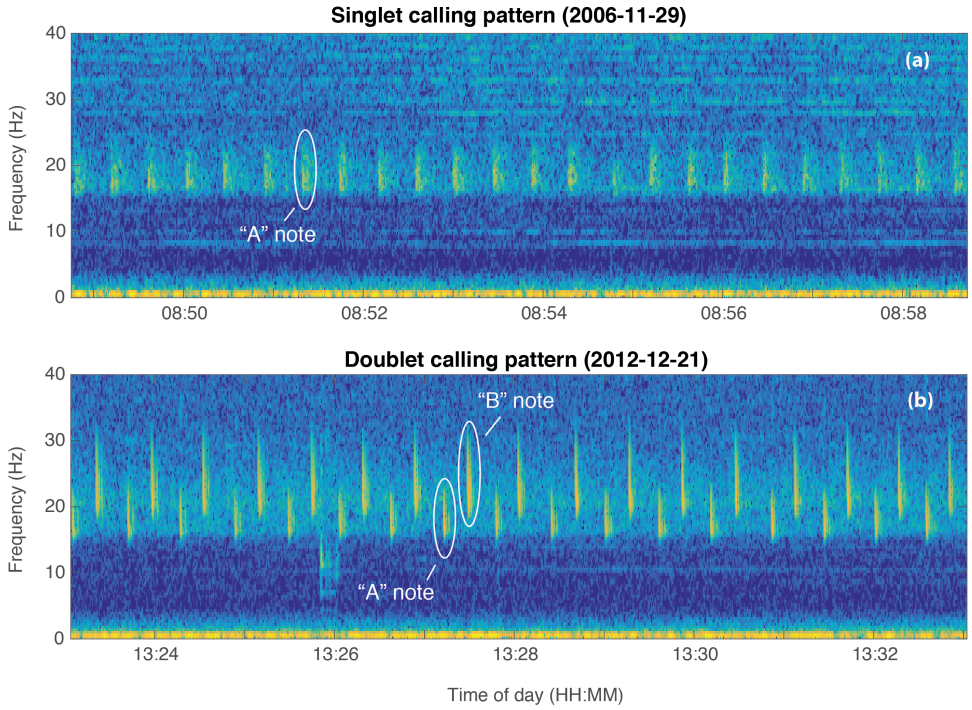

Figure 4.2: Example spectrograms from the Axial instrument showing the two primary song types observed in the datasets. The upper panel (a) shows a sequence with one primary frequency and a single IPI (singlet song). The lower panel shows a sequence with alternating notes, with two frequencies and two dominant IPIs (doublet song).

of combinations of two distinct notes. For simplicity, the two pattern types are hereafter referred to as singlet (IPI >22 s) and doublet songs (IPI $\leq$22 s), and the note types are referred to as A (<22 Hz) and B ($\geq$22 Hz). Examples of the two song types are shown in Figs 2a and 2b. Singlet songs consisted of a single, repeated note with a fixed IPI and center frequency (Fig 4.2a). Doublet songs had two primary notes, alternating between a low frequency, high IPI note (type A), and a higher frequency, low IPI note (type B, Fig 4.2b). This relationship between frequency and IPI has been described previously for calls in the NE Pacific Ocean [49].

Singlet songs were more common in earlier years of the study, with a gradual transition to doublet songs over the decade of recording. Although singlet songs were more common

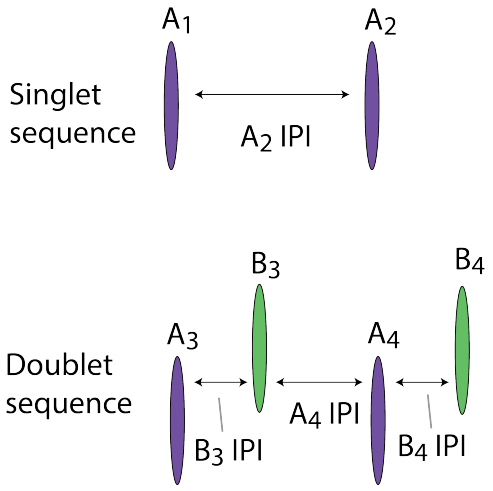

Figure 4.3: Illustration showing the relationship between notes and IPI for both the singlet and doublet sequence types. Axes indicate frequency and time, so this schematic is analogous to a spectrogram representation. The purple and green symbols indicate fin whale A and B calls, respectively. The IPI of a given note is the time between that note and the immediately preceding note, whether it is of the same type or not.

between 2003-2009, doublet songs were also occasionally observed. The introduction of the higher-frequency notes would effectively reduce the IPIs of the original sequence. In this transitory period, the spacing between A notes remained consistent, but between consecutive A notes, the higher frequency B notes began to occur. The gradual appearance of the B notes, and the stationary spacing between A notes, caused the B notes appear to be "interruptions". Since note type B did not occur at exactly halfway between two A-notes, it resulted in a bi-modal distribution of IPIs. The relationship between note types and IPI as described in this paper is illustrated in a sketch in Fig 4.3.

4.3.2 Decadal trends

Axial site

The 2D histograms for each month and year at the Axial site are shown in Fig 4.4. At Axial in earlier years (2006-2009), the dominant note had an IPI of ∼25 seconds and frequency

around 18 Hz. This can be observed in the 2D histograms as a single bright peak illustrating note A of a singlet song (i.e. January 2007). Gradually, note B becomes a more prominent feature and the doublet song begins to emerge but singlet songs are still recorded. Note B can be observed as a higher frequency, lower IPI peak in the 2D histograms (i.e. February 2011, Fig 4.4). By the final years of the dataset (2011-2013), doublet songs become much more dominant. The A notes were often lower in amplitude than B notes and were occasionally not detected. This resulted in the peaks seen in the upper right quadrant of some months (e.g. March 2011).

Additional recorders

The Axial dataset covered seven years (2006-2013), and data from nearby KENE (200 km to the NNE of Axial) were available from 2003-2006. Inclusion of these data extended temporal coverage to a full decade. To justify the use of these additional data, we looked at data from KEMF, which was located less than 10 km from KENE, but had temporal overlap with Axial data (2010-2013). The song data from KEMF showed the same characteristics in both frequency and IPI as the Axial data (Fig 4.5), thus we believe combining KENE and Axial for a full decadal analysis was justified.

Uncertainties associated with each monthly data point were determined by taking the width of the data distributions at half of the maximum amplitude. We assumed that the underlying distributions were Gaussian, so the full width at half amplitude can be scaled by a factor of 2.355 to obtain an estimate of the standard deviation of the data. We then computed standard error assuming that the number of independent measurements that contributed to the mean was equal to the number of sequences. The standard error for each data point shown in Fig 4.5 is between 0.06 s and 0.40 s for IPI and is between 0.04 and 0.13 Hz for frequency.

Both monthly IPI and frequency changed over time from 2003-2013 (Fig 4.5). Only singlet songs consisting of A notes were recorded at the start of the decade. The introduction of note B and doublet songs was well-established by 2008, and continued from that point onward.

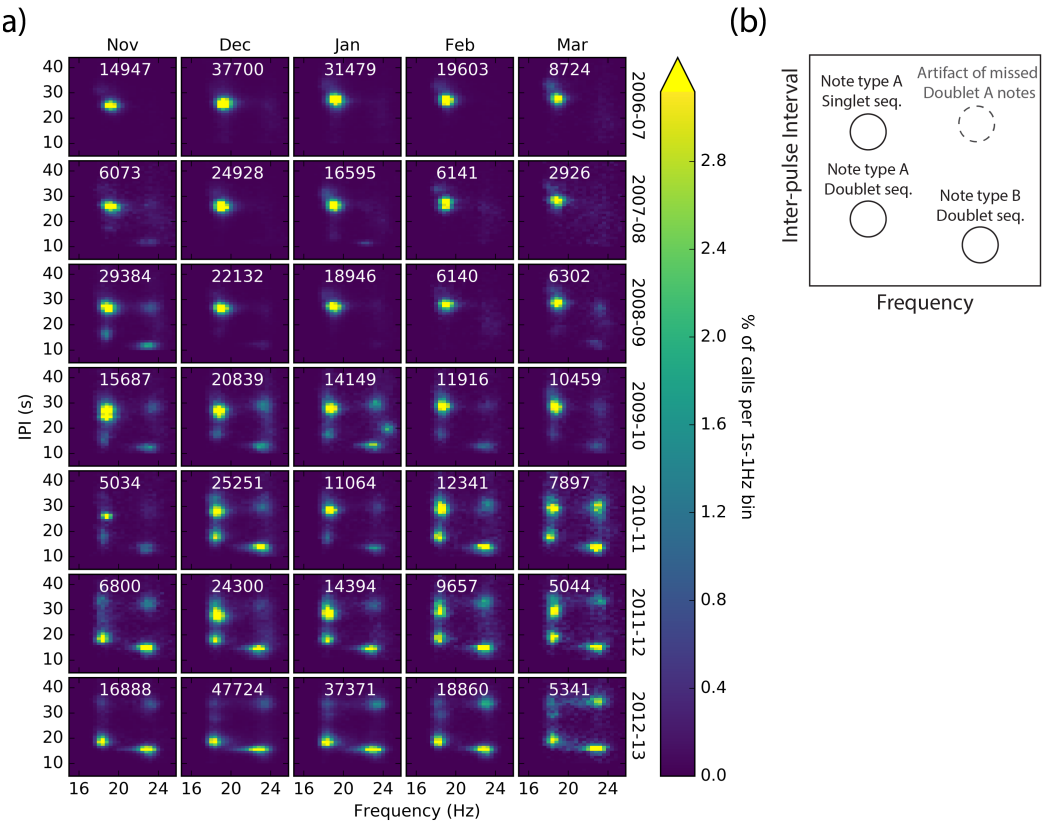

Figure 4.4: Panel (a) shows 2-dimensional histograms of IPI and frequency for each month (November-March) at the Axial NOAA-PMEL OBH from 2006-2013. Colors correspond to proportion of notes (in percent) observed within each month (total notes per month labeled in white). Panel (b) illustrates how the peaks in the 2D spectrograms can be interpreted in terms of note and sequences types.

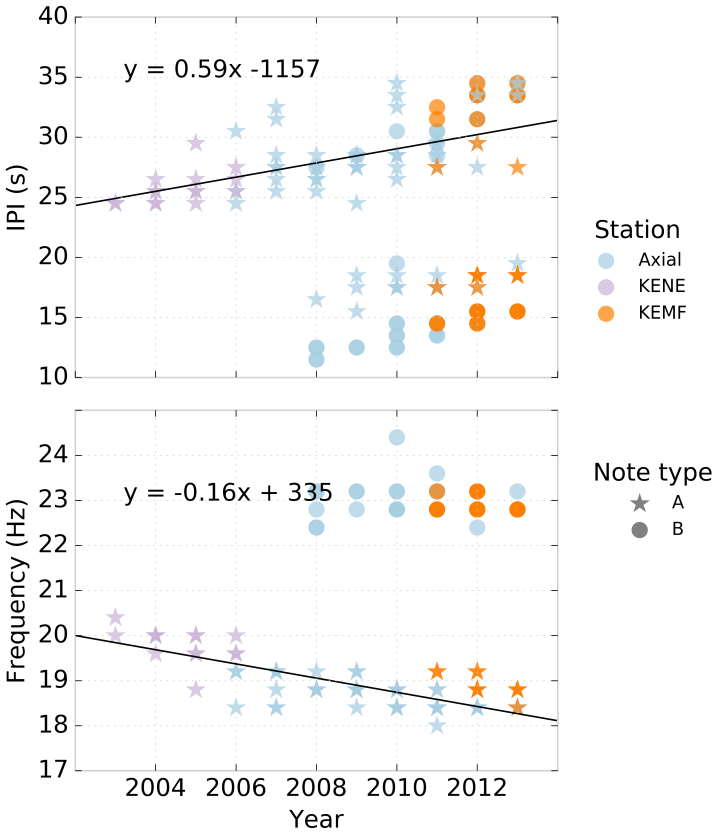

Figure 4.5: Frequency and IPI characteristics from three instruments plotted as a function of year from 2003-2013. Symbols are colored by station (Axial is blue, KENE is purple, and KEMF is orange), and note type is indicated by shape (Note type A shown by stars, note type B shown by circles)

The IPI of A-note singlet songs increased significantly, at a rate of 0.59 s/year (R^2=0.37, p<0.001), over the decade of observation (Fig 4.5a). The frequency of the same subset of sequences decreased significantly by 0.16 Hz/year (R^2=0.59, p<0.001) over the decade (Fig 4.5b). We also looked at the trends in doublet songs. Within that subset, we observed statistically significant increases in IPI for both the doublet A and B notes. IPI of doublet A notes increased at a rate of 0.39 s/year (R^2=0.46, p<0.001) and doublet B notes increased at a rate of 0.72 s/year (R^2=0.46, p<0.001). Frequencies of the doublet song notes did not show any significant decrease (R2=0.036, p=0.351) over the same time period.

Due to the volume of data, it was not possible to examine every spectrogram. However, several sample spectrograms were checked for each instrument and year. Exploring the transitional time between the singlet-only years and the years that also contained doublet calls revealed that there were sequences that contained both singlet and doublet characteristics. No sequences consisting solely of singlet B notes were observed.

4.3.3 Seasonal and inter-annual trends

In addition to the decadal, among-year trends described in the previous section, within-year patterns in IPI were also observed. Between 2005 and 2010, there was a within-year increase in IPI by month, followed by a reset to a shorter IPI (that was nevertheless greater than that of the same month the year prior) at the start of the following year (Fig 4.6). The pattern became less clear as doublet song types became more prominent in 2010, and by 2013, the monthly increase in IPI was no longer observed.

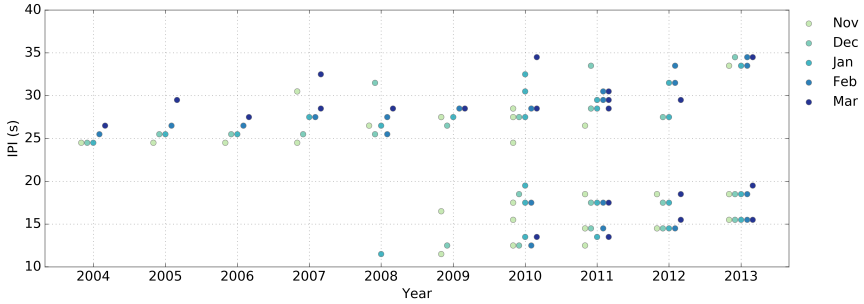

Figure 4.6: Monthly IPI peaks from KENE and Axial to illustrate the variations within years and from year to year (2003-2014). Colors indicate month, from November to March.

4.3.4 Geographic trends

The decadal trend is clear at Axial and the Endeavour segment locations (KENE/KEMF). Because we had access to data from locations to the east and south of the Axial/Endeavour region, but from fewer years, we wanted to examine if the annual patterns in song type occurrence and IPI were robust over a greater geographic range by including analysis from CI and Colza experiment sites (Fig 4.1). As the CI OBSs had an upper limit on bandwidth of ∼23.5 Hz, and our estimates of frequency could be biased low (as described in the methods), we chose to focus only on the IPI values for the geographic analysis. Other studies that have examined small-scale geographic variation in fin whales have relied on IPI alone to establish population identity ([115, 56] but see [37, 26] for the use of frequency components for geographic distinction).

IPIs for each location were extracted from 2D histograms computed over the entire calling season for singlet A notes, doublet A notes, and doublet B notes (Fig. 4.7). Standard error for each monthly IPI estimate varied between 0.08 s and 0.72 s. Although we did not observe a significant geographic trend in the IPI of doublet A or B notes, there appeared to be two distinct groupings of singlet A note IPIs. There was a higher IPI group that occurred at latitudes less than approximately 45°N, and a lower IPI group that occurred at latitudes greater than approximately 43°N. Two of the Cascadia Initiative instruments, CI-J23A and

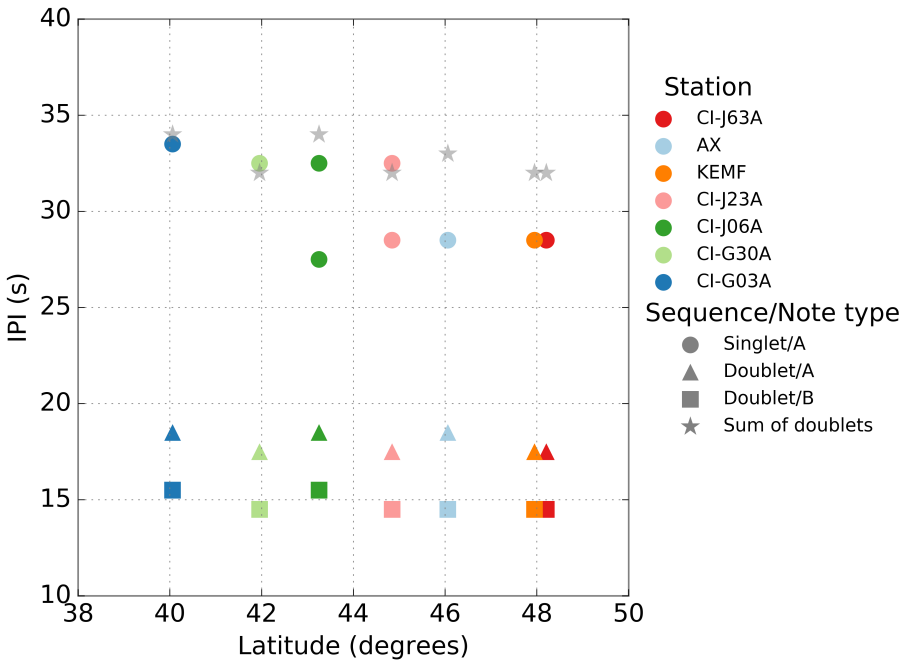

Figure 4.7: Annual summary IPIs as a function of latitude for each station recording during the 2011/2012 calling season. Doublet A-notes are indicated by triangles, doublet B-notes are indicated by squares, and singlet A-notes are indicated by circles. Colors correspond to station. Gray stars indicate the sum of doublets at the corresponding location.

CI-J06A recorded singlet A notes of both types.

For the higher IPI singlets, the sum of the corresponding doublets is approximately equivalent to the singlet song IPI at any given site. This aligns with the general notion that the doublets result from regularly-spaced interruptions of consistent singlet song IPIs. However, in the case of the lower IPI singlets, the sum of the doublet song IPIs at each location is higher than the corresponding singlet songs. The mean IPI of the lower singlet group was 28.3 $\pm$0.40 and the mean IPI of the higher singlet group was 32.8 $\pm$0.43. A two-tailed t-test showed a statistically significant difference between the higher IPI singlet group and the lower IPI singlet group ($p<0.001$).

A similar analysis was carried out for the 2007-2009 for Axial and Colza sites. The

Colza site is located approximately 350 km to the east of Axial, just west of the foot of the continental slope (Fig 4.1). Both the Colza and Axial instruments were sampled at rates that allowed for the analysis of both frequency and IPI. Singlet songs dominated both Axial and Colza sites during both years, although some doublets were observed in both years. Results from this comparison are shown in Fig 4.8. During the 2007-2008 calling season, less than 5% of calls were doublets, and these smaller peaks in the 2D monthly histograms were not reliably detected by the automatic algorithm, so are not included in the analysis. By the 2008-2009 calling season, doublet calls made up ∼24% of all recorded calls at Colza, and ∼16% of all recorded calls at Axial. Monthly standard error for the COLZA site varied between 0.12-0.38 s in IPI and 0.06-0.12 Hz in frequency.

Two-tailed t-tests between monthly means of each call type between stations showed statistically significant differences between the singlet A note frequencies in both years (2007-2008: $p < 0.001$; 2008-2009: $p = 0.001$). No other note types showed a significant difference between sites for either IPI or frequency. It is important to note that these results depend on the assumption that each sequence represents an independent measurement. If, however, a small number of animals are producing the calls at each of the locations, then the differences in singlet A note frequency might not be statistically significant.

4.4 Discussion

It is clear, from this work and other recent work on fin whale acoustics [74, 91], that fin whale sound production is more complicated than previously thought. Our work adds further support for intra-annual changes observed in inter-pulse interval [74]. In the northeast Pacific, IPI increased over the course of each month from November through March, but then partially reset to the previous year's value at the start of the following year. Over a decade however, the IPI for all song types increased significantly such that from 2003-2013, the IPI of singlet songs increased from 25.0 to 30.9 s. Over the same time period, the peak frequency decreased significantly from 19.8 Hz to 18.2 Hz. Further, over the decade, an additional note type was introduced and became more prominent. The two note types then

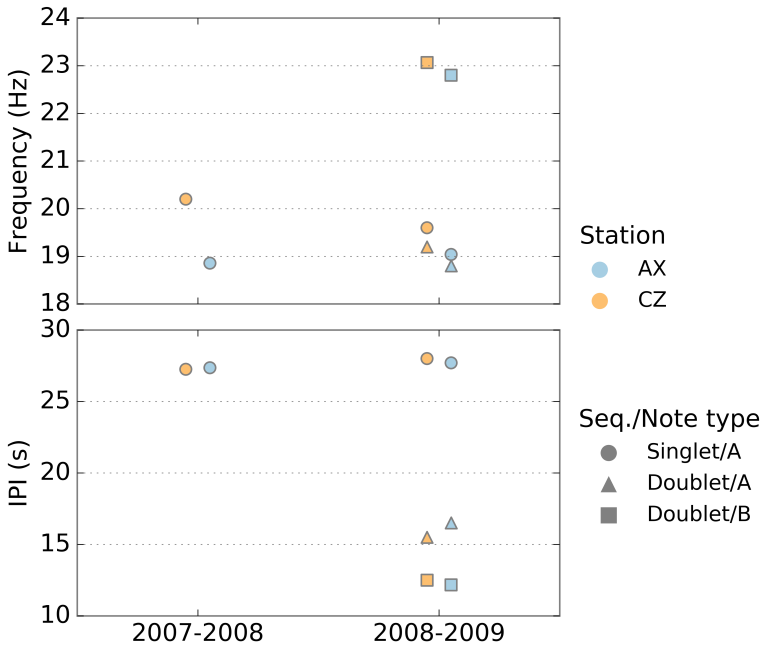

Figure 4.8: Annual means of frequency and IPI values at Colza and Axial sites for the 2007-2008 and 2008-2009 calling seasons. Station is indicated by color. Doublet A-notes are indicated by triangles, doublet B-notes are indicated by squares, and singlet A-notes are indicated by circles.

alternated in a doublet pattern resulting in a distinctly different song. Geographic patterns were also observed: within one calling season (2011-2012), two distinct singlet A note IPIs occurred. One group, occurring mostly below 44°N, had a mean IPI for singlet A notes of 32.8 ±0.43 s. The other group, occurring mostly north of 44°N, had a mean IPI for singlet A notes of 28.3 ±0.40 s.

A similar pattern of an annual change in frequency with a partial reset and overall decadal decrease in frequency has been documented in Antarctic blue whales recorded off Australia [37, 36]. A decrease in frequency in numerous blue whale populations over time has also been noted. McDonald et al. [56] explored a number of potential factors to explain the observed decline in tonal frequencies, and hypothesized that increasing population size was one possible explanation for decreasing frequencies. Gavrilov et al. [36] suggest that the underlying explanation for the shift is likely more complex than an increase in animal density and hypothesize that the interannual shifts might be related to changes in calling depth. Other marine mammal species have shown evidence of long term shifts in call frequency that have been attributed to anthropogenic noise, although these tend to be associated with an increase in frequency, rather than a decrease such as we observed. For example, Parks et al. [77, 78] observed a long-term increase in right whale calling frequency under high noise conditions. Foote et al. [29] describe a terrestrial analog, whereby birds were observed to sing at higher pitch in the presence of urban noise. To date, decreases in call frequency have not typically been attributed to increasing environmental noise.

A recent study of fin whale calls recorded between 2000 and 2006 found within-year increases in IPI from October to February in three regions: southern California, Hawaii, and the southeast Bering Sea [74]. Like our study, at least for the southern California region, there was an annual reset from the maximum IPI in February (in our data set, March) to a minimum in October. That study had 3 consecutive years of data from southern California but did not find any interannual trends. The data from Hawaii are intriguing in that for the month of December the median IPI increased from 2000 to 2005 (although only the December median IPIs are reported for the later calling season). The Bering Sea location,

however, did not show a corresponding increase over the same time period. Koot [49] also describes a within-year increase in IPI for doublet song of approximately 2.6 s from August to January for an instrument located just off the northwest coast of Vancouver Island in 2010-2011.

Oleson et al. [74] hypothesized that the within-year IPI trends might be linked to reproductive hormonal activity, and posited that a shorter IPI can be considered equivalent to a greater calling rate and evidence for increased male fitness either as a mate attractant or to mediate male-male assessment. Either (or both) of these motivators could result in a lower call rate later in the season and the argument presented by those authors is intriguing and well supported by examples from other taxa. It does not help explain, however, the emergence of a second song type in our data in which IPIs are necessarily decreased and do not change seasonally from roughly 2011 and onward. Further, the hypothesis attributing seasonal changes in call characteristics to reproductive activity cannot entirely explain the longer-term trends that we observed. These other changes that occur over longer time scales might reflect calling behaviors that are spread geographically throughout the region.

Thompson et al. [107] were the first to aggregate 20-Hz pulse characteristics from around the globe to highlight the potential for geographic variation in fin whale calls. Hatch [44] looked at acoustic and genetic data on fin whales from several sites in the Pacific and Atlantic Oceans, and found significant regional acoustical differences in call characteristics. Our timeline overlaps with that of the Oleson [74] study during the 2005-06 calling season, although the instruments they used were far from our study (the Bering Sea and off Hawaii). The IPIs they reported during that time period were between ∼25-35 s which is not substantially different from our results from the Axial dataset over the same time period (24.5-30.5 s).

The results from our geographic analysis of the 2011-2012 calling season show that there is a significantly lower singlet song IPI at the northern stations than at the southern stations in the network although doublet song IPI remains the same across the same boundary. The two middle latitude locations (CI-J06A and CI-J23A) show both types of singlet IPI. At the 2010-2011 study location off the northwest coast of Vancouver Island, Koot [49] reported that

both singlet and doublet songs were observed, with average doublet IPIs of 12.9 s and 17.3 s, which is consistent with IPIs observed in our study. Koot [49] also reported that the mean singlet IPI between consecutive lower frequency notes (which we refer to as A notes) was 28.8 s. Although their study location was at a slightly higher latitude (∼50°N), and in coastal waters (∼105 m water depth), their singlet A-note IPI was similar to the singlet A note IPIs observed in our data at higher latitudes. The distinct shift in singlet A note IPI with latitude is interesting since it reveals a difference in call characteristics between the northern and southern portions of our study region, which may be evidence of two acoustically distinct groups of fin whales. To determine whether these potentially socially distinct groups also have genetic differences, in situ sampling would be required.

The 2007-2009 comparison between the Colza and Axial sites allowed us to explore frequency and IPI at locations with similar latitudes, but differences in proximity to the coast. The only notable difference between the two locations was in the frequency - at the Colza site, during both years, the frequency of singlet A notes was significantly higher than the corresponding singlet A notes at Axial. This may be further evidence for acoustically distinct groups of fin whales. It would be informative to look at frequency characteristics of both singlet and doublet calls across a broader geographic area and over multiple years to determine how persistent this pattern is both spatially and temporally.

Our study illustrates that if song characteristics are going to be used for determining population structure in fin whales, then long term, decadal scale data need to be considered, or lacking this, data from the same months and the same year should be compared to avoid potentially identifying populations as acoustically distinct when they are not [74]. Additionally, instrument locations need to be sufficiently dense in order to capture geographic variations and difference between these and temporal changes, which occur simultaneously and could otherwise be difficult distinguish. For instance, the median "long" IPIs from December 2000 and February 2001 from southern California, Hawaii and the Bering Sea were all different [74]; determining whether these differences are robust enough to delineate populations will require more data.

Boyd and Richardson [7] define culture as "information or behavior acquired from conspecifics through some form of social learning". One way of studying animal culture is by observing behavioral change patterns in wild populations where the animals' genetics or environment are not clear causes [85]. The two types of shifts in our dataset - a gradual shift in IPI and frequency, and a more distinct shift from one calling pattern to another - could both potentially be a result of cultural transmission. Cultural transmission has been observed in cetaceans [16, 22, 34, 71], but also in terrestrial animals such as frogs [39], bats [105], and birds [46, 92, 121].

It is difficult to determine the causes of the variations observed here because we have a very limited understanding of the underlying population structure. We can only speculate based on what do know about fin whale distributions and migratory movements, as well as what has been observed in other species, both marine and terrestrial. Payne and Webb [81] suggest that fin whales might maintain contact over great distances and this ability allows them to be unconstrained by geography with regards to potential breeding aggregations. In this way, whales from different North Pacific populations could potentially interact on regions of high secondary productivity and possibly exchange, or as suggested by Oleson [74], synchronize song types. Several populations of marine mammals have been observed to adopt a new song type after encountering even a small number of "foreign" singers. For example, Noad et al. [71] describe humpback whales off the Australian east coast gradually adopting song originating from humpback whales off the Australian west coast over a period of three years. Over an 11-year observation time, several humpback whale song types in the western and central south Pacific were observed to transmit unidirectionally across multiple populations from east to west [34]. Stafford and Moore [99] observed a blue whale in the Gulf of Alaska that produced a song that combined features of both the eastern and western north Pacific blue whale populations, suggesting that blue whales can mimic each others' calls. Resident killer whales observed off the coast of British Columbia showed evidence of a gradual shift in one of the two call types studied over a duration of 13 years [22]. The authors hypothesized that it might be evidence of cultural drift in the call structure, combined with

transmission of the new call characteristics between members of the population.

In order to test the hypothesis that fin whale vocalizations are undergoing cultural transmission, it would be necessary to continue to simultaneously explore more data from sufficiently dense networks covering wide regions over long time periods. Mizroch et al. [64] proposed that there are two subpopulations of fin whales in the North Pacific Ocean: one western and one eastern. At least a subset of these are believed to mingle on the northern summertime feeding grounds, which would potentially allow them the opportunity to meet and exchange song types. It would be interesting to explore and compare long term calling characteristics from non-migratory populations, such as from the Gulf of California [6], or the East China Sea [32] where we would expect that calling characteristics would evolve separately. Reliably linking acoustic observations to cultural transmission would require a more thorough understanding of the underlying geographic population structure and migratory patterns of the animals being studied. It would also be informative to look at whether long-term trends in frequency and IPI are observed in other ocean basins around the world.

4.4.1 Analysis limitations

All of the Cascadia Initiative instruments have a sample rate of 50 Hz, and an effective upper frequency limit at ∼23.5 Hz. Although a large portion of even the higher frequency notes are lower than this, the weighted frequency estimation is biased by the lack of signal above that point. For this reason, Cascadia Initiative instruments were not analyzed for patterns in frequency. Since the higher frequency calls were still detected, however, they could still be used for IPI analysis.

To express the variability of monthly estimates of IPI and frequency derived from 2D histograms, we used standard error, where standard deviations in the measurements were scaled by the number of sequences in the corresponding month. This was based on the assumption that each sequence was produced by a different animal, so were therefore independent samples. A more conservative estimate of the number of independent variables would be to use the number of days containing sequences, rather than the number of sequences. If multiple

sequences occur during a given day, those sequences might be produced by a single animal [93]. When this alternate method of estimating the number of independent samples is used, estimates of standard error increase by a factor of approximately two. This does not affect the interpretation of any of the reported results, but is worth considering. The true number of independent samples is likely bracketed by the number of sequences in one month, and the number of days with recorded sequences.

The definition of inter-pulse interval used in this analysis was chosen partially based on convention, and also because it was a straightforward computation. It might be beneficial in future work to compute inter-note interval, that is, the time between successive notes of the same frequency. However, exploring patterns in this way allowed us to easily explore the relationship between frequency and IPI without making prior assumptions. Notes of a particular frequency tended to follow a particular IPI, giving rise to the various groupings described here.

In this paper we describe broad patterns in both frequency and IPI. Previous research based on more temporally and spatially focused datasets has revealed finer nuances in these parameters. From an in-depth analysis of call types observed at the Endeavour Segment location, four dominant note types were described in terms of both frequency and IPI, and these call types were linked to swimming behavior over an entire year [93]. That study used the same data we used for KENE from 2003-2004 and reported on finer subtleties in the frequency and IPI patterns. They described three distinct song types, along with 2 categories of mixed or irregular song types. The most commonly observed type had a dominant IPI peak at 24 s (similar to this study) and a smaller secondary peak at 30 s. Our methodology focused on the more dominant note types, and was not sensitive to the subtle patterns described by Soule et al. [93]. Future work might benefit from a more detailed examination of those notes that occur less frequently.

4.5 Conclusions

The use of calling characteristics to define distinct sub-populations for conservation purposes is more complicated for fin whales than previously believed. There is some evidence indicating that in addition to long term shifts in both frequency and IPI, there are also subtle shifts across the region, in particular for the singlet A note call sequences. Future studies will need to take into account the potential for both spatial and temporal variability when planning surveys and when interpreting the resulting data.

Future work in the exploration of fin whale IPI and frequency patterns would benefit from the analysis of additional stations both spatially and temporally. The Cascadia Initiative Experiment [109] consists of around 70 instruments deployed from 2011-2015 off the West Coast of Canada and the US. This scope of this study focused on a specific set of five of those instruments deployed for the first year of the experiment. Based on our findings, we suggest that further exploration of this valuable open source dataset would help to better understand geographic variations in calling in this region. Additionally, data from the Regional Scale Nodes [24] and Ocean Networks Canada Neptune [5] cabled observatories already provide several years of ongoing recordings that should also be mined to explore long-term trends.

It would also be useful to conduct similar exploration of recordings in different ocean basins. Seismic instruments such as those used in this study have been deployed in networks around the world and the data from many of these are also openly available. Fig 4.9 shows a global map of seismic experiments from 2003-2016 from the United States Ocean Bottom Seismograph Instrument Pool (OBSIP). More than 800 of the instruments deployed during this time period were used for passive acoustic monitoring, and most of the data are accessible on the IRIS database (Incorporated Research Institutions for Seismology). There are also substantial fleets of OBSs operated by Japan and several European countries that could potentially be explored. These instruments typically record frequencies of 50 to 100 Hz, but with improvements in technology higher frequencies are becoming increasingly feasible.

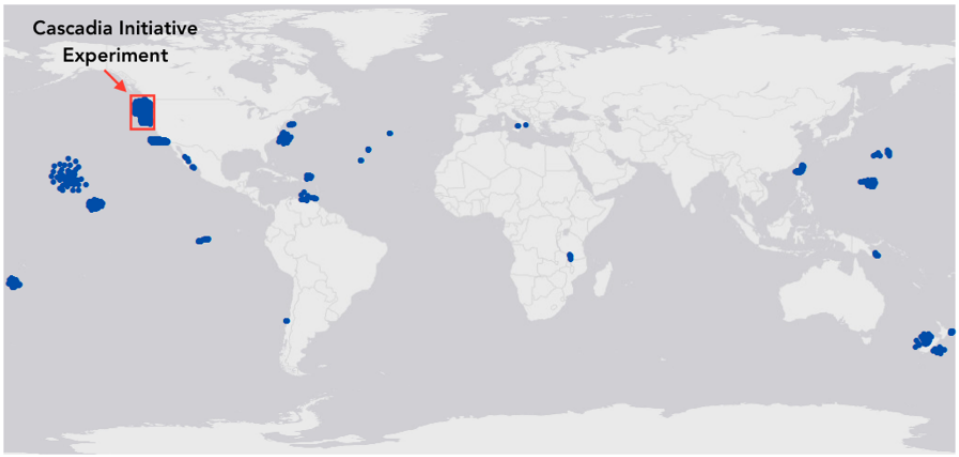

Figure 4.9: Locations of ocean bottom seismometers from US OBSIP experiments from 2003-2016. This map was generated using instrument metadata extracted from the IRIS global database.

Chapter 5

CONCLUSIONS

The over-arching goal of the three studies described in Chapters 2-4 was to explore the properties and patterns of fin whale calls recorded on OBSs in the northeast Pacific Ocean. Fin whales remain at risk from human activities in the ocean and to best protect them and mitigate these risks, we need to gain an understanding of their temporal and spatial distributions throughout their range.

The measurement of animal abundance over time is a critically important part of assessing and monitoring the recovery of endangered species. This has traditionally been done using visual surveys although the use of passive acoustic monitoring is becoming increasingly common. In order to turn passive measurements of underwater vocalizations into quantities that are relevant to conservation efforts requires a careful conversion from the number of calls to a normalized estimate of the number of animals at a particular location. Density estimation methods provide ways to carry out this conversion. Many of these methods, particularly distance sampling, borrow heavily from techniques originally developed for studying the abundance of terrestrial animals. The three studies described here looked at different aspects of fin whale calling that contribute in some way to our understanding of fin whale distributions, and all three have implications for density estimation.

The source levels study (Chapter 2) showed that fin whale calls in the northeast Pacific Ocean are consistently loud, averaging 189 $\pm$ 5.8 dB re 1Pa @ 1m. For individual animals producing a series of calls, there was no evidence of either a decrease or increase in amplitude within a sequence. Much of the variability observed in the estimated average source level can be attributed to uncertainties in the horizontal and vertical position of the fin whale at the time of the vocalization. Source levels estimated as part of this study were consistent

with previous studies, although they were at the higher end of the range. However, results were almost identical to a more recent study [112] which had a larger sample size than earlier studies. Source levels are useful in the calculation of acoustic communication space and the analysis of potential effects of anthropogenic noise. They are also a necessary component in the estimation of animal density using the energy in the frequency band of fin whale calls [62]. Source levels for 20 Hz calls were measured, and lower frequency backbeats were not included in the calculations. Analysis of later years (in Chapter 4) revealed the emergence of doublet calls. It would be informative to conduct similar analyses to look at the source levels of these other call types.

Using the timing and relative amplitude of multipaths allowed for estimates of range out to $\sim$20 km in 2-3 km water depth. Ranges up to $\sim$4 km could be reliably used for density estimation. The method was tested at two sites. One was in a mid-ocean ridge environment, with complex bathymetry and a basaltic seafloor. At this location, the basaltic seafloor resulted in strong reflections and typically between 4-5 multipath arrivals were visible for a single vocalization. However, the complex morphology of the seafloor introduced timing variability and made amplitudes difficult to predict. The other site was at a flat, heavily sedimented mid-plate location. At this site, the amplitude of multipath arrivals was suppressed and even after stacking nearby calls to increase signal to noise ratio, there were many cases when only two arrivals were detected. However, since the amplitude was more predictable at this location, amplitudes could be successfully used to aid in range determination when only two arrivals were detected.

Any future implementation of this method would require, first, that multipath arrivals can be detected. In heavily sedimented locations, there is the additional challenge introduced by interference from reflections from the base of the sediment layer. Simple modeling suggests that this is likely to occur when the sediment layer thickness is between 100 m and 1 km. For example, There are some full-ocean depth, sedimented locations where it appears that only the direct path is observed [54]. If weak multipaths can be amplified using stacking, multipath ranging might prove to be a valuable tool in sedimented sites since both timing

and amplitude are more predictable.

The multipath ranging method provides an important alternative to existing techniques for estimating density of vocalizing fin whales. Another method of estimating call density from OBS recordings uses the relative amplitudes on the three OBS components to estimate an incoming incidence angle. By combining the incidence angle with knowledge of the seafloor depth, the range to a vocalizing whale can be determined [54]. From that point, the estimation of call density is similar to the method presented here: it uses distance sampling [43]. It only works at ranges below the critical range, since the OBS channels are no longer coherent beyond that point. The third technique does not use individual calls, but instead measures the energy in the frequency band of fin whale calls, along with assumptions about call rate, source level, and knowledge of the acoustic propagation environment to estimate animal density [62]. Each of the methods has its strengths and weaknesses, and the ideal solution may involve a combination of all three. For example, the three-component method works best in deep water where all three OBS components are well-coupled to the seafloor. However, it is restricted to calls arriving within the critical range, so the coverage area is greatly reduced in shallower water. The multipath ranging method requires that distinct arrivals are detectable, which can be more challenging in deep, heavily-sedimented locations. The frequency band method has the potential to cover larger areas than either of the two distance sampling techniques but would potentially benefit from calibration using one of the first two methods which use individual calls in their calculations.

When converting call density to animal density, a major source of uncertainty is in the conversion of the number of calls to the number of animals, which depends on the proportion of animals calling and the amount of time an individual animal spends producing sounds. The calling patterns study revealed a lot about how challenging estimating call rate could be, at least in the northeast Pacific Ocean. In this study, both IPI and frequency were explored over the course of an entire decade. And in that decade, the IPI was observed to increase linearly over the course of the study. Furthermore, there was a change from mostly singlet call types to doublet call types about halfway through the decade of study. IPI, of course, relates

directly to calling rate: an increase in IPI could be erroneously linked to the presence of more animals, leading to a miscalculation in animal density. The observations of gradually shifting frequency and IPI have more implications than just estimates of animal density. They also impact efforts to delineate sub-populations acoustically due to the presence of a strong temporal trend. If differing fin whale calling patterns are observed at different locations and at different times, it is not possible to simply assume that they belong to different populations. The calls might be produced by a single population that has been gradually changing their song. Finally, the shifts in calling patterns also have implications for understanding the calling behavior of fin whales, and opens the door to the possibility of cultural transmission of call patterns across the region.

The calling patterns study, in particular, raises many questions that cannot be answered without extending the analysis to look at more locations and longer durations. Geographic differences, such as the singlet IPI shift between the northern and southern Cascadia Initiative Experiment stations (Fig. 4.7), or the shift in frequency between Axial and COLZA sites (Fig. 4.8) are difficult to explain. Are there some singing fin whales that remain to the north while others stay to the south of the northeast Pacific Ocean? Are there some that stay nearer to the coast while others remain further offshore? Fin whales are fast swimmers and can easily traverse entire ocean basins. It is unclear what would motivate them to segregate and restrict their movements, since having such broad mobility could be very beneficial in locating food resources or finding mates.

Expanded geographic analysis would help us to gain an understanding of fin whale calling behaviors, and how they reflect underlying distributions. This would require coverage over multiple years and at instrument density sufficient to distinguish geographic patterns. This type of study might reveal nuances in the rates of change of call characteristics along with information on how these changes propagate across the region. Cabled observatories such as the Regional Scale Nodes experiment or Ocean Networks Canadas Neptune Array can provide valuable long-term data to look at changing fin whale calls, and OBS arrays located around the world could enable better understanding fin whale calls on a global scale.

BIBLIOGRAPHY

[1] G.C. Anderson. The seasonal and geographic distribution of primary productivity off the Washington and Oregon coasts. *Limnology and Oceanography*, 9:284–302, 1964.

[2] J I Antonov, D Seidov, T P Boyer, R A Locarini, A V Mishonov, H E Garcia, O K Baranova, M M Zweng, and D R Johnson. *World Ocean Atlas 2009, Volume 2: Salinity.* U.S. Government Printing Office, Washington, D.C., 2010.

[3] R Aubauer, M O Lammers, and W W Au. One-hydrophone method of estimating distance and depth of phonating dolphins in shallow water. *The Journal of the Acoustical Society of America*, 107(5 Pt 1):2744–9, may 2000.

[4] Jay Barlow and Karin A. Forney. Abundance and population density of cetaceans in the California Current ecosystem. *Fishery Bulletin*, 105(4):509–526, 2007.

[5] C. R. Barnes, M. M. R. Best, F. R. Johnson, and B. Pirenne. NEPTUNE Canada: Installation and initial operation of the world's first regional cabled ocean observatory. In *SEAFLOOR OBSERVATORIES*, pages 415–438. Springer Berlin Heidelberg, Berlin, Heidelberg, 2015.

[6] Martine Bérubé, Jorge R. Urbán, Andrew E Dizon, Robert L Brownell, and Per J Palsbøll. Genetic identification of a small and highly isolated population of fin whales (Balaenoptera physalus) in the Sea of Cortez , México. *Fisheries Science*, 3:183–190, 2002.

[7] Robert Boyd and Peter J. Richerson. *Culture and the evolutionary process.* University of Chicago Press, 1988.

[8] Eli Brookner. *Tracking and kalman filtering made easy.* Wiley, 1998.

[9] Susahhah J. Buchan, Rodrigo Hucke-Gaete, Luke Rendell, and Kathleen M. Stafford. A new song recorded from blue whales in the Corcovado Gulf, Southern Chile, and an acoustic link to the Eastern Tropical Pacific. *Endangered Species Research*, 23(3):241–252, mar 2014.

[10] S T Buckland, D R Anderson, K P Burnham, J L Laake, D L Borchers, and L Thomas. Introduction to Distance Sampling: Estimating abundance of biological populations. pages 1–10. Oxford University Press, New York, NY, USA, 2001.

[11] Brenda J Burd and Richard E Thomson. Hydrothermal venting at endeavour ridge: effect on zooplankton biomass throughout the water column. *Deep Sea Research Part I: Oceanographic Research Papers*, 41(9):1407–1423, 1994.

[12] Brenda J Burd, Richard E Thomson, and Glen S Jamieson. Composition of a deep scattering layer overlying a mid-ocean ridge hydrothermal plume. *Marine Biology*, 113(3):517–526, 1992.

[13] R.L. Carlson and C.N. Herrick. Densities and porosities in the oceanic crust and their variations with depth and age. *J. Geophys. Res. Solid Earth*, (95):9153–9170, 1990.

[14] James V Carretta, Erin M. Oleson, D.W. Weller, A.R. Lang, Karin A. Forney, J. Baker, M.M. Muto, B. Hanson, A.J. Orr, H. Huber, M.S. Lowry, J. Barlow, J.E. Moore, D. Lynch, L. Carswell, and R.L. Brownell. U.S. Pacific Marine Mammal Stock Assessments: 2014. Technical report, U.S. Department of Commerce, NOAA Technical Memorandum, NOAA-TM-NMFS-SWFSC-549, 2015.

[15] Manuel Castellote, Christopher W. Clark, and Marc O. Lammers. Fin whale (Balaenoptera physalus) population identity in the western Mediterranean Sea. *Marine Mammal Science*, 28(2):325–344, apr 2012.

[16] S. Cerchio, J. K. Jacobsen, and T. F. Norris. Temporal and geographical variation in

songs of humpback whales, Megaptera novaeangliae: synchronous change in Hawaiian and Mexican breeding assemblages. *Animal Behaviour*, 62(2):313–329, 2001.

[17] R A Charif, D K Mellinger, K J Dunsmore, K M Fristrup, and C W Clark. Estimated source levels of fin whale (Balaenoptera physalus) vocalizations: Adjustments for surface interference. *Marine Mammal Science*, 18(1):81–98, 2002.

[18] G. L. Christeson, G.M. Purdy, and G.J. Fryer. Seismic constraints on shallow crustal emplacement processes at the fast spreading East Pacific Rise. *Journal of Geophysical Research*, 99(B9):17,957–17,973, 1994.

[19] Donald a Croll, Christopher W Clark, Alejandro Acevedo, Bernie Tershy, Sergio Flores, Jason Gedamke, and Jorge Urban. Only male fin whales sing loud songs. *Nature*, 417(6891):809, jun 2002.

[20] Connie F. Cudrak and Ron. M. Clowes. Crustal Structure of Endeavour Ridge Segment, Juan de Fuca Ridge, From a Detailed Seismic Refraction Survey. *Journal of Geophysical Research*, 98(B4):6329–6349, 1993.

[21] Keith R. Curtis, Bruce M. Howe, and James A. Mercer. Low-frequency ambient sound in the North Pacific: Long time series observations. *The Journal of the Acoustical Society of America*, 106(6):3189, 1999.

[22] V.B. Deecke, J.K.B. Ford, and P. Spong. Dialect change in resident killer whales: implications for vocal learning and cultural transmission. *Animal behaviour*, 60(5):629–638, 2000.

[23] V. A. Del Grosso. New equation for the speed of sound in natural waters (with comparisons to other equations). *The Journal of the Acoustical Society of America*, 56(4):1084, 1974.

[24] J. R. Delaney and D. S. Kelley. Next-generation science in the ocean basins: Expanding the oceanographer's toolbox utilizing submarine electro-optical sensor networks. In

SEAFLOOR OBSERVATORIES, pages 465–502. Springer Berlin Heidelberg, Berlin, Heidelberg, 2015.

[25] Julien Delarue, Bruce Martin, David Hannay, and Catherine L. Berchok. Acoustic Occurrence and Affiliation of Fin Whales Detected in the Northeastern Chukchi Sea, July to October 200710. *Arctic*, 66(2):159–172, 2013.

[26] Julien Delarue, Sean K Todd, Sofie M Van Parijs, and Lucia Di Iorio. Geographic variation in Northwest Atlantic fin whale (Balaenoptera physalus) song: implications for stock structure assessment. *The Journal of the Acoustical Society of America*, 125(3):1774–1782, 2009.

[27] Robert a Dunn and Olga Hernandez. Tracking blue whales in the eastern tropical Pacific with an ocean-bottom seismometer and hydrophone array. *The Journal of the Acoustical Society of America*, 126(3):1084–94, sep 2009.

[28] W. M. Ewing, W. S. Jardetzky, F. Press, and Arthur Beiser. Elastic Waves in Layered Media. *Physics Today*, 10(12):27, 1957.

[29] Andrew D. Foote, Richard W. Osborne, and A. Rus Hoelzel. Whale-call response to masking boat noise. *Nature*, 428(April):910, 2004.

[30] J. Forcada, A. Aguilar, P. Hammond, X. Pastor, and R. Aguilar. Distribution and abundance of fin whales (Balaenoptera physalus) in the western Mediterranean sea during the summer. *Journal of Zoology*, 238(1):23–34, jan 1996.

[31] Karin A Forney and Jay Barlow. Seasonal patterns in the abundance and distribution of California Cetaceans, 1991-1992. *Marine Mammal Science*, 14(3):460–489, 1998.

[32] Kazuo Fujino. Immunogenetic and marking approaches to identifying subpopulations of the North Pacific whales. *Sci. Rep. Whales Res. Inst., Tokyo*, 15:84–142, 1960.

[33] J.V. Gardner, D.A. Cacchione, D. Drake, B. Edwards, M. Field, M. Hampton, and H.A. Karl. Map showing the sediment isophachs in the deep-sea basins of the Pacific continental margin, Cape Mendocino to Point Conception, 1993.

[34] Ellen C. Garland, Anne W. Goldizen, Melinda L. Rekdahl, Rochelle Constantine, Claire Garrigue, Nan Daeschler Hauser, M. Michael Poole, Jooke Robbins, and Michael J. Noad. Dynamic horizontal cultural transmission of humpback whale song at the ocean basin scale. *Current Biology*, 21(8):687–691, 2011.

[35] Oriol Gaspa Rebull, Jordi Diaz Cusi, Mario Ruiz Fernandez, and Josep Gallart Muset. Tracking fin whale calls offshore the Galicia Margin, North East Atlantic Ocean. *The Journal of the Acoustical Society of America*, 120(4):2077–2085, 2006.

[36] Alexander N Gavrilov, Robert D McCauley, and Jason Gedamke. Steady inter and intra-annual decrease in the vocalization frequency of Antarctic blue whales. *The Journal of the Acoustical Society of America*, 131(6):4476–80, jun 2012.

[37] Alexander N. Gavrilov, Robert D. McCauley, Chandra Salgado-Kent, Joy Tripovich, and Chris Burton. Vocal characteristics of pygmy blue whales and their change over time. *The Journal of the Acoustical Society of America*, 130(6):3651, 2011.

[38] Jason Gedamke and Sarah M. Robinson. Acoustic survey for marine mammal occurrence and distribution off East Antarctica (30-80E) in January-February 2006. *Deep Sea Research Part II: Topical Studies in Oceanography*, 57(9):968–981, 2010.

[39] H. Carl Gerhardt. The Evolution of Vocalization in Frogs and Toads. *Annual Review of Ecology and Systematics*, 25(1994):293–324, 1994.

[40] Lisa A. Gilbert and H. Paul Johnson. Direct measurements of oceanic crustal density at the Northern Juan de Fuca Ridge. *Geophysical Research Letters*, 26(24):3633–3636, dec 1999.

[41] Jeremy A. Goldbogen, John Calambokidis, Robert E. Shadwick, Erin M. Oleson, Mark A. McDonald, and John A. Hildebrand. Kinematics of foraging dives and lunge-feeding in fin whales. *The Journal of experimental biology*, 209(Pt 7):1231–44, 2006.

[42] Edward J Gregr, Linda Nichol, John K B Ford, Graeme Ellis, and Andrew W Trites. Migration and population structure of Northeastern Pacific whales off coastal British Columbia: An analysis of commercial whaling records from 1908-1967. *Marine Mammal Science*, 16(4):699–727, 2000.

[43] Danielle Harris, Luis Matias, Len Thomas, John Harwood, and Wolfram H Geissler. Applying distance sampling to fin whale calls recorded by single seismic instruments in the northeast Atlantic. *The Journal of the Acoustical Society of America*, 134(5):3522–3535, 2013.

[44] L T Hatch and C W Clark. Acoustic differentiation between fin whales in both the North Atlantic and North Pacific Oceans, and integration with genetic estimates of divergence. Technical report, 2004.

[45] Luc T. Ikelle and Lasse Amundsen. *Introduction to petroleum seismology*. Society of Exploration Geophysicist, Tulsa, OK, 2005.

[46] P. F. Jenkins. Cultural transmission of song patterns and dialect development in a free-living bird population. *Animal Behaviour*, 26(PART 1):50–78, 1978.

[47] Eric Jones, Travis Oliphant, and Pearu Peterson. SciPy: Open source scientific tools for Python.

[48] Lawrence E. Kinsler, Austin R. Frey, Alan B. Coppens, and James V. Sanders. *Fundamentals of Acoustics*. John Wiley & Sons, Inc., New York, NY, 4th edition, 1999.

[49] Barbara Koot. *Winter behaviour and population structure of fin whales (Balaenoptera physalus) in British Columbia inferred from passive acoustic data*. PhD thesis, University of British Columbia, 2015.

[50] Elizabeth T Küsel, David K Mellinger, Len Thomas, Tiago Marques, David Moretti, and Jessica Ward. Cetacean population density estimation from single fixed sensors using passive acoustics. *The Journal of the Acoustical Society of America*, 129(6):3610–3622, 2011.

[51] David W. Laist, Amy R. Knowlton, James G. Mead, Anne S Collet, and Michela Podesta. Collisions Between Ships and Whales. *Marine Mammal Science*, 17(1):35–75, jan 2001.

[52] R A Locarini, A V Mishinov, J I Antonov, T P Boyer, H E Garcia, O K Baranova, M M Zweng, and D R Johnson. *World Ocean Atlas 2009, Volume 1: Temperature*. U.S. Government Printing Office, Washington, D.C., 2010.

[53] Tiago a Marques, Len Thomas, Jessica Ward, Nancy DiMarzio, and Peter L Tyack. Estimating cetacean population density using fixed passive acoustic sensors: an example with Blainville's beaked whales. *The Journal of the Acoustical Society of America*, 125(4):1982–94, apr 2009.

[54] Luis Matias and Danielle Harris. A single-station method for the detection, classification and location of fin whale calls using ocean-bottom seismic stations. *The Journal of the Acoustical Society of America*, 138(1):504–520, 2015.

[55] Mark A McDonald and Christopher G Fox. Passive acoustic methods applied to fin whale population density estimation. *October*, 105(5):2643–2651, 1999.

[56] Mark A McDonald, John A Hildebrand, and Sarah Mesnick. Worldwide decline in tonal frequencies of blue whale songs. *Endangered Species Research*, 9:13–21, 2009.

[57] Mark A McDonald, John A Hildebrand, and Spahr C Webb. Blue and fin whales observed on a seafloor array in the Northeast Pacific. *Journal of the Acoustical Society of America*, 98(2):712–721, 1995.

[58] Mark A. McDonald, Sarah L. Mesnick, and John A. Hildebrand. Biogeographic characterisation of blue whale song worldwide: using song to identify populations. *Journal of Cetacean Research and Management*, 8(1):55–65, 2006.

[59] P. R. McGill, W. S. Wilcock, D. S. Stakes, A. H. Barclay, T. M. Ramirez, and D. R. Toomey. A Long-Term Seismic Array on the Endeavour Segment of the Juan de Fuca Ridge. *American Geophysical Union, Fall Meeting 2003, abstract #B12A-0748*, 2003.

[60] D K Mellinger and C W Clark. Recognizing transient low-frequency whale sounds by spectrogram correlation. *The Journal of the Acoustical Society of America*, 107(6):3518–29, jun 2000.

[61] David K Mellinger and Christopher W. Clark. Blue whale (Balaenoptera musculus) sounds from the North Atlantic. *Journal of the Acoustical Society of America*, 114(2):1108–1119, 2003.

[62] David K. Mellinger, E.T. Küsel, D. Harris, L. Thomas, and L. Matias. Estimating singing fin whale population density using frequency band energy. *Journal of the Acoustical Society of America*, (136):2275–2275, 2014.

[63] David K. Mellinger, Kathleen M. Stafford, Sue E. Moore, Robert P. Dziak, and Haru Matsumoto. An Overview of Fixed Passive Acoustic Observation Methods for Cetaceans. *Oceanography*, 20(4):36–45, 2007.

[64] Sally a. Mizroch, Dale W. Rice, Denny Zwiefelhofer, Janice Waite, and Wayne L. Perryman. Distribution and movements of fin whales in the North Pacific Ocean. *Mammal Review*, 39(3):193–227, jul 2009.

[65] Sue E Moore, Kathleen M. Stafford, Marilyn E Dahlheim, Christopher G Fox, Howard W Braham, Jeffrey J Polovina, and David E Bain. Seasonal variation in reception of fin whale calls at five geographic areas in the North Pacific. *Marine Mammal Science*, 14(3):617–627, 1998.

[66] Janelle L. Morano, Daniel P. Salisbury, Aaron N. Rice, Karah L. Conklin, Keri L. Falk, and Christopher W. Clark. Seasonal and geographical patterns of fin whale song in the western North Atlantic Ocean. *The Journal of the Acoustical Society of America*, 132(2):1207, 2012.

[67] David Mouillot and Denise Viale. Satellite tracking of a fin whale (Balaenoptera physalus) in the north-western Mediterranean Sea and fractal analysis of its trajectory. *Revue*, pages 163–171, 2001.

[68] M.R. Nedimović, S. M. Carbotte, J. B. Diebold, A. J. Harding, J. P. Canales, and G. M. Kent. Upper crustal evolution across the Juan de Fuca ridge flanks. *Geochemistry Geophysics Geosystems*, 9(9), 2008.

[69] Sharon L. Nieukirk, David K. Mellinger, Sue E. Moore, Karolin Klinck, Robert P. Dziak, and Jean Goslin. Sounds from airguns and fin whales recorded in the mid-Atlantic Ocean, 19992009. *The Journal of the Acoustical Society of America*, 131(2):1102, 2012.

[70] Sharon L. Nieukirk, Kathleen M. Stafford, David K. Mellinger, Robert P. Dziak, and Christopher G. Fox. Low-frequency whale and seismic airgun sounds recorded in the mid-Atlantic Ocean. *The Journal of the Acoustical Society of America*, 115(4):1832, 2004.

[71] Michael J. Noad, Douglas H. Cato, M. M. Bryden, Micheline N. Jenner, and K. Curt S. Jenner. Cultural revolution in whale songs. *Nature*, 408(6812):537–537, nov 2000.

[72] Guust Nolet and Leroy M. Dorman. Waveform Analysis of Scholte Modes In Ocean Sediment Layers. *Geophysical Journal International*, 125(2):385–396, may 1996.

[73] J. Northrop, William C. Cummings, and Paul O. Thompson. 20-Hz Signals Observed in the Central Pacific. *Journal of the Acoustical Society of America*, 43(2):13–14, 1968.

[74] Erin M. Oleson, Ana Širović, Alexra R. Bayless, and John A. Hildebr. Synchronous seasonal change in fin whale song in the North Pacific. *PLoS ONE*, 9(12):1–18, 2014.

[75] Erin Marie Oleson. *Calling Behavior of Blue and Fin Whales off California*. PhD thesis, University of California, San Diego, 2005.

[76] Simone Panigada, Giovanna Pesante, Margherita Zanardelli, Frédéric Capoulade, Alexandre Gannier, and Mason T. Weinrich. Mediterranean fin whales at risk from fatal ship strikes. *Marine Pollution Bulletin*, 52(10):1287–1298, 2006.

[77] Susan E. Parks, C. W. Clark, and P. L. Tyack. Short- and long-term changes in right whale calling behavior: The potential effects of noise on acoustic communication. *The Journal of the Acoustical Society of America*, 122(6):3725, 2007.

[78] Susan E. Parks, Ildar Urazghildiiev, and Christopher W. Clark. Variability in ambient noise levels and call parameters of North Atlantic right whales in three habitat areas. *The Journal of the Acoustical Society of America*, 125(2):1230, 2009.

[79] B. Patterson and G.R. Hamilton. Repetitive 20 cycle per second biological hydroacoustic signals at Bermuda. *Marine bioacoustics*, 1964.

[80] Katharine Payne and Roger Payne. Large Scale Changes over 19 Years in Songs of Humpback Whales in Bermuda. *Zeitschrift für Tierpsychologie*, 68(2):89–114, apr 1985.

[81] Roger Payne and Douglas Webb. Orientation by means of long range acoustic signaling in baleen whales. *Annals of the New York Academy of Sciences*, 188:110–141, 1971.

[82] Michael B. Porter and Homer P. Bucker. Gaussian beam tracing for computing ocean acoustic fields. *The Journal of the Acoustical Society of America*, 82(4):1349, 1987.

[83] V Premus and J L Spiesberger. Can acoustic multipath explain finback (B . physalus) 20-Hz doublets in shallow water ? *Journal of the Acoustical Society of America*, 101(August 1987):1127–1138, 1997.

[84] S.B. Reilly, J. L. Bannister, P. B. Best, Brown M., R.L. Brownell Jr., D.S. Butterworth, P.J. Clapham, J. Cooke, G.P. Donovan, Jorge R. Urbán, and A.N. Zerbini. Balaenoptera physalus: The IUCN Red List of Threatened Species 2013: e.T2478A44210520. Technical report, 2013.

[85] Luke Rendell and Hal Whitehead. Culture in Whales and Dolphins. *Mar. Ecol. Prog. Ser*, 24(2):309–382, 2001.

[86] B. Romanowicz, D. Stakes, R. Uhrhammer, P. McGill, D. Neuhauser, T. Ramirez, and D. Dolenc. The MOBB experiment: A prototype permanent off-shore ocean bottom broadband station. *Eos Trans. AGU*, 84(34):325, 2003.

[87] Mrinal K Sen, L N Frazer, S Mallick, and N R Chapman. Analysis of multipath sound propagation in the ocean near 49N, 128W. *The Journal of the Acoustical Society of America*, 83(2):588–597, 1988.

[88] Malene Simon, Kathleen M. Stafford, Kristian Beedholm, Craig M Lee, and Peter T Madsen. Singing behavior of fin whales in the Davis Strait with implications for mating, migration and foraging. *The Journal of the Acoustical Society of America*, 128(5):3200–10, nov 2010.

[89] Ana Širović, John A. Hildebrand, Sean M. Wiggins, Mark A. McDonald, Sue E. Moore, and Deborah Thiele. Seasonality of blue and fin whale calls and the influence of sea ice in the Western Antarctic Peninsula. *Deep Sea Research Part II: Topical Studies in Oceanography*, 51(17):2327–2344, 2004.

[90] Ana Širović, John A. Hildebrand, Sean M. Wiggins, and Deborah Thiele. Blue and fin whale acoustic presence around Antarctica during 2003 and 2004. *Marine Mammal Science*, 25(1):125–136, jan 2009.

[91] Ana Širović, Lauren N. Williams, Sara M. Kerosky, Sean M. Wiggins, and John A.

Hildebrand. Temporal separation of two fin whale call types across the eastern North Pacific. *Marine Biology*, 160(1):47–57, jan 2013.

[92] P.J.B. Slater. The cultural transmission of bird song. *Trends in Ecology & Evolution*, 1(4):94–97, 1986.

[93] Dax C. Soule and William S. D. Wilcock. Fin whale tracks recorded by a seismic network on the Juan de Fuca Ridge, Northeast Pacific Ocean. *The Journal of the Acoustical Society of America*, 133(3):1751, 2013.

[94] Dax C. Soule, William S. D. Wilcock, and Richard E. Thompson. Statistical analysis of fin whale vocalizations recorded by a seismic network at the Endeavour Segment of Juan de Fuca Ridge, N. E. Pacific Ocean. *The Journal of the Acoustical Society of America*, 129(4):2638, 2011.

[95] Kathleen M. Stafford. Two types of blue whale calls recorded in the Gulf of Alaska. *Marine Mammal Science*, 19(4):682–693, oct 2003.

[96] Kathleen M. Stafford, Emily Chapp, DelWayne R. Bohnenstiel, and Maya Tolstoy. Seasonal detection of three types of pygmy blue whale calls in the Indian Ocean. *Marine Mammal Science*, 27(4):828–840, oct 2011.

[97] Kathleen M. Stafford, John J. Citta, Sue E. Moore, Mary Ann Daher, and Joseph E. George. Environmental correlates of blue and fin whale call detections in the North Pacific Ocean from 1997 to 2002. *Marine Ecology Progress Series*, 395:37–53, dec 2009.

[98] Kathleen M. Stafford, Christopher G Fox, and Christopher W Clark. Long-range acoustic detection and localization of blue whale calls in the northeast Pacific Ocean. *The Journal of the Acoustical Society of America*, 104(6):3616–25, dec 1998.

[99] Kathleen M Stafford and Sue E Moore. Atypical calling by a blue whale in the Gulf of Alaska (L). *Journal of the Acoustical Society of America*, 117(5):2724, 2005.

[100] Kathleen M. Stafford, Sharon L. Nieukirk, and Christopher G. Fox. An acoustic link between blue whales in the Eastern Tropical Pacific and the Northeast Pacific. *Marine Mammal Science*, 15(4):1258–1268, oct 1999.

[101] Kathleen M. Stafford, Sharon L. Nieukirk, and Christopher G. Fox. Low-frequency whale sounds recorded on hydrophones moored in the eastern tropical Pacific. *The Journal of the Acoustical Society of America*, 106(6):3687, 1999.

[102] Kathleen M Stafford, Sharon L Nieukirk, and Christopher G Fox. Geographic and seasonal variation of blue whale calls in the North Pacific. *Journal of Cetacean Research and Management*, 3(1):65–76, 2001.

[103] D. Stakes, J. McClain, T. Zandt, P. McTill, and M. Begnaud. Corehole seismometer development for low-noise seismic data in a long-term seafloor observatory. *Geophys. Res. Lett*, 25:2745–2748, 1998.

[104] Alison K Stimpert, Stacy L DeRuiter, Erin A Falcone, John Joseph, Annie B Douglas, David J Moretti, Ari S Friedlaender, John Calambokidis, Glenn Gailey, Peter L Tyack, and Jeremy A Goldbogen. Sound production and associated behavior of tagged fin whales (Balaenoptera physalus) in the Southern California Bight. *Animal Biotelemetry*, 3(1):23, dec 2015.

[105] Keping Sun, Li Luo, Rebecca T. Kimball, Xuewen Wei, Longru Jin, Tinglei Jiang, Guohong Li, and Jiang Feng. Geographic Variation in the Acoustic Traits of Greater Horseshoe Bats: Testing the Importance of Drift and Ecological Selection in Evolutionary Processes. *PLoS ONE*, 8(8):1–10, 2013.

[106] S.A. Swift, D. Lizarralde, R.A. Stephen, and H. Hoskins. Velocity structure in upper ocean crust at Hole 504B from vertical seismic profiles. *J. Geophys. Res. Solid Earth*, (103):15361–15376, 1998.

[107] P.O. Thompson, L.T. Findley, and O. Vidal. 20-Hz Pulses and Other Vocalizations of Fin Whales, Balaenoptera-Physalus, in the Gulf-of-California, Mexico. *Journal of the Acoustical Society of America*, 92(6):3051–3057, 1992.

[108] Christopher O Tiemann, Aaron M Thode, Janice Straley, Victoria O'Connell, and Kendall Folkert. Three-dimensional localization of sperm whales using a single hydrophone. *The Journal of the Acoustical Society of America*, 120(4):2355, 2006.

[109] Douglas Toomey, Richard Allen, Andrew Barclay, Samuel Bell, Peter Bromirski, Richard Carlson, Xiaowei Chen, John Collins, Robert Dziak, Brent Evers, Donald Forsyth, Peter Gerstoft, Emily Hooft, Dean Livelybrooks, Jessica Lodewyk, Douglas Luther, Jeffrey McGuire, Susan Schwartz, Maya Tolstoy, Anne Trehu, Michelle Weirathmueller, and William Wilcock. The Cascadia Initiative: A Sea Change In Seismological Studies of Subduction Zones. *Oceanography*, 27(2):138–150, jun 2014.

[110] A.M. Trehu. Coupling of ocean bottom seismometers to sediment: Results of tests with the US Geological Survey ocean bottom seismometers. *Bulletin of the Seismological Society of America*, 75:271–289, 1985.

[111] R.J. Urick. *Principles of Underwater Sound*. Peninsula Publishing, Los Altos, CA, 3rd edition, 1983.

[112] Ana Širović, John A. Hildebrand, and Sean M Wiggins. Blue and fin whale call source levels and propagation range in the Southern Ocean. *The Journal of the Acoustical Society of America*, 122(2):1208–15, aug 2007.

[113] E. M. Van Ark, R. S. Detrick, J. P. Canales, S. M. Carbotte, A. J. Harding, G. M. Kent, M. R. Nedimovic, W. S. D. Wilcock, J. B. Diebold, and J. M. Babcock. Seismic structure of the Endeavour Segment, Juan de Fuca Ridge: Correlations with seismicity and hydrothermal activity. *Journal of Geophysical Research*, 112(B2):B02401, feb 2007.

[114] W A Watkins, P Tyack, K E Moore, and J E Bird. The 20-Hz signals of finback whales (Balaenoptera physalus). *The Journal of the Acoustical Society of America*, 82(6):1901–12, dec 1987.

[115] WA Watkins. Activities and underwater sounds of fin whales. *Sci. Rep. Whales Res. Inst.*, 33:83–117, 1981.

[116] William A Watkins, Mary Ann Daher, Gina M Reppucci, Joseph E George, Dare L Martin, Nancy A Dimarzio, and Damon P Gannon. Seasonality and Distribution of whale calls in the North Pacific. *Oceanography*, 13(I):62–67, 2000.

[117] William A Watkins, Karen E Moore, Johann Sigurjonsson, Douglas Wartzok, and Guiseppe Notobartolo di Sciara. *Fin whale (Balaenoptera physalus) tracked by radio in the Irminger Sea*. Reykjavic: Hafrannsoknastofnunin, 1984.

[118] William A Watkins and William E Schevill. Sound source location by arrival-times on a non-rigid three-dimensional hydrophone array. *Deep-Sea Research*, 19:691–706, 1972.

[119] Michelle J Weirathmueller, William S D Wilcock, and Dax C Soule. Source levels of fin whale 20 Hz pulses measured in the Northeast Pacific Ocean. *The Journal of the Acoustical Society of America*, 133(2):741–749, 2013.

[120] Gordon M. Wenz. Acoustic Ambient Noise in the Ocean: Spectra and Sources. *The Journal of the Acoustical Society of America*, 34(12):1936–1956, dec 1962.

[121] Meredith J. West, Andrew P. King, and Thomas J. Harrocks. Cultural transmission of cowbird song (Molothrus ater): Measuring its development and outcome. *Journal of Comparative Psychology*, 97(4):327–337, 1983.

[122] Sean M. Wiggins, Mark A. Mcdonald, Lisa M. Munger, Sue E. Moore, and John A. Hildebrand. Waveguide propagation allows range estimates for north Pacific Right Whales in the Bering Sea. *Canadian Acoustics*, 32(2):146–154, 2004.

[123] W S D Wilcock. Tracking fin whales in the Northeast Pacific Ocean with a seafloor seismic network. *The Journal of the Acoustical Society of America*, 132:2408–2419, 2012.

[124] William S. D. Wilcock, Stephen D. Archer, and G. M. Purdy. Microearthquakes on the Endeavour segment of the Juan de Fuca Ridge. *Journal of Geophysical Research: Solid Earth*, 107(B12):EPM 4–1–EPM 4–21, dec 2002.

[125] William S. D. Wilcock, Dax C. Soule, and Richard E. Thomson. Tracking fin and blue whales above the Juan de Fuca Ridge with a local seafloor seismic network. *The Journal of the Acoustical Society of America*, 125(4):2588–2588, apr 2009.

[126] Rob Williams and Patrick O'Hara. Modelling ship strike risk to fin, humpback and killer whales in British Columbia, Canada. *Journal of Cetacean Research and Management*, 11(1):1–8, 2010.

[127] A.N. Zerbini, J.M. Waite, J.L. Laake, and P.R. Wade. Abundance, trends and distribution of baleen whales off Western Alaska and the central Aleutian Islands. *Deep Sea Research Part I: Oceanographic Research Papers*, 53(11):1772–1790, nov 2006.